**UNIVERSITÀ DEGLI STUDI DI NAPOLI "FEDERICO II"**

**Corso di dottorato in Ingegneria dei Prodotti e dei Processi Industriali (XXIX ciclo)**

# Organic and Inorganic Material-Based Functional Surfaces for Sensors and Biosensors: Synthesis and Design

<u>**Dottorando:**</u>

**Aldobenedetto Zotti**

<u>**Coordinatore:**</u>

**Ch.mo Prof.
Giuseppe Mensitieri**

<u>**Relatori:**</u>

**Dott.ssa
Anna Borriello**

**Ch.mo
Prof. Giuseppe Mensitieri**

**ANNO ACCADEMICO 2016/2017**

*In memory of my father*
*Aldo Zotti (1951-2016)*

# List of Content

# List of abbreviations

EI - electromagnetic interference

RI – Refractive Index

FBG – Fiber Bragg Grating

LPG – Long Period Grating

GPL – Liquefied Petroleum Gas

a-PS – Atactic Polystyrene

VOC - Volatile Organic Compounds

ppm – Part per million

RH – Relative Humidity

AAO - Anodic Aluminum Oxide

QCM – Quartz Crystal Microbalance

PEI - Poly (ethylenimine)

PAA - poly (acrylic acid)

GOD - glucose oxidase

SRI - Surrounding Medium RI

MFC – Mass Flow Controller

LHC - Large Hadron Collider

BL - β-lactamases

ESBL - Extended-spectrum BL

3-APBA – 3 Aminophenyl boronic acid

EDC - N-ethyl-N'-(3- (dimethylamino)propyl)carbodiimide

NHS - N-hydroxysuccinimide

# 1.  Introduction

Advancement of sensor technology over the past few decades has led to significant progress in all scientific and technological fields, such as environmental and atmospheric monitoring, agriculture, industrial processing, medicine and biotechnology. Environmental and atmospheric monitoring, i.e., the control of air pollution caused by industry and exhaust gases from automobiles, has become a critical issue. In agriculture, sensors can be used for animal and plant disease diagnostics, detection of contaminants and pathogens in milk, meat, and other foods and determination of product quality such as the ripeness and flavors of fruits and vegetables in the field. Medicine is another important field for sensor applications: emerging requirements for sensors in the medical and healthcare sector are being driven by movement toward the continuous monitoring of patients. Breath analysis is one of the possible applications of ~~gas~~ sensors in medicine. At present there are a wide variety of devices based on different materials and operating on diverse principles which can be applied for analytes detection. Physics, chemistry, and technology of sensors require a better understanding of both the bulk and surface properties of the sensing materials. One expects that a sensing material should have high sensitivity and selectivity, small response and recovery times, minimum environmental degradations, room temperature operation and low power consumption. Therefore, the selection and development of an active material is a challenge. The active sensing materials acts as a catalyst for sensing a particular analyte or a set of analytes. The recent development in the nanotechnology has paved the way for large number of new materials and devices of desirable properties which have useful functions for numerous chemical sensor and biosensor applications. Basically by creating nanostructure, it is possible to control the fundamental properties of materials even without changing their chemical composition.

The study of the interface between the analyte and the sensitive material represents a fundamental step in the design, development and understanding of any chemical and biological analysis. In first approximation, the problem of compatibility is solved by operating an appropriate choice of materials which act as an interface and are adapted to the interaction of molecules and macromolecules.

The interface is designed not only as a measuring environment, but as an integral part of the measurement system. Modern chemical sensors are focused on the study of applications in which analyte, sensor, and elaboration unit are integrated, in order to achieve measuring elements that are portable and easy to use. In this context, it is fundamental the engineering of the interface, i.e., the part that interacts with the analyte and which can be modified by means of different techniques, in order to obtain specific characteristics; these concern not only the compatibility, but also other surface properties that may be required by the application (wettability, surface tension, chemical reactivity, etc.).

The sensing material is the main component of a sensor, but without an appropriate transducer it is not possible to convert the sensible material property change in a readable signal. On the other hand, the transducer itself is not able of interacting with the external medium: the sensor is then blind. Therefore, to develop an efficient sensor different aspects must be considered: the sensible material, the transducer typology and the interaction between material and transducer.

During the last decades, the technology and applications of optical fibers have evolved very quickly. Sensors employing optical fibers as transducers exhibit many advantages over their electrical counterparts, including higher responsivity, higher detection bandwidth, capability of operating in a wide temperature range, immunity to EI, possibility of using any material as sensing film regardless of its dielectric nature, greater environmental resistance and flexibility. Moreover, in applications where the working

space is stringent or where physical intrusion must be minimized, it become highly desirable to develop ultra-compact sensors that can maintain the level of performances despite the miniaturization. Among all fiber-based optical sensors, Long Period Gratings are the most popular devices used for developing chemical sensors and biosensors.

The thesis is focuses on the realization of integrated optical bio/sensors by the engineering of materials and interfaces and by means of innovation of the transduction platforms. The transducer is the Long Period Gratings (LPGs) with different organic and/or inorganic materials as sensitive elements. The careful study of the sensing materials, as well as the optimization of the deposition process, can lead to an improved sensor (chemical and biological), in term of compactness, responsivity, detection bandwidth and response time, compared to commercial sensors. In particular, three different devices as been developed during these three years:

- GPL sensor based on a-PS coatings, in the framework of the OPTOFER Project (Cap. 5);

- Cryogenic humidity sensors based on Titanium Oxide coatings, during a collaboration agreement with CERN (Cap.6);

- Drug resistant bacteria biosensor based on a-PS/PMMA coatings, in the framework of the OPTOBACTERIA European Project (Cap. 7);

All results in this thesis derived by integrating knowledges in different scientific areas (optical engineering, biochemistry, polymer materials, etc.) fulfil the interdisciplinary scope.

# 2. State of art on sensor and biosensors

Recently, gas sensing, as a typical application in intelligent systems, is receiving increasing attention in both industry and science. Sensing technology has become more significant because of its widespread and common applications in the following areas: industrial production (e.g., methane detection in mines) [1]; automotive industry (e.g., detection of polluting gases from vehicles) [2]; medical applications (e.g., electronic noses simulating the human olfactory system) [3]; indoor air quality supervision (e.g., detection of carbon monoxide) [4]; environmental studies (e.g., greenhouse gas monitoring) [5].

To evaluate the performance of gas sensing methods or gas sensors, several indicators should be considered: *sensitivity* - the minimum target gases volume detectable; *selectivity* - the ability of gas sensors to identify a specific gas among a gas mixture; *response time* - the period from the time when gas concentration reaches a specific value to that when sensor signal reaches a plateau value; *energy consumption*; *reversibility* - whether the sensing materials could return to its original state after detection; *adsorptive capacity* (also affects sensitivity and selectivity); *fabrication cost*.

Sensors are classified on the basis of the property that is measured in presence of the analyte. Fig. 1 shows the classification proposed by Liu et al. [6]. As it is evident, the most developed class of sensor is that of the electrochemical sensors, in which the transducing signal is the electric conductivity change in presence of the analyte. Most of the electrochemical sensors are based on metal oxide semiconductor, which exhibit significantly greater sensitivity to inorganic gases like ammonia and a few kinds of VOCs like alcohol ($C_2H_5OH$) and formaldehyde [6]. However, metal oxide semiconductor-based sensors are not able to detect VOCs with high selectivity, and their inability to discriminate between different gasses is a remarkable drawback. As humans could easily

breathe VOCs since they are commonly used as ingredients in household products or in industrial processes, it is important to selectively monitor the concentration of these vapors to safeguard the health of residents and workers, and to keep atmospheric emissions under control in order to avoid environmental hazards. Unlike metal oxide semiconductors, polymer are suitable to discriminate between different gasses and vapors classes. Furthermore, these inorganic materials need high operative temperature (over 300°C).
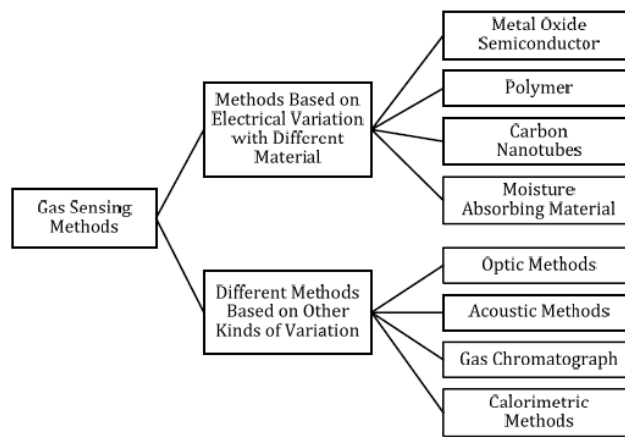


**Figure 1** Sensor classification proposed by Liu et al. [6]

For these reasons, polymers have begun to be studied and employed in the sensing area. Although conductive polymers are also used as electrochemical sensors, the area where polymers find most successful is the optical sensing: in fact, they are extensively used as sensible coating for optical fiber sensors.

The optical fiber sensors have advantages that include immunity to EI, lightweight, small size, large bandwidth, and ease in implementing multiplexed or distributed sensors. Moreover, optical fiber sensors could achieve higher sensitivity, selectivity, stability and lower response time (which enables on-line real time detection) than non-optical methods, with much longer lifetime. Strain, temperature and pressure are the most widely studied measurands and the fiber grating sensor represents the most widely studied technology for optical fiber sensors as shown in Fig. 2, which shows the technologies involved in the optical fiber sensors presented at 15th Optical Fiber Sensors Conference (OFS-15) [7].
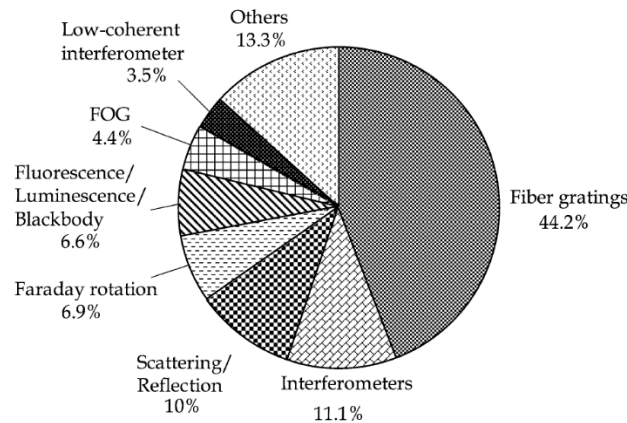
8

**Figure 2** Distribution of OFS-15 papers according to technologies. [7]

Although the formation of fiber gratings had been reported in 1978 [8], intensive study on fiber gratings began after a controllable and effective method for their fabrication, developed in 1989 [9]. Extensive studies have been performed on fiber grating sensors and some of which have now reached commercialization stages. Fig. 3 shows some types of fiber gratings. Under phase matching conditions, a FBG couples the forward propagating core mode to the backward propagating core mode. A LPG can couple the forward propagating core mode to one or a few of the forward propagating cladding modes.
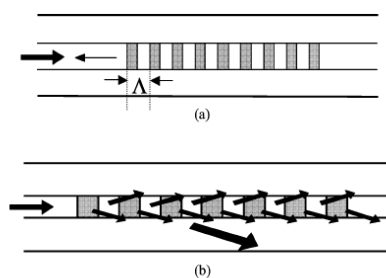


**Figure 3** Types of fiber gratings. (a) Fiber Bragg grating, (b) long-period fiber grating. [7]

In particular, LPG has been used as a RI sensor because of its high RI sensitivity. If the coating or jacket is removed from the optical fiber, the evanescent field of the cladding mode that exists outside the cladding experiences the RI change of the outside material. The selectivity and sensitivity can be tuned by depositing a thin film overlay on the grating region, as reported by Rees et al. [10]; he has coated an LPG with an organic film by the Lamgmuir–Blodgett technique and studied the influence of the overlay material

9

thickness on the LPG response: the film has been proved to be chemically sensitive, so the LPG film sensors could be used as species-specific chemical sensors.

## 2.1   VOCs and GPL sensors

VOCs are organic chemical compounds that have a high vapor pressure at ordinary room temperature. Their high vapor pressure results from a low boiling point, which causes large numbers of molecules to evaporate from the liquid form of the compound and enter the surrounding air. VOCs are numerous varied, and some examples are the followers: aromatic and aliphatic hydrocarbons (such as methane, propane, butane and benzene), aldehydes (such as formaldehyde), alcohol (such as ethanol and propanol) and chlorofluorocarbons. In addition, GPL is classified as a VOC.

GPL or liquid petroleum gas, are flammable mixtures of hydrocarbon gases used as fuel in heating appliances, cooking equipment, and vehicles. Varieties of GPL bought and sold include mixes that are mostly propane ($C_3H_8$), mostly butane ($C_4H_{10}$) and, most commonly, mixes including both propane and butane. Propylene, butylene and various other hydrocarbons are usually also present in small concentrations. LPG is prepared by refining petroleum or "wet" natural gas, and is almost entirely derived from fossil fuel sources, being manufactured during the refining of petroleum (crude oil), or extracted from petroleum or natural gas streams as they emerge from the ground.

As reported in the previous paragraph, metal oxide semiconductor are the most common materials used to develop electrochemical VOCs sensors. Generally, the used oxide are n type semiconductors [11-13] (charge carrier are electrons), but this is not a general rule because $NiO_x$ oxides, that are p type semiconductors (charge carrier are holes), result widely employed in VOCs detection. The most employed oxides as sensing material in VOCs sensors are:  iron oxide ($Fe_2O_3$) [11], tin oxide ($SnO_2$) [12] and titanium oxide (TiO2) [13]. Thin $Fe_2O_3$ layers, deposited using catodic sputtering, have been employed

by *Siroky et al.* [11] to realize an hydrogen and VOCs detector; the operative temperature is 350-400°C. In order to obtain a device able to discriminate between toluene and o-xylene, in 1997 *Llobet et al.* [12] developed a sensors array based on $SnO_2$ films: the simultaneous tracking of the stationary (response absolute value) and in time (response time) signal has allowed to evaluate the device selectivity. Using different sol-gel methods is possible to realize $TiO_2$ based sensors with different sensing performances, as studied by *Garzella et al.* [13] in 2000. In this work, developed devices have shown promising response toward ethanol and methanol, although operative temperature are very high (400-500°C). Fig. 4 shows the performances obtained in the cited.
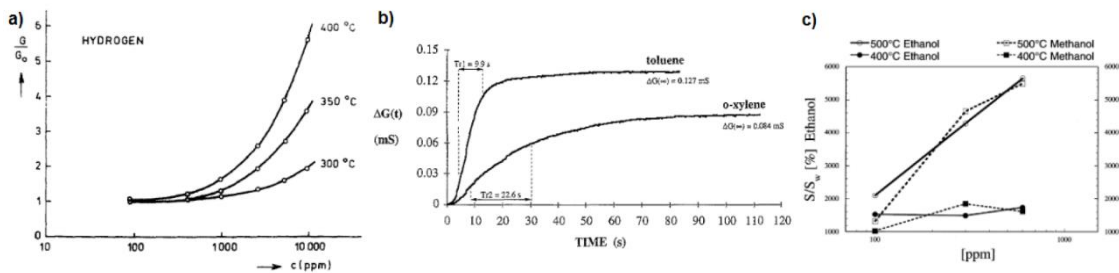


**Figure 4** (a) Response as function of hydrogen concentration (ppm) for the $Fe_2O_3$ sensor at different operative temperature [11]; (b) in time response for the $SnO_2$ sensors array [12]; (c) response as function of ethanol and methanol concentration (ppm) for the $TiO_2$ sensor at different operative temperature [13].

GPL has characterized by a boiling point lower than room temperature. It is heavier than air, unlike natural gas, and thus it flows along floors and tend to settle in low spots, such as basements. GPL results very dangerous for two reasons: the first is the risk of explosion if the mixture of gas and air is within the explosive limits and there is an ignition source; the second is suffocation due to gas displacing air, causing a decrease in oxygen concentration.

For these reasons, great efforts are done to obtain sensible and selective GPL sensors. At now, commercial GPL sensors are based on metal oxide semiconductor, in particular: pure oxides (e.g. ZnO [14], $SnO_2$ [15], $Fe_2O_3$ [16]), mixed oxides (e.g. $NiFe_2O_4$ [17]) and heterojunctions [18]. In 2011, *Chaisitsak et al.* [15] have developed a GPL sensor based

on SnO$_2$ layers doped with F: as shown in Fig. 5, operative temperature is a critical parameter in device sensing performance.
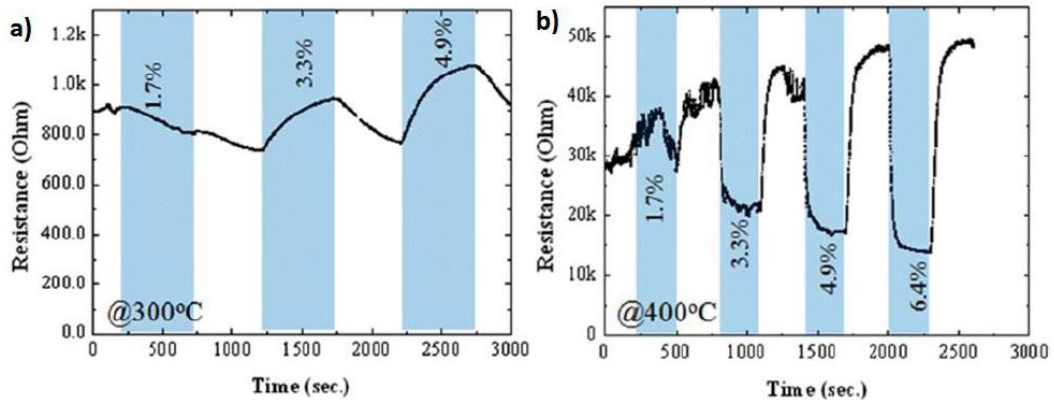


**Figure 5** Resistance variation as function of time for SnO$_2$:F sensor, in presence of either pure N$_2$ or N$_2$/GPL mixture, at (a) 300°C and (b) 400°C. [15]

Although GPL sensors are generally realized using planar architecture (the sensing meaurand is the electrical conductibility variation), some researchers have proposed to develop sensors using optical fibers. An example is the work of *Abdelghani et al.* [16], who have coated optical fibers with porous silica (realized with a sol-gel method). Results are shown in Fig. 6, and it is evident the sensor ability to discriminate between chlorinated hydrocarbons and alkanes (main components in GPL). The firsts have higher RI than the optical fiber cladding (n$^{clad}$ = 1.4), while the seconds are characterized by a lower RI, and that justify the selectivity of the sensor.
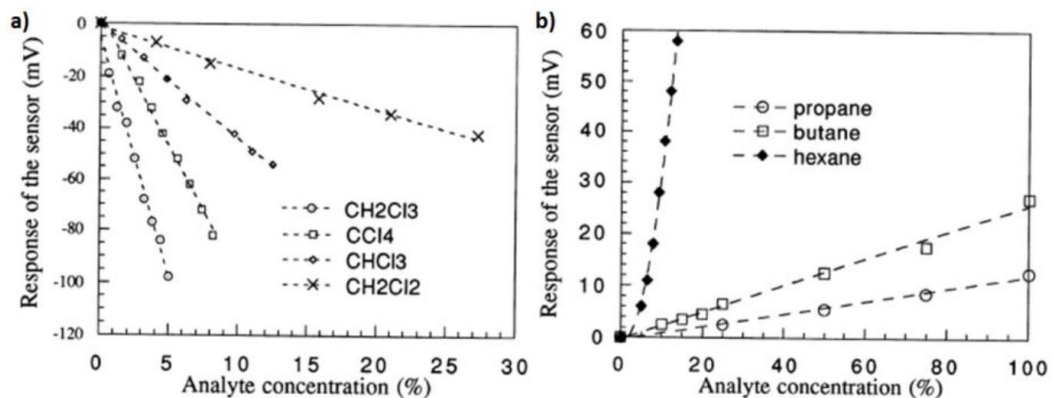


**Figure 6** Response as function of analyte concentration; analyte is: (a) chlorinated hydrocarbons and (b) alkanes. [16]

## 2.2 Humidity sensors

Humidity and temperature are among the most frequently measured physical quantities in measurement science. Whereas the measurement of temperature can nowadays be done with a satisfactory accuracy, measurement of the water vapor content of gaseous atmospheres, i.e. hygrometry, appears much more complex. Water vapor is a natural component of air, and it plays an important role in a wide and various range of practical measurement situations. Today, different humidity sensors exist for miscellaneous applications [19, 20]. Recent achievements in miniaturization have certainly encouraged the development of miniaturized humidity sensors. Today, roughly 75% of the humidity sensors in commerce are based on the capacitive technique [21]. There are, on the other hand, multitudes of other hygrometers based on different transducing techniques, such as gravimetric and optical techniques.
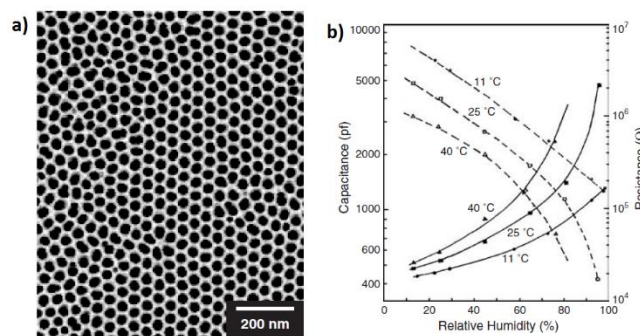


**Figure 7** a) Honeycomb structure of AAO [22]; b) Capacitance (—) and resistance (- - - -) response of the Al2O3 sensor to RH at 11°C, 25°C, and 40°C [23].

Capacitive sensors are based on dielectric changes of thin films in presence of water vapors. $Al_2O_3$ is one of the most favorable ceramic sensing materials due to its negligible dependence of temperature at nearly all range of RH from 25°C to 80°C [24]. The small pore radius makes $Al_2O_3$ sensitive to very low water vapor pressure. The discovery of the AAO sensibility toward humidity dates back to 1950, but it was practically employed only in 1978, when researcher discover that it could form regular microstructure [25]. Low voltage anodization at certain conditions in acidic electrolyte solution forms $Al_2O_3$

layer consisting of hexagonal closepacked cylindrical pores perpendicular to the metal surface (Fig. 7.a). Figure 7.b shows the electrical characteristics of the $Al_2O_3$ sensors versus RH at various temperatures [23].

$TiO_2$ has three phases: anatase, rutile, and brookite. The third one is seldom used in humidity sensing. When heated strongly ($\sim$1000°C), anatase automatically transforms to the rutile structure. Rutile is the most common phase of $TiO_2$, while anatase is very rare in nature. For humidity sensing applications, anatase $TiO_2$ are usually made by sol–gel method. The sintering must be at low temperatures (e.g., <500°C) for short time. Otherwise, $TiO_2$ may be turned into rutile. Due to its higher water adsorption capacity, anatase is a preferred humidity sensing material. However, most $TiO_2$-based sensors are not sensitive at low humidity levels and have limited detection ranges from 10 to 30%RH [26, 27]. A newly developed TiO2 nanowire/Nafion composite sensor is capable to detect RH levels between 12 and 98%RH (Fig. 8), with low hysteresis and good stability [28].
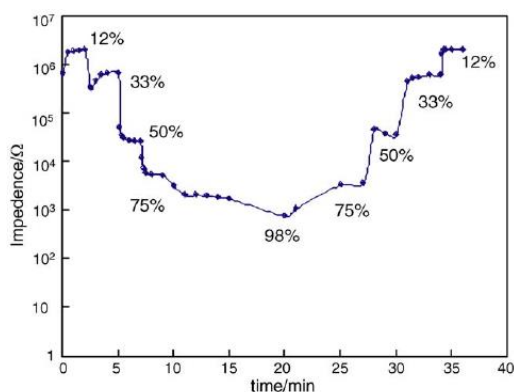


**Figure 8** Humidity response curve of $TiO_2$nanowires/Nafion. [28]

The most widely known gravimetric humidity sensor is the QCM. Thin plates of pietzoelectric quartz have resonance frequencies in the MHz- range. Coated with a hygroscopic layer, the change of frequency acts as a measure of the humidity. In 2009, a novel humidity sensor was fabricated by electrospinning deposition of nanofibrous polyelectrolyte membranes as sensitive coatings on a quartz crystal microbalance (QCM). The results of sensing experiments indicated that the response of the sensors increased by

more than two orders of magnitude with increasing RH from 6 to 95%RH (Fig. 9.a) at room temperature, exhibiting high sensitivity, and that, in the range of 20–95% RH, the Log($\Delta f$) showed good linearity (Fig. 9.b) [29].
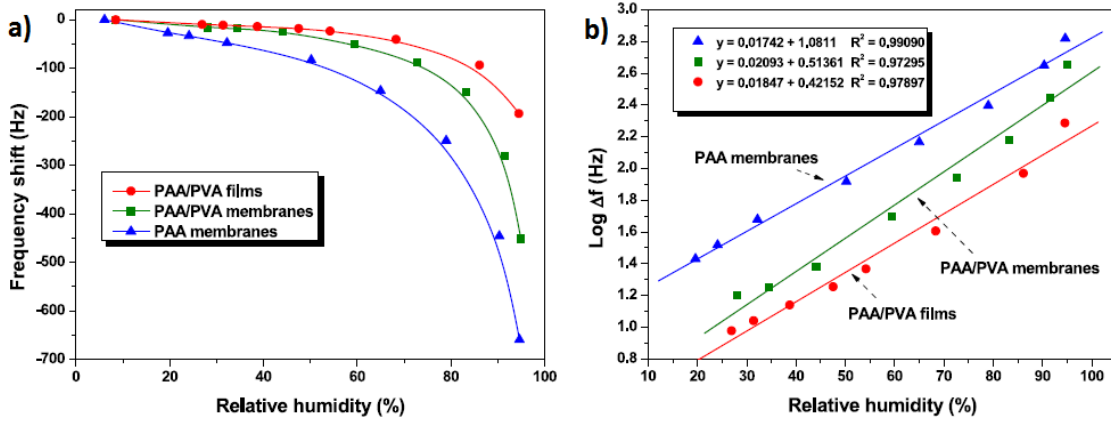


**Figure 9** a) Frequency shifts of polyelectrolyte coated QCM humidity sensors as a function of the RH. b) The dependence of the frequency shifts of sensors on RH (20–95%) and the calibration curves obtained from (a). [29]

All the sensors discussed so far, are generally not suitable to be employed in an environment of a potentially hazardous or explosive nature and also in situations where requirements such as immunity to electromagnetic interference, multi sensor operation, in situ and remote monitoring are, for example, required. Fiber optics offers a new approach to this new measurement problem. The fiber grating sensor represents a class of intrinsic fiber optic sensor that has gained widespread popularity in recent years and, as previously stated, they are generally classified into two main categories, i.e. FBG and LPG.

As an example, work reported by *Yeo et al.* [30] demonstrates the applicability of polymer-coated FBG as humidity sensors. The swelling of the polyimide coating as a result of the moisture absorption changes the Bragg wavelength of the FBG, thus giving a direct indication of the humidity level. The results obtained are plotted in Fig. 10, showing the Bragg wavelength shift of the PI-coated sensors with different coating thickness used. For each, the RH response of the sensors was found to be linear with increasing RH from 23 to 97%RH.
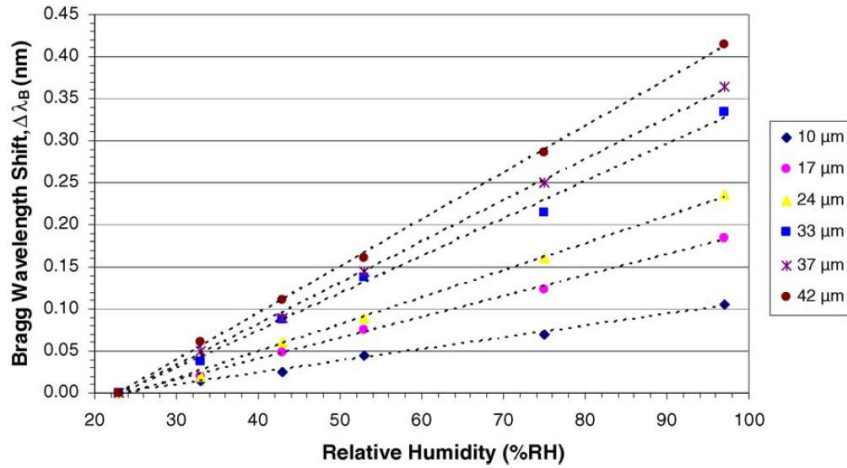
**Figure 10** RH response of the sensors with different coating thicknesses from 23 to 97%RH at constant room temperature. [30]

Recent studies by *Venugopalan et al.* [31] have shown the use of polyvinyl alcohol (PVA) film as a sensing material for LPG-based humidity detection. In this work, a ~4μm thick PVA layer was deposited onto the grating of an LPG with a 300μm period. The sensor was evaluated over a relative humidity range from 33 to 97% using the resonance loss band at 1500 nm where the change in transmission dip was monitored and calibrated against humidity change. The results are shown in Fig. 11: the change of the spectral characteristics of the sensor with %RH leads to the calibration graph of resonance loss vs. %RH.
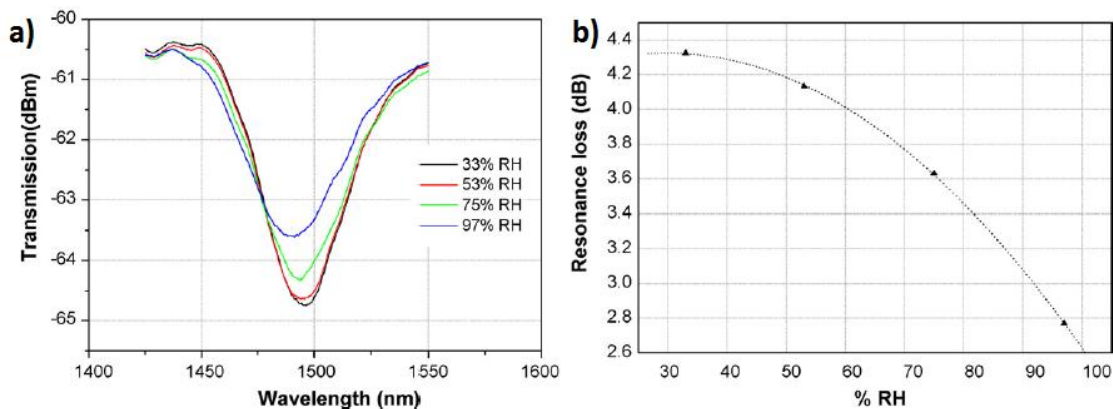


**Figure 11** a) Spectral characteristics of PVA-coated LPG at 1500 nm. b) Transmission dip variation at various RH levels [31].

## 2.3   Biosensors

A biosensor is a device for the detection of an analyte that combines a biological component with a physicochemical detector component. It consists of 3 parts (see Fig. 12):

- A sensitive biological element (a biological material, e.g. tissue, microorganisms, organelles, cell receptors, enzymes, antibodies, nucleic acids, etc.);

- A transducer or the detector element (optical, piezoelectric, electrochemical, etc.) that transforms the measurand variation, due to the interaction of the analyte with the biological element, into a measurable signal;

- A signal processors that are primarily responsible for the display of the results in a user-friendly way.
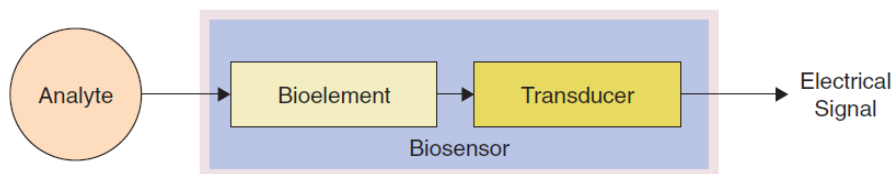


**Figure 12** A schematic representation of biosensors.

A biosensor is any device able to convert the interaction between its surface and a biological element into a readable signal, rejecting any other nonspecific signal.

**Table 1** Elements of a biosensor.

| Biosensors | |
|---|---|
| **Biological element** | **Sensor element** |
| Enzyme | Electric conductivity |
| Antibody | Electromagnetic radiation |
| Nucleic Acid | Mass |
| Tissue | Temperature |
| Microbial | Viscosity |
| Polysaccharide | |

Affinity biosensors are based on interaction between the immobilized biological components on the transducer surface and target molecules. The bioelement is very specific to the analyte to which it is sensitive, and it does not recognize other analytes. Biological elements used in affinity biosensors are for example, antibody, DNA and

receptor protein. A detailed list of different possible bioelements and sensor-elements is shown in table 1. These sensors can provide high sensitivity, selectivity and low detection limit.

Biosensors can have a variety of biomedical, industry, and military applications, as shown in Fig. 14. A major application is in blood glucose sensing because of its abundant market potential. However, biosensors have tremendous potential for commercialization in other fields of application such as biosensor-based instruments in food and beverage production, environmental sampling, and noninvasive instruments for clinical analysis. However, commercial adoption has been slow because of several technological difficulties. For example, due to the presence of biomolecules along with semiconductor materials, biosensor contamination is a major issue.
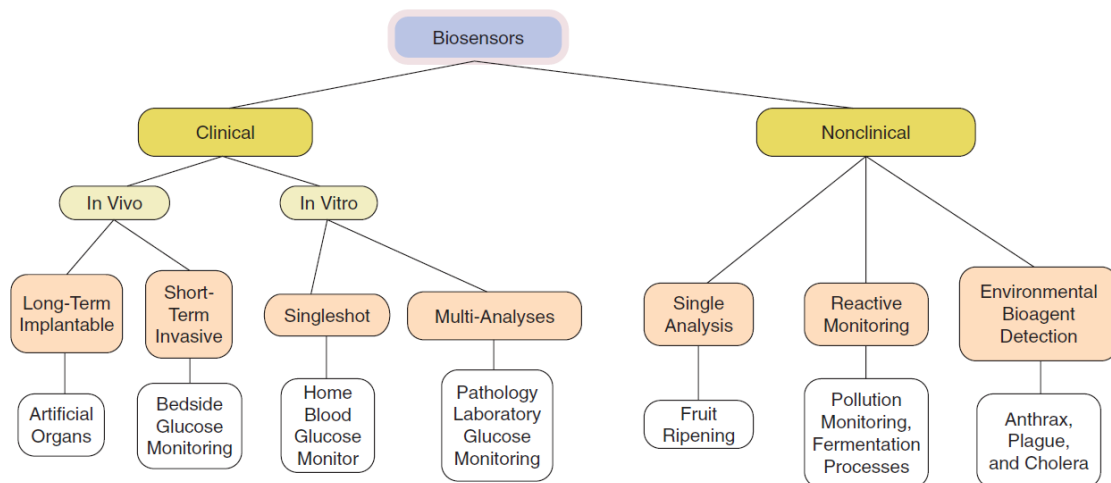


**Figure 13** Biosensors application fields.

The history of biosensors started in 1962 with the development of enzyme electrodes by scientist Clark et al. [32]. Since then, research communities from various fields such as very large scale integration (VLSI), physics, chemistry, and material science have come together to develop more sophisticated, reliable, and mature biosensing devices.

Various types of biosensors being used are enzymebased, tissue-based, immunosensors, DNA biosensors, and thermal and piezoelectric biosensors. *Updike et al.* [33] reported the first enzyme-based sensor in 1967. Enzyme biosensors have been devised on

immobilization methods, i.e. adsorption of enzymes by van der Waals forces, ionic bonding or covalent bonding. The commonly used enzymes for this purpose are oxidoreductases, polyphenol oxidases, peroxidases, and aminooxidases [34].

An enzyme is a large protein molecule that acts as a catalyst in chemical reactions but remains unchanged at the end of the reaction; its working principle is illustrated in Fig. 14.a. An enzyme, upon reaction with a substrate, forms a complex molecule that, under appropriate conditions, forms the desirable product molecule releasing the enzyme at the end. The enzymes are extremely specific in their action: enzyme X will change a specific substance A, to another specific substance B, as illustrated in Fig. 14.b. This extremely specific action of the enzymes is the basis of biosensors.
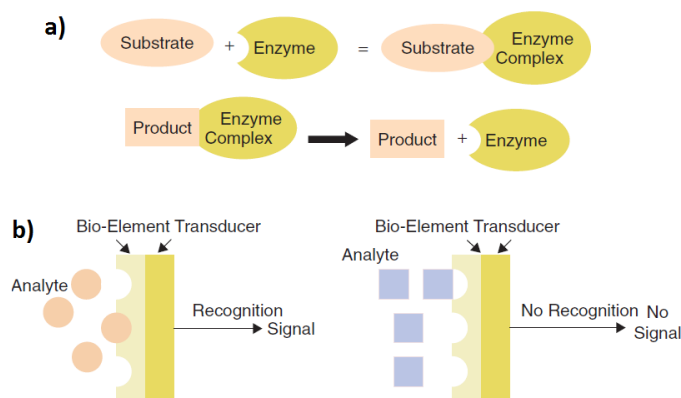


**Figure 14** a) Working principle of enzymes; b) Specificity of enzymes.

The first microbe-based or cell-based sensor was actualized by Diviès et al. [35]. The tissues for tissue-based sensors arise from plant and animal sources. The analyte of interest can be an inhibitor or a substrate of these processes. However, for this type of biosensor, the stability was high, but the detection time was longer, and the specificity was reduced.

Immunosensors were established on the fact that antibodies have high affinity towards their respective antigens, i.e. the antibodies specifically bind to pathogens or toxins, or interact with components of the host's immune system. The DNA biosensors were devised on the property that single-strand nucleic acid molecule is able to recognize and bind to

its complementary strand in a sample. The interaction is due to the formation of stable hydrogen bonds between the two nucleic acid strands [36].

As reported in table 1, there are different types of transducing signals (sensor elements), which define as many types of biosensors. In resonant biosensors, an acoustic wave transducer is coupled with an antibody, or bioelement. When the analyte molecule, or antigen, gets attached to the membrane, the mass of the membrane changes. The resulting change in the mass subsequently changes the resonant frequency of the transducer. This frequency change is then measured.

Since the anthrax spore bioterrorism attacks in America in 2001, the early detection of *Bacillus anthracis* spores and vegetative cells has gained significant interest. In 2008, *Hao et al.* [37] have developed a novel QCM sensors for detection of *Bacillus anthracis*. This biosensor is based on a QCM sensor functionalized with an anti-Bacillus anthracis monoclonal antibody designated to 8G3 (mAb 8G3, IgG). Optimized mAb 8G3 was immobilized onto the Au electrode with protein A on a mixed self-assembled monolayer (SAM) of 11-mercaptoundecanoic acid (11-MUA) and 6-mercaptohexan-1-ol (6-MHO) as adhesive layer. The schematic illustration of mAb functionalized QCM sensor is depicted in Fig. 15.
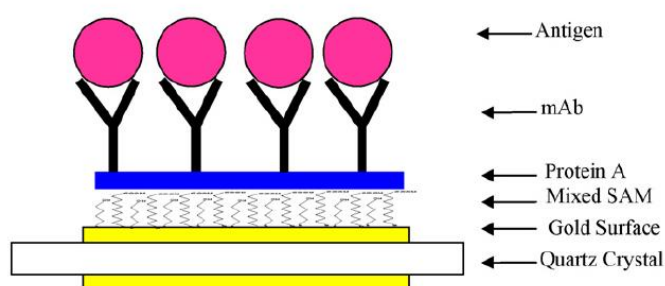


**Figure 15** Schematic illustration of mAb functionalized QCM sensor. [37]

In Fig. 16 is shown the response of the QCM biosensor to a range of concentrations of *Bacillus anthracis* vegetative cells, from $7 \times 10^2$ to $7 \times 10^8$ CFU/ml, and their calibration curve in log–log plot. It was shown that the frequency shift of the QCM biosensor increased, along with the concentration of *Bacillus anthracis* vegetative cells.
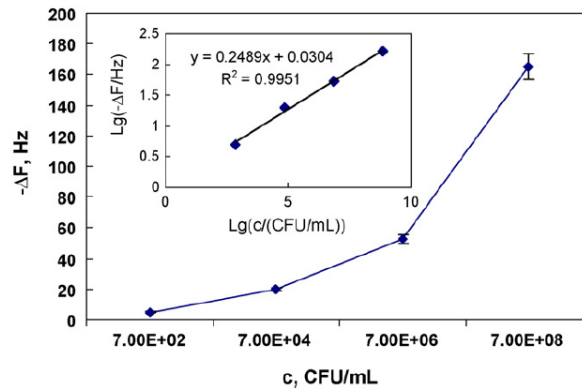
**Figure 16** Changes of frequencies of mAb functionalized QCM biosensor response to *Bacillus anthracis* vegetative cells in range of concentrations. [37]

Another wide class of biosensors is based on the optical fibers: fibers are a convenient material for optical sensor design because they can be inexpensive and provide easy and efficient signal delivery. LPGs, have attracted a great deal of attention in recent years for biochemical sensing applications although the advantages of LPGs have been known since the early 1990's. The earliest demonstration of biomolecule detection with LPGs was in 2000, when etched LPGs were used to detect antibodies [38], where goat anti-human IgG antibodies were linked to the fiber surface with glutaraldehyde and were then used to detect aqueous human IgG. These results showed repeatable detection down to 2µg/mL with a dynamic range of 2–100µg/mL.
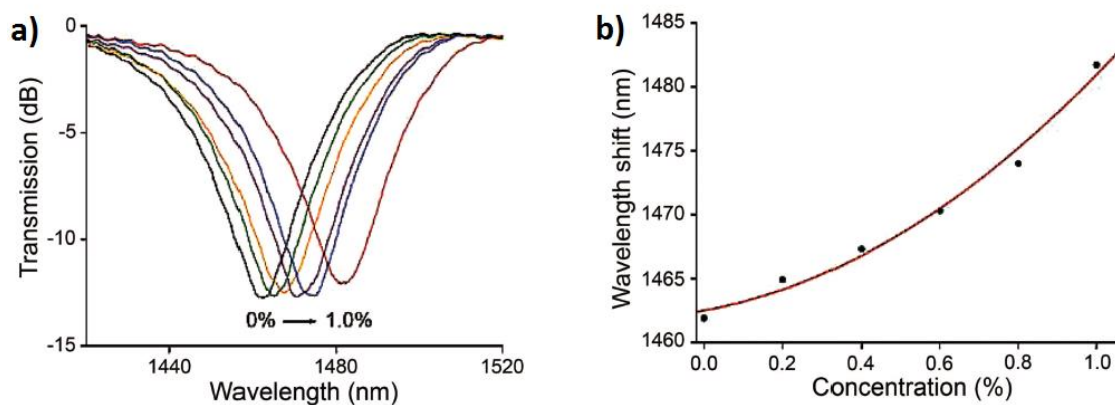


**Figure 17** a) Spectral evolution of LPG resonance peak with different hemoglobin concentrations; b) wavelength shifts against hemoglobin concentration. [39]

In 2007, *Chen et al.* [39] were able to use etched LPGs for detection of hemoglobin. In this work, the hemoglobin was allowed to adsorb non-specifically, yielding an estimated DL of around 0.005% for hemoglobin in water. Fig. 17.a shows the spectra of the

21

resonance peak under different solutions, and Fig. 17.b plots its central wavelength shift against the hemoglobin concentration.

In 2016, Yin et al. [40] have developed an highly sensitive glucose microfluidic chip integrated with specialty optical fiber LPG sensor (inscribed in a small-diameter single-mode fiber). A layer-by-layer self-assembly technique has been successfully applied to prepare PEI/PAA multilayers on the surface of the LPG sensor. The negatively charged GOD layer was then immobilized on the multilayer film for glucose sensing (Fig. 18).
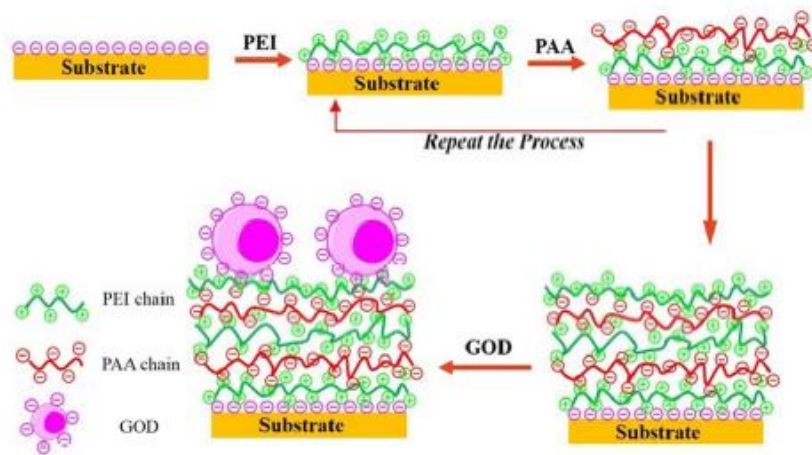


**Figure 18** The layer-by-layer self-assembly scheme for the preparation of multilayer sensing film. [40]
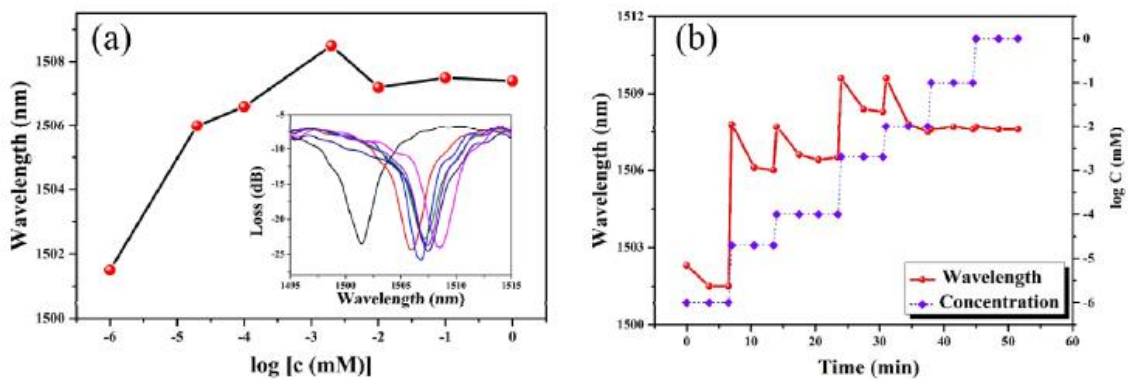


**Figure 20** (a) Response of the SDSMF-LPG biosensor to different glucose concentrations. The inset shows the measured transmission spectra; (b) the measured dynamic response of the biosensor. [40]

When the glucose is oxidized with the GOD catalyst, gluconic acid will be produced, and the pH of mixture solution changes with it. Since the swelling degree of the $(PEI/PAA)_n$ multilayer sensing film depends on the pH of surrounding medium, the sensing film will

22

swell with glucose concentration increasing and the induced RI change leads to a spectra shift of the LPG sensor [41, 42].

The fabricated glucose biosensors were tested in glucose solutions with different concentrations. Fig. 20.a shows the response of the LPG (with $(PEI/PAA)_9(PEI/GOD)_1$ multilayer film) to different glucose concentrations. It can be seen that the resonant wavelength shifts to longer values when the concentration of glucose increases, in accordance with the previous explanation. The spectral dip stops red shift when the glucose concentration increases to 2 μM. It is mainly because that the pH no longer changes after reacting for a specific period of time. The dynamic response of the LPG sensor is shown in Fig. 20.b, and two aspect are evident: 1) the *response time* is about 6 mins (time needed by the sensor to reach a stable signal); 2) the *detection limit* is 1 nM.

# References

[1] Y. Wang, M.M. Tong, D. Zhang. *Sensors*, **11**, 19–31 (2011).

[2] R. Frodl, T. Tille. *IEEE Sens. J*., **6**, 1697–1705 (2006).

[3] J. Qu, Y. Chai, S.X. Yang. *Sensors*, **9**, 895–908 (2009).

[4] E. Cordos, L. Ferenczi, S. Cadar. *In Proceedings of 2006 IEEE International Conference on Automation, Quality and Testing, Robotics*, pp. 208–211, Romania, 25–28 May 2006.

[5] G.F. Fine, L.M. Cavanagh, A. Afonja. *Sensors*, **10**, 5469–5502 (2010).

[6] X. Liu, S. Cheng, H. Liu. *Sensors*, **12**, 9635-9665 (2012).

[7] L. Byoungho. *Optical Fiber Technology*, **9**, 57–79 (2003).

[8] K.O. Hill, Y. Fujii, D.C. Johnson. *Appl. Phys. Lett.*, **32**, 647–649 (1978).

[9] G. Meltz, W.W. Morey. *Opt. Lett.*, **14**, 823–825 (1989).

[10] N. D. Rees, S. W. James, R. P. Tatam. *Opt. Lett.*, **27**, 686 (2002).

[11] K. Siroky, J. Jiresova, L. Hudec. *Thin Solid Films*, **245**, 211-214 (1994).

[12] E. Llobet, J. Brezmes, X. Vilanova. *Sensors and Actuator B*, **41**, 13-21 (1997).

[13] C. Garzella, E. Comini, E. Tempesti. *Sensors and Actuators B*, **68**, 189–196 (2000).

[14] P. Mitra, A.P. Chatterjee, H.S. Maiti. *Materials Letters*, **35**, 33–38 (1998).

[15] S. Chaisitsak. *Sensors*, *11*, 7127-7140 (2011).

[16] D. Patil, V. Patil, P. Patil. *Sensors and Actuators B,* **152**, 299–306 (2011).

[17] L. Satyanarayana, K.M. Reddya, S.V. Manorama. *Materials Chemistry and Physics*, **82**, 21–26 (2003).

[18] D.S. Dhawale, R.R. Salunkhe, U.M. Patil. *Sensors and Actuators B,* **134**, 988–992 (2008).

[19] Y. Ma, S. Ma, W. Fang. *Sensors and Actuators A*, **49**, 47-50 (1995).

[20] V. Matko, D. Donlagic. S*ensors and Actuators A*, **61**, 331-334 (1997).

[21] G. Scholz. *Technisches Messen*, **59**, 88-109 (1992).

[22] Z. Chen, C. Lu. *Sensors Letters*, **3**, 274-295 (2005).

[23] Z. Chen, M.-C. Jin. *in Proc. 27th Annual Conf. IEEE Industry Appl. Soc.*, **2**, pp. 1668, Houston(TX), 1992.

[24] S. Chakraborty, K. Nemoto, K. Hara. *Smart Materials and Structure*, **8**, 274 (1999).

[25] G. E. Thompson, R. C. Furneaux, G. C. Wood. *Nature*, **272**, 433 (1978).

[26] L.L. Chow, M.M.F. Yuen, P.C.H. Chan. S*ensors and Actuators B*, **76**, 310 (2001).

[27] M.K. Jain, M.C. Bhatnagar, G.L. Sharma. S*ensors and Actuators B*, **55**, 180 (1999).

[28] R. Wu, Y. Sun, C. Lin. *Sensors and Actuators B*, **115**, 198-204 (2006).

[29] X. Wang, B. Ding, J. Yu. *Nanotechnology*, **21**, 55502-55508 (2010).

[30] T.L. Yeo, T. Suna, K.T.V. Grattan. *Sensors and Actuators B*, **110**, 148–155 (2005).

[31] T. Venugopalan, T.L. Yeo, T. Sun. *In Proceedings Third European Workshop on Optical Fibre Sensors*, **6619**, pp. 661925-1–661925-4, Naples (Italy) (2007).

[32] L.C. Clark, C. Lyons. *Annals New York Academy of Sciences*, **102**, 29-45 (1962).

[33] S.J. Updike, G.P. Hicks. *Nature*, **214**, 986-988 (1967).

[34] J. Wang. *Chem. Rev.*, **108** (2), 814-825 (2008).

[35] C. Diviès. *Ann Microbiol.*, **126A**, 175-186 (1975).

[36] J. Wang. *Biosensors and Bioelectronics*, **13**(7-8), 757-762 (1998).

[37] R. Hao, D. Wang, X. Zhang. *Biosensors and Bioelectronics*, **24**, 1330–1335 (2009).

[38] M.P. DeLisa, Z. Zhang, M. Shiloach. *Anal. Chem.*, **72**, 2895 (2000).

[39] X. Chen, K. Zhou, L. Zhang. *Appl. Opt.*, **46**, 451 (2007).

[40] M. Yin, B. Huang, S. Gao. *Biomedical Optics Express*, **7**(5), 2067-2077 (2016)

[41] M.J. Yin, B.B. Gu, J.W. Qian. *Anal. Methods*, **4**(5), 1292-1297 (2012).

[42] I. Tokarev, I. Tokareva, V. Gopishetty. *Adv. Mater.*, **22**(12), 1412–1416 (2010).

# 3.   Long Period Gratings

## 3.1   Principle of Operation

Long Period Fiber Gratings are photonic devices realized by inducing a periodic refractive index modulation ($\Lambda$=100-500 μm) of the core of a single mode optical fiber along few centimeters (L=2-3 cm) of its length [1]. This periodic perturbation makes possible the power transfer from the fundamental guided core mode to a discrete number of forward propagating cladding modes and to each of them at a distinct wavelength where the so-called phase matching condition is satisfied:

$$\lambda_{res,0i} = (n_{eff,co} - n_{eff}{}^{0i}{}_{,cl}) \cdot \Lambda \qquad \text{(eq. 1)}$$

where $n_{eff,co}$ and $n_{eff}{}^{0i}{}_{,cl}$ are the core and i[th] cladding mode effective indices respectively, $\Lambda$ is the grating period (see Fig. 1.a). As a result of this process, referred to as mode coupling, the LPG transmission spectrum shows several attenuation bands or dips related to the different excited optical fields: the cladding modes (see Fig. 1.b). LPGs are sensitive to a number of environmental parameters (temperature, strain, bending, ambient refractive index) which affect the phase matching condition changing, in turn, the attenuation bands spectral position [2]. However, appropriate simple countermeasures can be used to minimize the effect of the parameters not of interest.
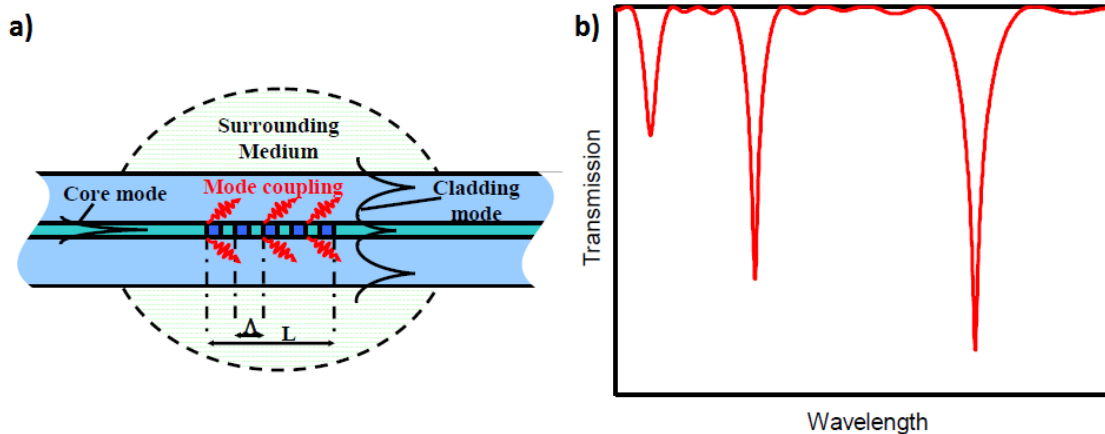


**Figure 1** a) Pictorial description of mode coupling in LPGs; b) typical LPG transmission spectrum.

The dependence of LPGs spectral features on SRI changes is what makes them very attractive for chemical and biomolecular sensing applications [3, 4]. However bare LPGs show the highest sensitivity for SRIs close to cladding refractive index (approx. 1.45), while they have poor performance in gaseous and watery environments [5]. Moreover they lack any chemical selectivity.

The influence of SRI changes for a bare LPG is expressed by:

$$\frac{d\lambda_{res,0i}}{dn_{sur}} = \frac{d\lambda_{res,0i}}{dn_{eff,cl}^{0i}} \frac{dn_{eff,cl}^{0i}}{dn_{sur}} \qquad \text{(eq. 2)}$$

where $n_{sur}$ is the refractive index of the external medium. The factor $dn_{eff,cl}^{0i}/dn_{sur}$ is different for each cladding mode, and hence, the spectral response of an LPG depends strongly on the order of the coupled cladding mode. The higher sensitivity is shown by the higher order modes and, as stated previously, it occurs at refractive indexes approaching that of the cladding. For a given cladding mode, the wavelength shift resulted from the refractive index changes may be positive or negative depending on the local slope of the phase matching curve $d\lambda/d\Lambda$, where for low order modes, it is typically negative. Although it is possible to enhance the sensitivity of an LPG by manipulating the fiber parameters to obtain the appropriate order of the coupled cladding mode, however, it is not possible to provide chemical selectivity with a bare LPG.

It was recently demonstrated that the sensitivity of LPGs can be greatly enhanced by the deposition of a thin overlay onto the cladding along the grating region, provided that the overlay has higher refractive index than the cladding [6]. Moreover the sensitivity can be optimized for a specific working environment by acting on thickness (ranging in hundreds of nanometers) of the high RI layer which is in contact with the surface of the LPG itself. Therefore, the deposition of thin high RI overlay of suitable thickness allows the enhancement and optimization of the device sensitivity against SRI changes and parametrical variations of the overlay features (RI and thickness). In addition, if the

overlay is made of a material able to respond to chemical/physical stimuli, the coated LPG can operate as an extremely sensitive sensor.

When a thin high RI overlay is deposited onto a LPG the effective index of the cladding modes increases and, as it follows from eq. 1, the attenuation bands experience a blue shift (see Fig. 2). By increasing the overlay thickness the attenuation bands move from their initial position toward that initially occupied by the adjacent cladding mode of lower order and this migration follows a transition function trend (see Fig. 3) [7].
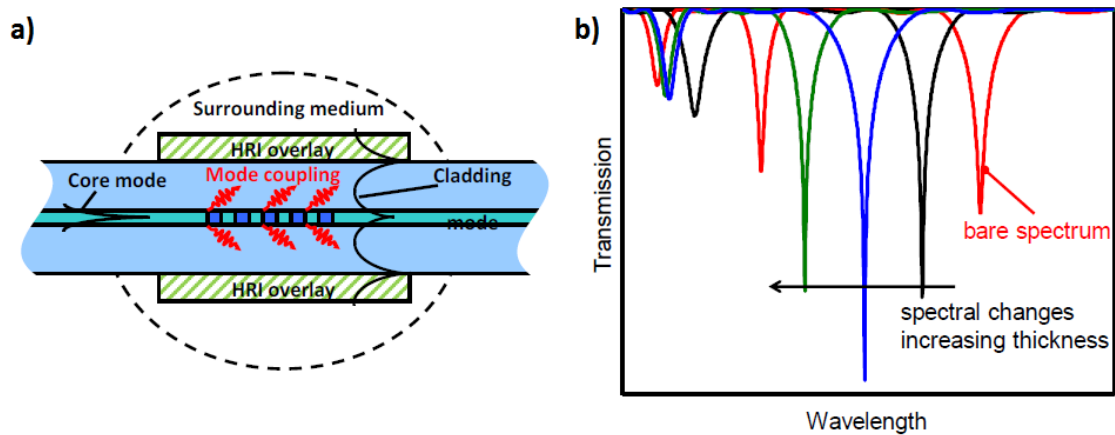


**Figure 2** a) Sketch of a LPG coated with a high RI overlayer; b) spectral changes against an increasing overlayer thickness.

When the attenuation bands of the coated LPG are tuned at the center of the spectral separation of two consecutive attenuation bands as defined by the original bare device then the device is working in the transition region or in transition mode. A LPG working in transition mode has the highest sensitivity to parametrical variations of the overlay (thickness and RI) and to the SRI changes (see Fig. 3.b). From the physical point of view, the high RI overlay draws the optical field towards the external medium extending its evanescent wave. As a result, there is an increased sensitivity of the device to the SRI changes. At the same time, an increasing evanescent wave in the surrounding medium corresponds to an increasing optical power fraction confined in the overlay.

Therefore, the sensitivity to the refractive index changes of the high RI overlay is even bigger than that to the SRI changes. High RI coated LPGs have been successfully

exploited for chemical and biomolecular sensing applications and are expected to become a key technology in the sensing field within the next few years [8-10].
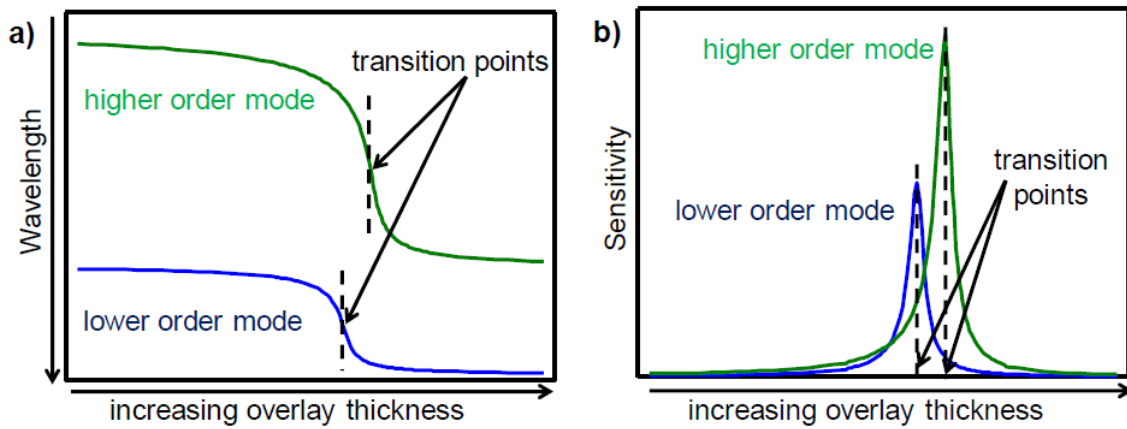


**Figure 3** a) Conceptual plot explaining the wavelength shift of the attenuation bands as function of the overlay thickness of a fixed SRI and given material; b) sensitivity trend as a function of the overlay thickness.
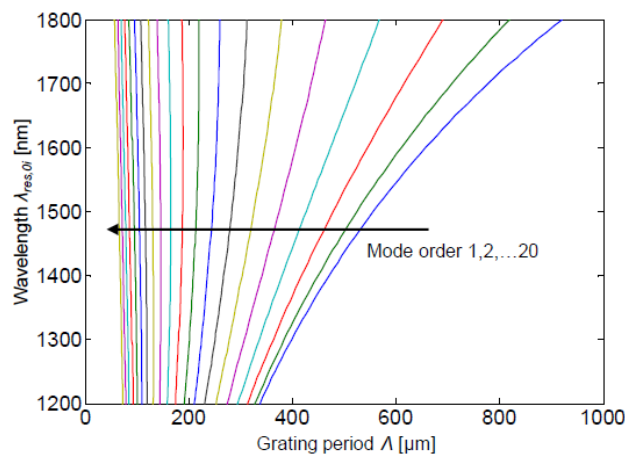


**Figure 4** Modal dispersion diagram for the first 20 cladding modes.

Figure 4 shows the so called modal dispersion diagram for the cladding modes, relative to a generic optical fiber. Each curve in the plot is related to a different cladding mode and the mode order increases moving from right to left in the plot, in particular the dispersion curves for the first 20 cladding modes is reported. The wavelength range reported on the y-axis is 1200-1800 nm that is the common wavelength range for optical spectrum analyzers (OSA). These curves are the result of a complex numerical processing, obtained solving the coupled mode equation that is a system of differential equations derived by the coupled mode theory [11].

This plot is useful to determine the central wavelengths of the attenuation bands present in the transmission spectrum, and to which cladding mode they are related, given a specific grating period. As an example, in Fig. 5 it is reported the same modal dispersion diagram with a vertical line corresponding to a period $\Lambda$=400 μm. This line intercepts the modal curves of the first 5 cladding modes at the wavelengths 1302.8 nm, 1325.9 nm, 1369.6 nm, 1444.3 nm, 1581 nm respectively.
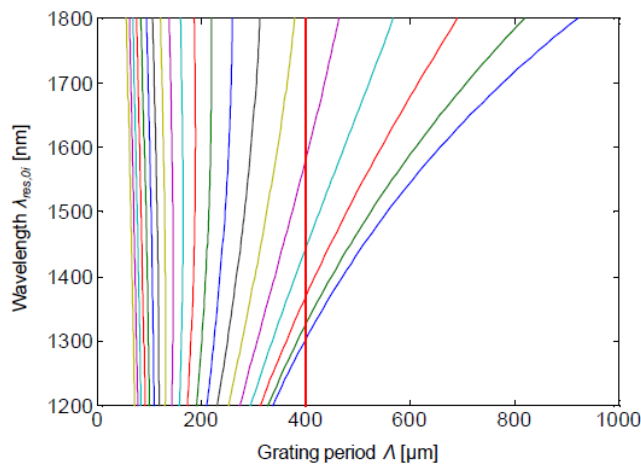


**Figure 5** Modal dispersion diagram with intercept at 400 μm period.

The complete solution of the coupled mode equations for the device under consideration leads to the spectral features reported in Fig. 6.
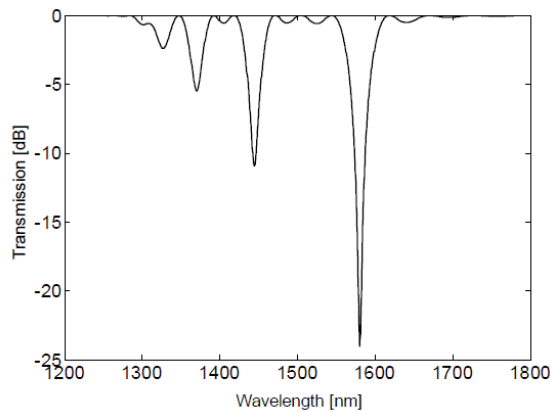


**Figure 6** Transmission spectrum for a LPG with grating period at 400 μm.

## 3.2 LPGs Typologies

The fabrication of LPGs relies upon the introduction of a periodic modulation of the optical properties of the fiber. This may be achieved by permanent modification of the refractive index of the core of the optical fiber or by physical deformation of the fiber.

### 3.2.1 UV-Induced LPGs

LPG fabrication method based on UV radiation is the most common approach for grating fabrication and thus most of the results reported in literature are referred to this type of fabrication. The UV-induced index modulation is typically achieved in Ge-doped silica fibers using wavelengths between 193 and 266 nm [12]. This is the most widely utilized method for the fabrication of LPGs. The refractive index change is associated with the formation of Ge-related glass defects. Fibers with high photosensitivity have been developed by co-doping the core with boron and germanium [13]. The refractive index modulation may be built up on a point-by-point basis, or the entire length of the LPG may be formed simultaneously by exposure of the fiber though an amplitude mask [14], via a patterned mirror [15] or using a microlens array [16], facilitating rapid and reproducible LPG fabrication.
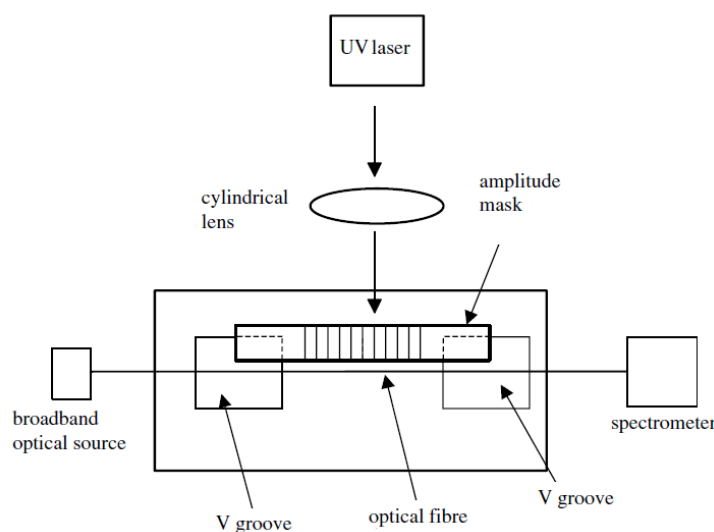


**Figure 7** LPG fabrication using a UV laser. [17]

A typical LPG fabrication configuration, using UV irradiation through an amplitude mask, is shown in figure 7. The output from a UV laser source is used to illuminate the optical fiber through an amplitude mask of appropriate period, which may be fabricated in chrome-plated silica or from a metal foil, for example by milling a copper foil using a Cu vapor laser. The cylindrical lens produces a line focus oriented parallel to the axis of the fiber.

## 3.2.2 Arc-Induced LPGs

In LPG fabrication method based on Electric arc discharge, the grating is written by periodical local heating of the fiber using electric arc discharges and by applying lateral stress on a standard fiber: this provides good performances as well as high thermal stability to the LPG [18]. The electrical arc technique is much simpler and does not need expensive laser equipment. Typically, the electrodes of a fusion-splicing machine are used, exposing a region of fiber with a length of the order of 100 μm to the arc, limiting the minimum period of LPG that may be fabricated.
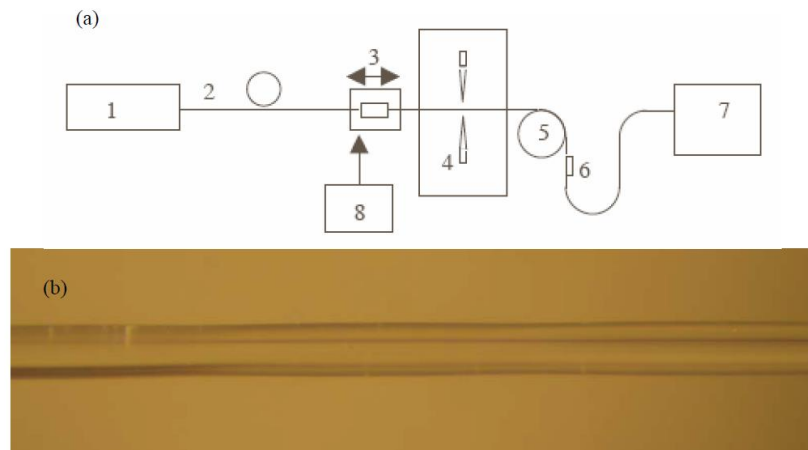


**Figure 8** a) Apparatus for manufacturing of taperd LPG: 1) broadband light source, 2) optical fiber, 3) motorized translation stage, 4) arc-generating electrodes, 5) pulley, 6) weight, 7) optical spectrum analyzer (OSA), 8) computer; b) microscope image of the investigated tapered LPG with Λ=600 μm. [19]

When a tensile load is applied to the fiber, the periodic variation in the diameter of the fibre results in a periodic strain variation across the corrugated structure, with a concomitant periodic refractive index induced via the photoelastic effect. The grating

period in arc-induced LPGs is determined by the moving step of the translation stage (controlled by a computer) and by some other factors such as arc intensity, arc duration time, and pulling weight. A schematic diagram of the fabrication setup is plotted in Fig. 8.

# References

[1] A. M. Vengsarkar, P.J. Lemaire, J.H. Judkins. *J. Lightwave Technol.*, **14**(1), 58-65, (1996).

[2] S.W. James, R.P. Tatam. *Meas. Sci. Technol.*, **14**(5), 49-61 (2003).

[3] R. Falciai, A.G. Mignani, A. Vannini. *Sens. Actuators B*, **74**(1-3), 74-77 (2001).

[4] M.P. DeLisa, Z. Zhang, M. Shiloach. *Anal. Chem.*, **72**(13), 2895-2900 (2000).

[5] H. J. Patrick, A. D. Kersey, F. Bucholtz. *J. Light. Technol.*, **16**(9), 1606-1612 (1998).

[6] A. Cusano, A. Iadicicco, P. Pilla. *Opt. Express*, **14**(1), 19-34, (2006).

[7] A. Cusano, A. Iadicicco, P. Pilla. *Appl. Phys. Lett*, **89**(20), 201116:1-3 (2006).

[8] A. Cusano, A. Iadicicco, P. Pilla. *J. Lightwave Technol.*, **24**(4), 1776-1786 (2006).

[9] A. Cusano, P. Pilla, M. Giordano. *Advanced Photonic Structure for Biological and Chemical Detection*, Ed. X. Fan, pp. 35-75 (Springer, 2009).

[10] P. Pilla, P. Foglia Manzillo, V. Malachovska. *Opt. Express*, **17**(22), 20039-20050 (2009).

[11] T. Erdogan. *J. Opt. Soc. Am.*, **14**(8), 1760-1773 (1997).

[12] R. Kashyap. *Fibre Bragg Gratings* (London: Academic) (1999).

[13] D.L. Williams, B.J. Ainslie, J.R. Armitage. *Electron. Lett.*, **29**, 45-47 (1993).

[14] A.M. Vengsarkar, P.J. Lemaire, J.B. Judkins. *J. Lightwave Technol.*, **14**, 58-64 (1996).

[15] H.J. Patrick, C.G. Askins, R.W. Mcelhanon. *Electron. Lett.*, **33**, 1167-1168 (1997)

[16] S.Y. Lu, H.Y. Tan, M.S. Demokan. *Electron. Lett.*, **35**, 79–80 (1999).

[17] S.W. James, R.P. Tatam. *Meas. Sci. Technol.*, **14**, 49-61 (2003).

[18] G. Rego, O. Okhotnikov, E. Dianov. *Journal Lightwave Technology*, **19**(10), 1574-1579 (2001).

[19] A. Iadicicco, S. Campopiano, A. Cutolo. *International Journal On Smart Sensing And Intelligent Systems*, 1(2), 354-369 (2008).

# 4.   Methods and Instrumentations

## 4.1   LPG reflection probes and optoelectronic set-up

Generally, LPGs are interrogated in transmission configuration, i.e. the light enters from a side of the fiber and come out of the other side. Through the manipulation of the fiber, it is possible to interrogate the LPG in reflection mode, in order to transform an LPG-based device in a more practical probe. As schematically represented in Fig. 1.a, this requires the integration of a selective mirror at the end of the optical fiber. To this aim, the optical fiber inside which the LPG is written has to be properly cut, and the fiber end-face has to be coated by a reflecting metallic layer, acting as a mirror.
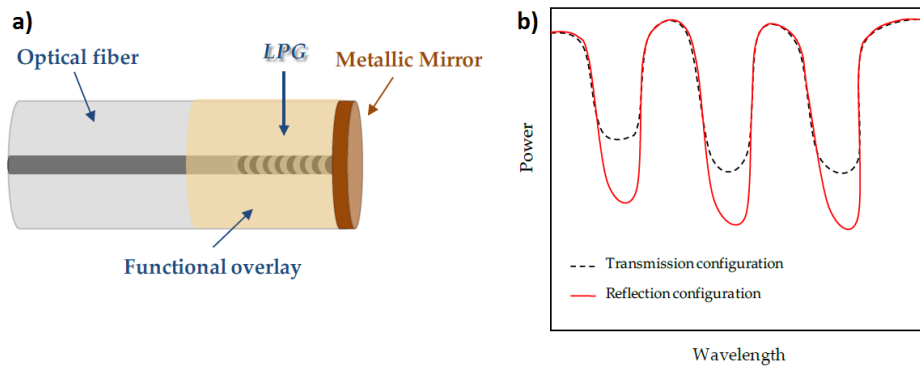


**Figure 1** a) Schematic representation of an LPG working in reflection configuration and b) of the consequent visibility increase in its attenuation bands.

A key aspect in this step relies on the identification of the precise LPG position within the optical fiber, which is of fundamental importance in order to cut the fiber just after the grating. To understand this concern, it must be considered that when the metallic layer is realized on the fiber facet, light passing through the LPG is reflected back and passes through it for the second time. This means that, if the optical fiber containing the LPG is cut immediately after the grating, this will be equivalent to an LPG working in transmission configuration and having a double length, which also leads to the positive implication of an increased resonance visibility, as schematically represented in Fig. 1.b.

Differently, if the optical fiber is not cut just after the grating, but at a distance L from it, the LPG will result in the cascade of two identical LPGs spaced by a distance d=2L. This would lead to the formation of interference fringes within the attenuation bands, similarly to those observed in a Mach–Zehnder interferometer, as schematically illustrated in Fig. 2 [1]. In light of these considerations, a correct identification of the LPG position inside the optical fiber is mandatory.
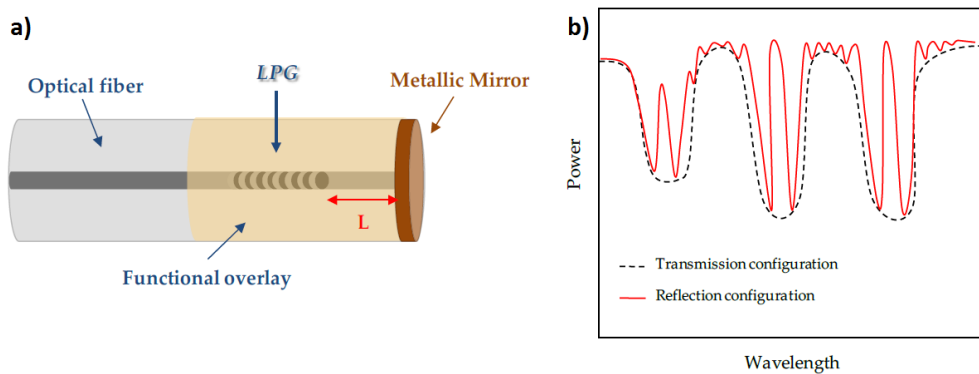


**Figure 2** a) Schematic representation of an LPG working in reflection configuration with the mirror integrated at a distance L from the grating and b) of the consequent interference fringes in the attenuation bands. [2]

After having identified the LPG position, a high precision fiber cleaver (Fujikura CT-30 Series) is used to cut the optical fiber just after the grating, followed by the integration of an Ag reflecting layer (i.e. the mirror) on the terminal face of the cut optical fiber.
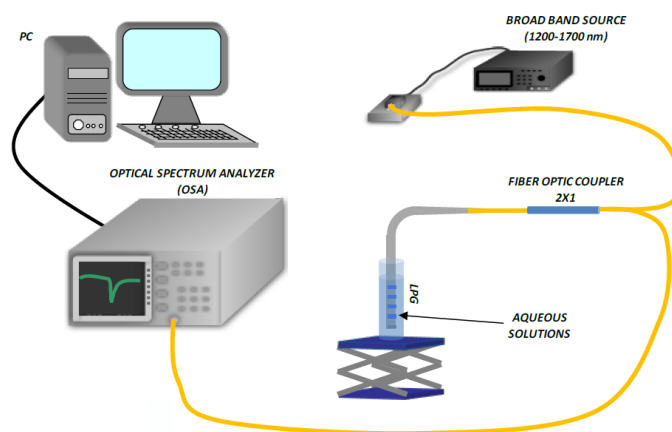


**Figure 3** Schematic of the optoelectronic set-up used for the LPG transducer.

Fig. 3 shows a schematic of the optoelectronic set-up used during the LPG based sensors manufacturing, and for the SRI characterization of the final device. It mainly comprises

a broadband light source (with bandwidth 1200-1700nm), a 2x1 directional coupler and an optical spectrum analyzer connected to a PC.

## 4.2   Silver Mirror Deposition

There are different method to deposit a reflective layer on the tip of the LPG. To this aim, a silver mirror reaction (Tollens' test) was adopted [3]. Tollens' test (or Tollens' reagent) is a chemical reagent used to determine the presence of an aldehyde functional groups in a solution. A positive test with Tollens' reagent is indicated by the precipitation of elemental silver, often producing a characteristic "silver mirror" on the inner surface of the reaction vessel.

Specifically, silver nitrate ($AgNO_3$ 0.1M) was dissolved in aqueous solution of potassium hydroxide (KOH 0.8M); the brown precipitate formed was dissolved in two drops of ammonia ($NH_3$ 30% w/w) with stirring. The $Ag^+$ ions reacted with OH- to produce a brown precipitate of $Ag_2O$, which was dissolved in an excess of aqueous ammonia, forming $[Ag(NH_3)_2]^+$. The resulting silver diamine complex was reduced in dextrose solution (0.25 M) to obtain the metallic silver. Successively the LPG fiber tip was dipped into the Tollens' reagent for about 35 minutes, after which an uniform Ag coating formed on the tip of the optical fiber.
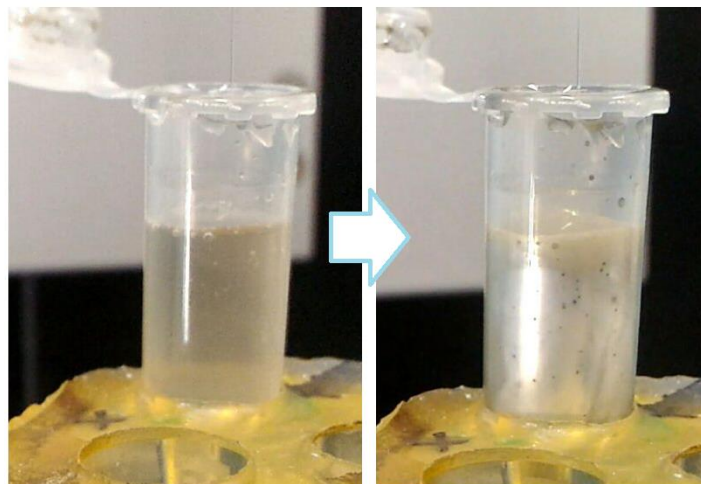


**Figure 4** Mirror formation on the inner surface of the reaction vessel during a Tollens' test.

## 4.3 Dip-Coating Technique

In order to obtain homogeneous and defect-free layers on the optical fiber grating, it was used the dip-coating technique, which provides a substrate to be immersed in a liquid solution and then withdrawn with a well-defined extraction speed under controlled temperature and atmospheric conditions. The steps through which a thin film is deposited onto a substrate by this technique are essentially five: immersion, extraction, wet layer formation, drainage and solvent evaporation. They are schematically reported in Fig. 5. The film thickness depends upon many parameters such as the withdrawal speed, the solid content and the viscosity of the liquid. If the withdrawal speed is chosen such that the shear rates keep the system in the Newtonian regime, then the coating thickness depends upon the aforementioned parameters by the Landau-Levich equation [4]:

$$th \; = \; 0.94 \cdot \frac{(\eta \cdot v)^{2/3}}{\gamma_{LV} \cdot (\rho \cdot g)^{1/6}} \qquad \text{(eq. 1)}$$

where $th$ is the coating thickness, $\eta$ the solution viscosity, $\rho$ the density, $\gamma_{LV}$ the liquid-vapor surface tension, g the gravity and $v$ is the withdrawal speed.
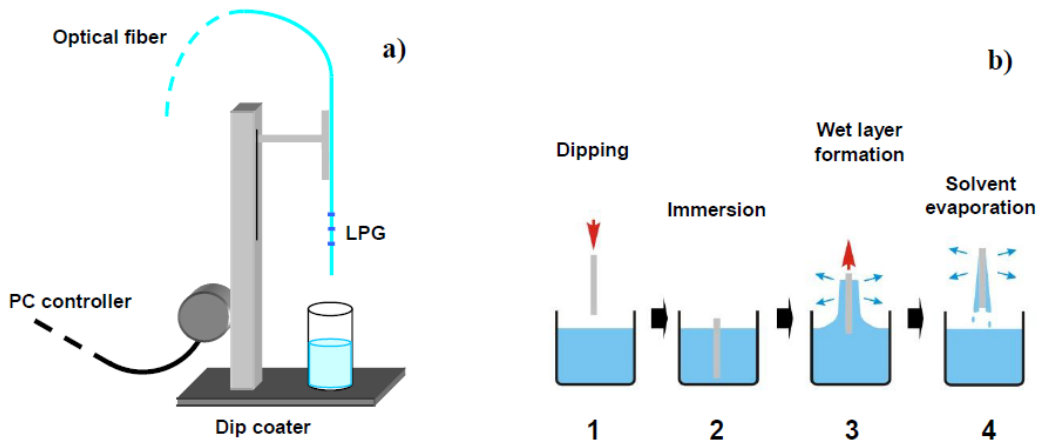


**Figure 5** a) Schematic view of the deposition setup; b) Dip coating process.

This deposition technique is relatively simple and less time consuming compared to electrostatic self-assembly and Langmuir-Blodgett, and has been demonstrated to provide a lower roughness of the layer which in turn determines its higher optical quality [5]. Moreover this technique can be realized with much less expensive equipment than the

sophisticated physical vapor deposition or chemical vapor deposition. A drawback of the technique is the not accurate control of the thickness compared to electrostatic self-assembly or  Langmuir-Blodgett techniques since it depends on too many parameters which are not easily controlled.

# References

[1] P. Pilla, C. Trono, F. Baldini. *Opt. Lett.*, **37**, 4152-4154 (2012).

[2] R.P. Murphy, S.W. James, R.P. Tatam. *Journal of Lightwave Technology*, **25**, 825-829 (2007).

[3] Y. Yin, Z. Li, Z. Zhong. *S. J. Mater. Chem.*, **12**, 522-527 (2002).

[4] L.E. Scriven. *Mater. Res. Soc. Symp. Proc.*, **121**, 717-729 (1988).

[5] I. Del Villar, I.R. Matias, F.J. Arregui. J. *Lightwave Technol.*, **23**, 4192 (2005).

# GAS SENSORS

# 5. GPL sensors based on a-PS coatings

## 5.1 Introduction

In the framework of the OPTOFER project: "Innovative Optoelectronic Technologies for the Monitoring and Diagnostics of Railway Infrastructure" (PON 03PE_00155), it has been developed an optoelectronic device for the detection and monitoring of GPL in railway tunnels.

The present situation of the Italian railway tunnels is characterized by a remarkable heterogeneity in term of typology, building year and management (ordinary and high speed railway network). When a tunnel is designed, it is necessary an accurate study of the possible accident scenarios, as only providing for the risks it is possible to establish an emergency plan.

Besides the obvious risk associated with the derailment, which can start a fire inside the tunnel, another source of danger is the accidental release of hazardous substances, either during the train travel or as a result of an accident. Many of the daily transported substances on rail track can be potentially fatal if dispersed in the environment, especially in a closed environment. Examples are flammable, explosive, radioactive and carcinogenic substances. Gasses are among the most hazardous substances that can be released in a gallery, as they can spread rapidly, can be flammable, explosive and/or toxic and, in the better situation, can be asphyxiating.

Actually, GPL is the most transported hazardous substances in Italy, with a frequency of 6-12 trains per day. The Viareggio train derailment, occurred in 2009, is an example of the GPL transport dangerousness. In this dangerous scenario, it is necessary to have sophisticated monitoring instruments, which must have the following properties: 1) short response time (for an early warning); 2) on-line monitoring (in order to monitor in real

time the gallery status, also during the disaster); 3) integrability with the preexisting warning alarms.

Optical sensing is one of the most suitable technique able to provide these features to a sensor. In this work, different LPGs have been coated with atactic polystyrene in order to develop a novel GPL sensor. This polymer has been chosen for two reason:

1) the chemical affinity between its hydrophobic chains and the short hydrocarbons molecules constituting the GPL;

2) the ability to quickly depositing homogeneous and defect-free films on optical fibers, making the sensor easy to manufacture.

## 5.2 Materials and GPL sensing test set-up

### 5.2.1 Materials

Polystyrene is a synthetic aromatic polymer made from the monomer styrene (Fig. 1). This polymer, with a higher refractive index compared to the cladding one, exhibits high sorption capacity and an improved selectivity toward low molecular weight substances, if compared to other polymers. As a thermoplastic polymer, polystyrene is in a solid (glassy) state at room temperature but flows if heated above about 100 °C, its glass transition temperature.
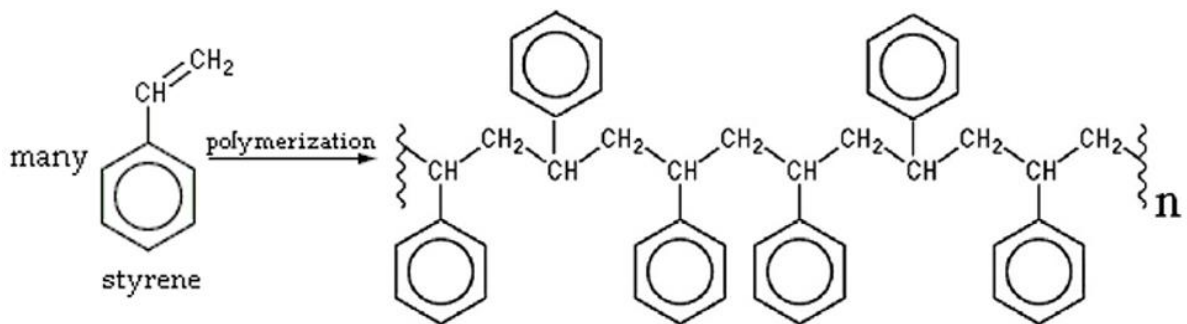


**Figure 1** *(left)* Styrene and *(right)* Polystyrene chemical structure.

Ordinary a-PS is one of the most common plastics in everyday life and it can be deposited on optical fibers in the form of thin films by dip-coating from a solution. The structure of this atactic polymer is shown in Fig. 2. Thin films of polystyrene are an ideal choice from the point of view of the device optical design since they are easily deposited by dip-coating, have excellent optical quality with low losses and have a suitable high refractive index that enables the modal transition [1-3].
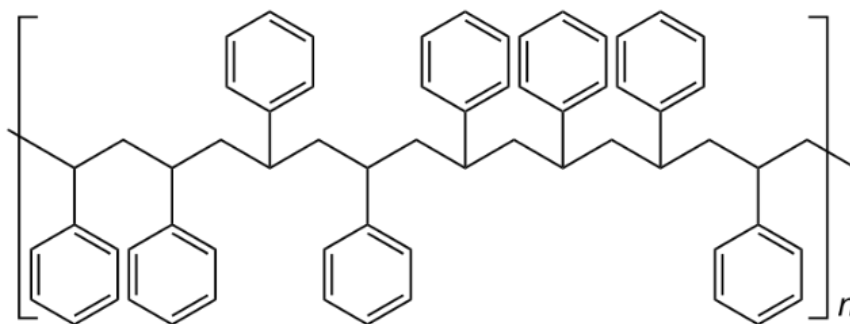


**Figure 2** a-PS chemical structure.

Dip-coating technique was used to deposit thin films of a-PS (Mw = 280,000, Aldrich – RI = 1.555 [4]) onto the grating region of different LPGs.

In the framework of OPTOFER Project two different type of LPGs has been employed: commercial UV-induced LPGs (bought by O/E Land Inc., Canada) and arc-induced LPGs (manufactured by the researchers of the University of Naples Parthenope). These optical devices has been used in reflection mode, and therefore a silver mirror was deposited on the tip of the fiber. The manufactured devices have been tested in presence of butane/nitrogen mixtures at different concentration: butane was chosen as analyte because is the main component of GPL, together with propane.

## 5.2.2 GPL sensing test set-up

In order to obtain the calibration curve of the manufactured devices, i.e. the curve of the optical shift as function of the gas concentration, it is necessary to perform GPL sensing tests with an appropriate set-up. For that purpose, it has been designed and purchased a gas sensing apparatus, schematized in Fig. 3 and showed in Fig. 4.



**Figure 3** (left) frontal and (right) top view of the gas sensing apparatus.
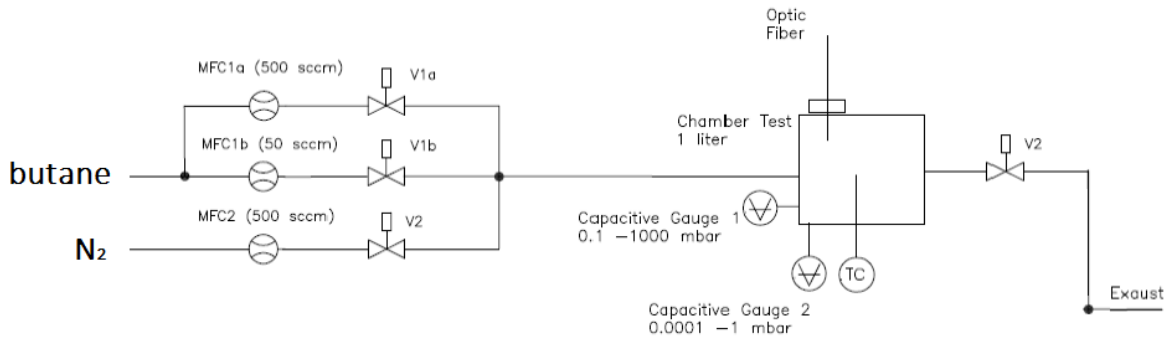
**Figure 4** Gas sensing apparatus project.

Set-up is constituted of two lines and in them flows nitrogen and butane, respectively. In the butane channel flows a mixture of nitrogen and butane, with a 1vol% of butane in nitrogen. The gas flow is tuned using Mass Flow Controller. The line where flows the butane is divided in two sub-lines: the first, that contains a low flow range MFC (50 sppm) and the second, that contains an high flow range MFC (500 sppm).

Using MFC it is possible to evaluate the gas concentration (expressed in ppm) which enter in the test chamber. A software has been designed and realized (in Labview) in order to set the MFCs flows and to calculate the gas concentration on the basis of the MFCs readings. The developed software is shown in Fig. 5.
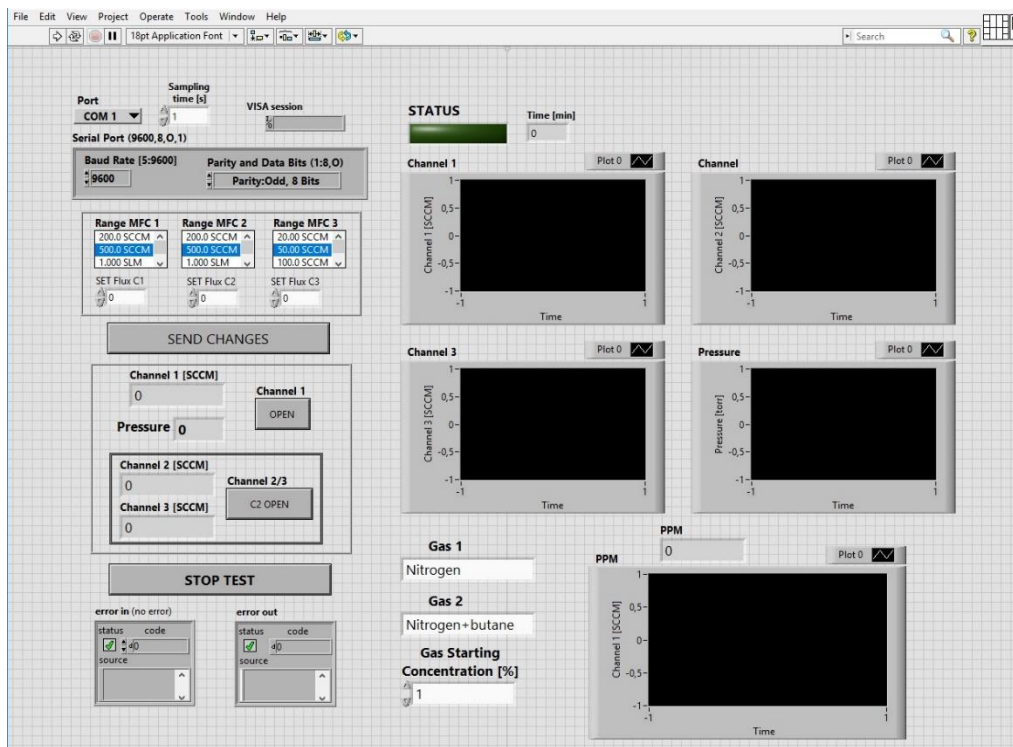


**Figure 4** Software Control Panel.

Through this software is possible to set the operative range of the MFCs (MFC1, MFC2 and MFC3), the starting butane concentration, and the gas flows (Flux C1, C2 and C3). In particular, channel C1 is relative to nitrogen line, while channels C2 and C3 are relative to the butane lines. On the right side of the panel are plotted the fluxes and the chamber pressure as function of time. On the basis of these readings, the software calculates the concentration of the output gas, and plot it on the bottom-right side of the panel.

## 5.3 Results and discussion

### 5.3.1 Fabrication of coated LPGs

The main manufacturing steps (summarized in the table below) refer to three main objectives to achieve, such as the realization of a reflection type LPG transducer, the realization of the coated LPG working in transition mode and the characterization and validation of the manufactured LPG probe.

**Table 1** Manufacturing steps of the a-PS coated LPG.

| Objective | Manufacturing steps |
|---|---|
| Reflection type LPG transducer | - Cleaning of the LPGs surface<br>- mirror integration at the end-face of the cut optical fiber |
| Coated LPG working in transition mode | - a-PS deposition |
| LPG probe characterization and validation | - butane sensing characterization |

The surface of the grating must be accurately cleaned to avoid that impurities (dust and/or fingerprints) can affect the homogeneity of the deposited film. Because a mechanical cleaning could damage the grating, it is necessary to use a chemical etching to perform the fiber treatment. In this case, a basic ("piranha") etching is performed. A solution of water, ammonia ($NH_4O_4$) and hydrogen peroxide ($H_2O_2$) in the ratio of 3:1:1 is wormed up to the boiling point (80 °C). The basic reaction and the boiling bubbles clean the surface from impurities leaving the glass surface perfectly smooth and scratch free. Before the application of the piranha solution, the optical fiber is dipped in chloroform for about 30 minutes to remove the any polymeric coating traces.

To obtain a reflection probe it is necessary to deposit a silver mirror on the tip of the LPG. This mirror is obtained using a Tollens' reagent, as reported in the previous chapter.

Fig. 5 shows the signal just after the cleaning step (black curve) and the signal after the mirror deposition (red curve). It can be seen that, before the mirror deposition baseline is very low, and that occurs because the light passing through the LPG is mostly transmitted

at the fiber/air interface, and only a small portion (~3-4%) of it is reflected back into the fiber as a consequence of the small refractive index contrast between the two media. Nevertheless, as soon as the Ag reflecting metallic layer is formed at the fiber termination, almost all the initial power is recovered. These curves refer to an arc-induced LPG with a grating period $\Lambda = 470\mu m$.
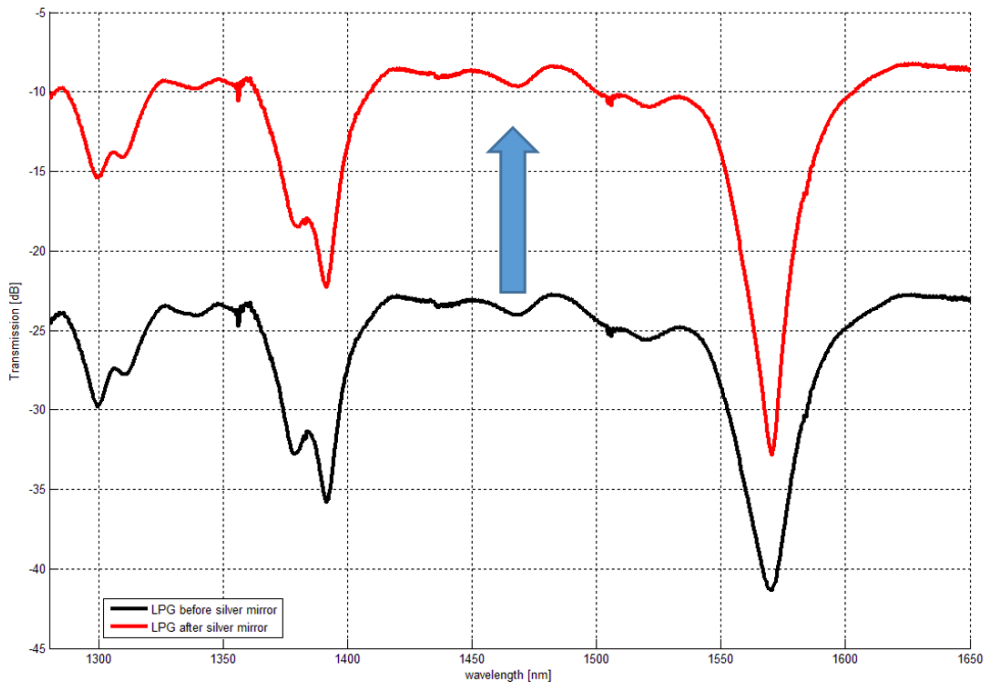


**Figure 5** Baseline variation due to the silver mirror deposition.
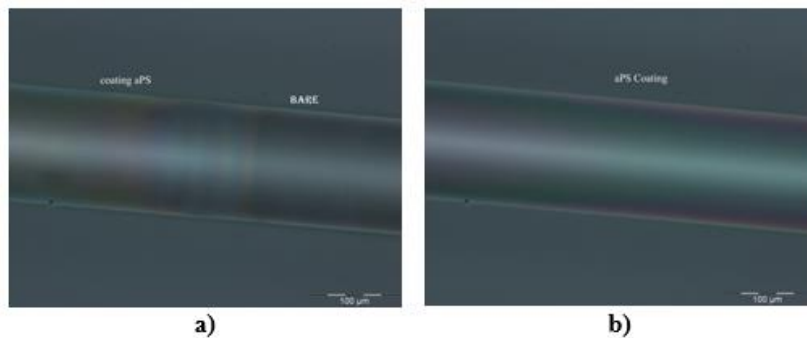


**Figure 6** Optical micrographs of the a-PS coated fibers.

As reported in table 1, the next step to the mirror formation is the sensible layer deposition using the dip-coating technique. Polymeric film is deposited starting from a solution of a-PS in chloroform (9.5w/w%). The deposition technique employed ensures the formation of a thin and homogenous a-PS film on the grating surface, as reported in Fig. 6. Comparing figs 6.a and 6.b it is evident that the presence of the polymeric film gives

an iridescent color to the fiber, likely due to the homogeneity and the low thickness of the layer.

In order to obtain the highest sensibility toward the analyite, LPG devices must be properly designed. There are two methods to increase the sensibility of the device:

1) Inducing the modal transition phenomenon.

2) Reducing the grating period $\Lambda$ it is possible to excite the higher order cladding modes in order to make them appear in the optical analysis region (1200-1700 nm); as reported in chapter 3, higher order cladding modes show higher sensitivity to the SRI variations;

To induce the modal transition phenomenon, the thickness of a-PS must be tuned accurately (as reported in chapter 3). The dip-coating technique allows this thickness tuning process in a simple and repeatable way: in fact, varying the withdrawal speed or the solution temperature it is possible to quickly change the layer thickness. As reported in Fig. 7, increasing the withdraw speed (50 to 200 mm/min) increases the shift undergone by the ith order cladding mode, which is consequence of the a-PS layer thickening. Fig. 7 refers to an arc-induced LPG with a grating period $\Lambda = 470\mu m$ (the same of Fig. 5).
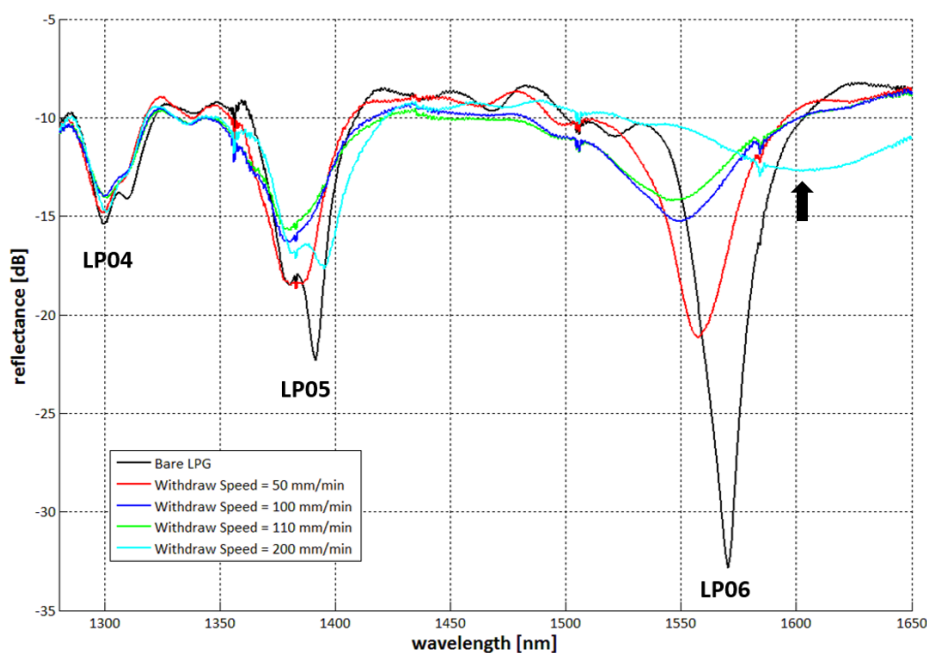


**Figure 7** LPG Spectra during the a-PS deposition.

According simulation in Fig. 8, the a-PS layer thickness with a withdrawn speed of 100 mm/min is ~280-300 nm. It is noteworthy that using a too high withdrawn speed (200 mm/min), the layer becomes too thick and the device exceed the transition region: this effect is evident in the cyan curve, where the shift is so high that the 7th cladding mode appears in the optical analysis region (black arrow).
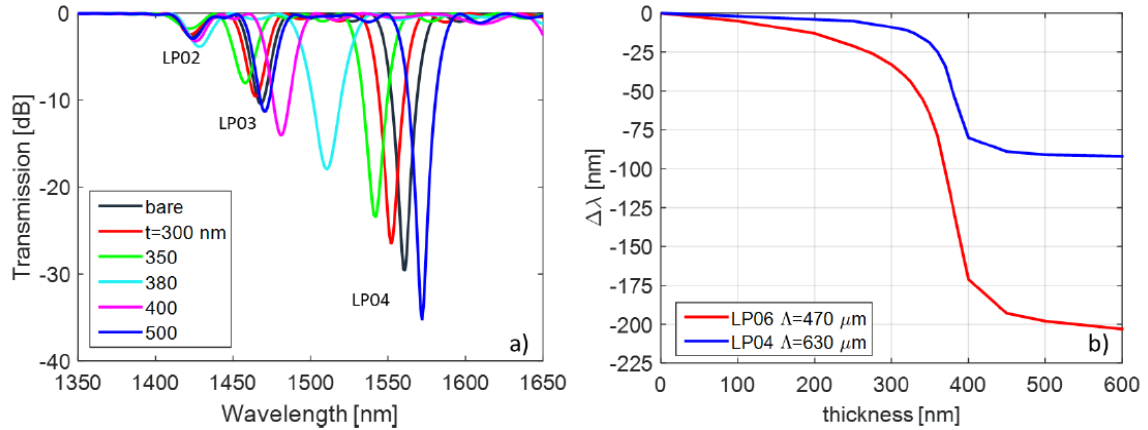


**Figure 8** Simulation of the wavelength shift ($\Delta\lambda$) as function of coating thickness (a-PS refractive index = 1.555).

The reduction of the grating period is another efficient method to increase the sensibility of the LPG device. Fig. 9 shows two a-PS coated LPGs with different grating periods, i.e. 630μm (Fig. 9.a) and 470μm (Fig. 9.b). The device with a grating period of 630μm shows a 12nm blue shift of the 4th order cladding mode; instead, the total shift undergone by the 6th order cladding mode, in the LPG with Λ=470μm, is 40nm. This implies that, to obtain a more sensible device it is preferable to use LPGs with grating period of 470μm.
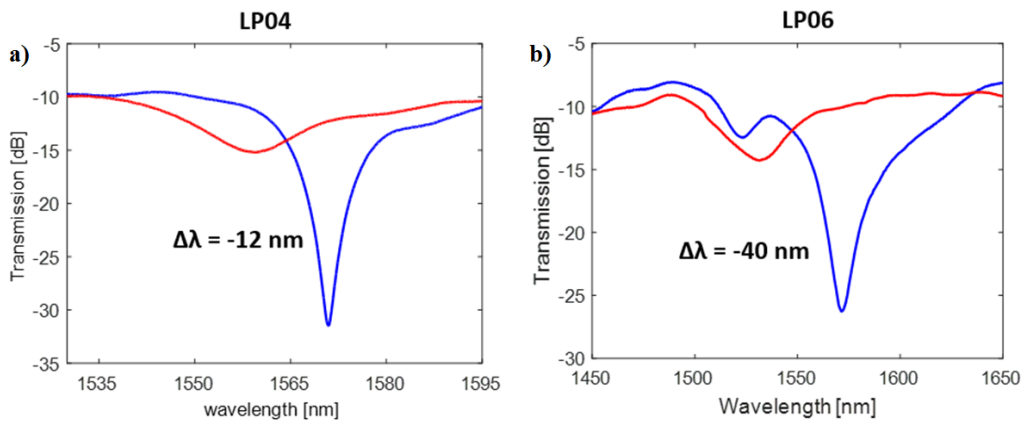


**Figure 9** Shifts undergone by LPGs with different grating period Λ, with the same a-PS coating thickness: a) Λ = 630μm and b) 470μm; blue and red curves are relative to the signal before and after the a-PS deposition, respectively.

Results have shown that to obtain an LPG probe with high sensibility toward butane it is necessary:

1) To work in transition mode: with dip-coating technique, using a withdrawn speed of 100 mm/min it is possible to obtain a ~300 nm thick a-PS layer; this thickness allows to work in transition mode with the employed LPG;

2) To use LPGs with shorter grating period: reducing $\Lambda$ up to 470μm it is possible to move the 6$^{th}$ order cladding mode inside the; this cladding mode is extremely more sensitive to the SRI variation compared to the 4$^{th}$ order cladding mode, excited in the LPG with $\Lambda$=630μm;
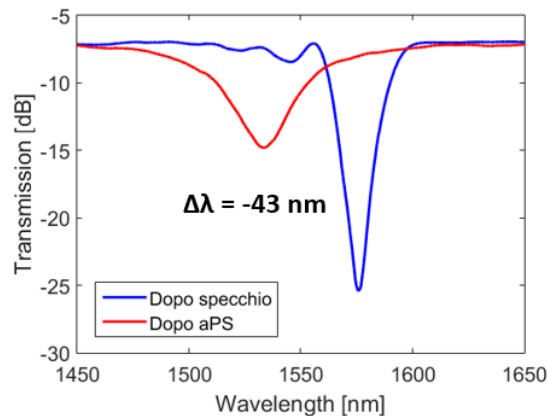


**Figure 10** Shift undergone by the commercial LPG after the a-PS deposition; blue and red curves are relative to the signal before and after the a-PS deposition, respectively.

Also commercial UV-induced LPG has been coated with an a-PS layer. The total shift due to the presence of the polymeric coating is shown in Fig. 10. It is evident that the shift is comparable to that undergone by the arc-induced LPG with $\Lambda$=470μm.

## 5.3.2 Butane Sensing Characterization

The manufactured fibers have been tested in presence of butane to evaluate the sensitivity toward this gas.

Preliminary tests have been carried out without a gas concentration control, in order to verify the maximum shift undergone by the device in presence of the analyte. Fig. 11 shows the shift undergone by the 6$^{th}$ order cladding mode (in an arc-induced LPG with

Λ=470μm and a-PS thickness of about 300nm) in presence of butane vapors. The curve

behavior indicates an absorption/desorption trend, with a response time of about 4 mins.

After exposition to air the total shift come back to zero, indicating device reversibility.
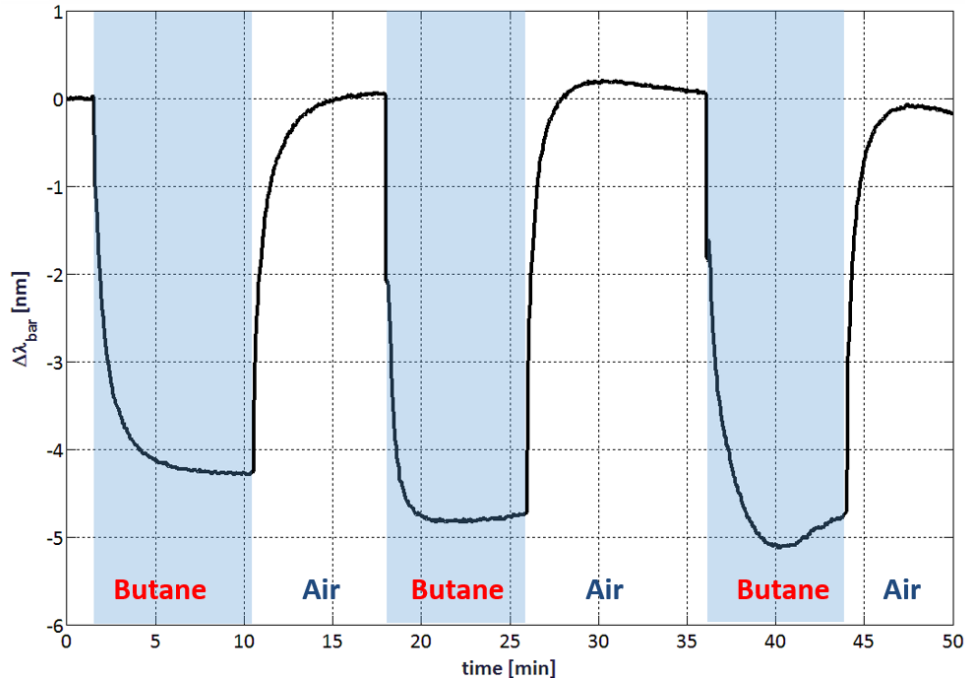


**Figure 11** Butane sensor behavior of the a-PS coated device (arc-induced LPG with Λ=470μm and a-PS thickness of about 300nm).

Test has been conducted using a three-necked flask filled with two spray of commercial

butane: the fiber is placed in one of the necks, and the flask is filled with two sprays of

commercial butane; after the spraying, the system is closed in order to evaluate the

response at a constant gas concentration. Butane has removed from the flask by a fan.

The same test is performed on a couple of UV-induced LPG coated with a-PS, as reported

in Fig. 12. It is evident that the maximum response is of the same order of magnitude as

the device in Fig. 11. During this test temperature has been monitored with a FBG.

Moreover, a bare LPG has been employed to verify the response of the device without

the sensible coating: results show that the butane devices sensitivity is entirely due to the

a-PS coating, as bare LPG response is not affected by the gas presence.

The difference in response value between these two devices (~1nm) could be attributable

to minimum difference in a-PS thickness: in fact, because the devices operate in the

transition region (maximum sensitivity region), minor variations in the coating thickness can cause large variation of the gas sensing response. Also in this case there is an absorption/desorption trend, with response time similar to that of the device in Fig. 11.
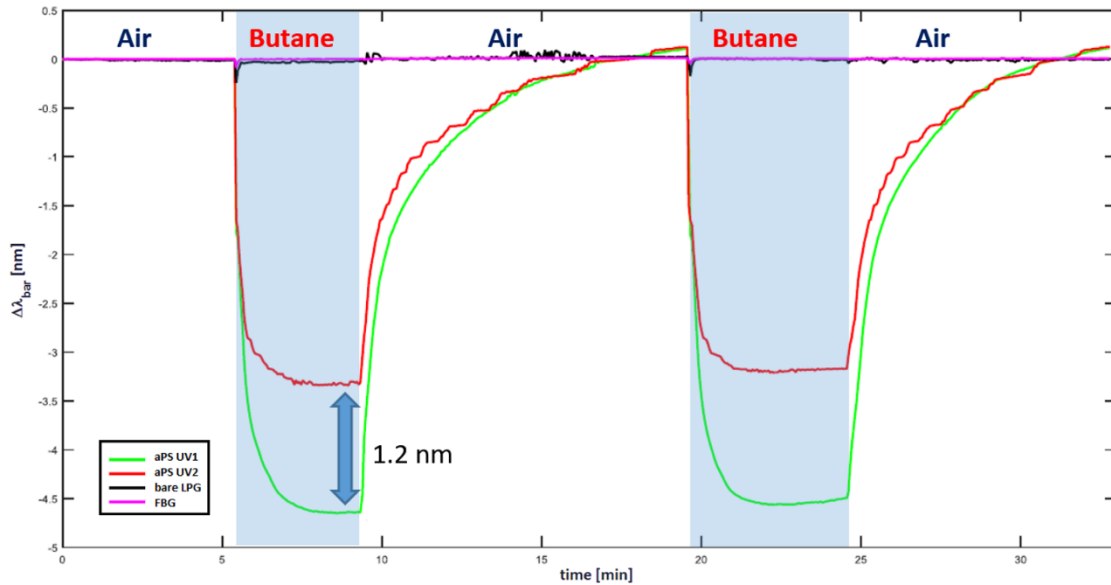


**Figure 12** Butane sensor behavior of two a-PS coated devices (UV-induced LPG with a-PS thickness of about 300nm).

Because arc-induced and UV-induced LPG show essentially the same gas sensing behavior (Figs 11 and 12), next tests have been performed only on the UV-induced LPG: this choice is due both to the lower optical losses after the layer deposition and to the more uniformity of the UV-induced LPG optical spectrum.

Other tests has been done to evaluate the instantaneous sensor response toward butane in an open environment: goal of these tests is to study the device response in a real situation (GPL leak after the train transit), where the gas run over the fiber and then expand in the surrounding environment, moving away from the device. To perform this test the set-up in Fig. 13 was employed. It consisting of an aluminum package used to bear and protect the devices, on which is sprayed butane with the help of a syringe. The latter is employed because if the gas is sprayed directly with the spray can the nebulized butane drops could condense onto the probes, polluting it.
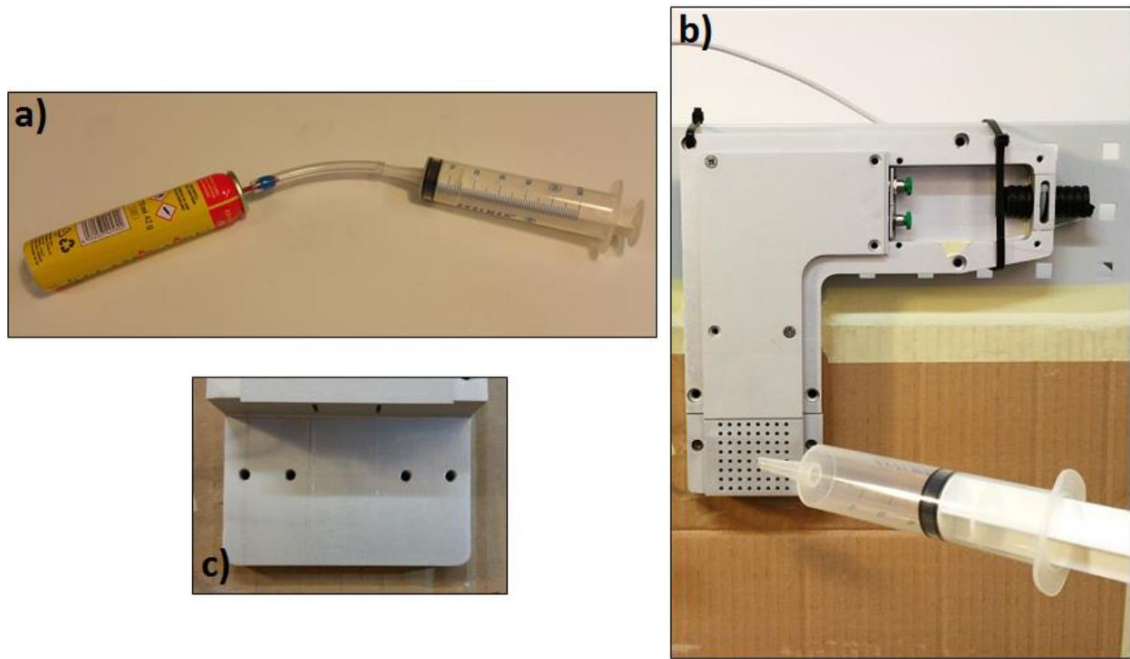
**Figure 13** a) Butane transfer in the syringe; b) butane spraying on the device packaging; c) package without protective cover.

Results of this test are shown in Fig. 14. As it is evident, the under examination device (UV-induced LPG coated with 300nm thick a-PS) undergoes an initial shift of about 0.7nm, which gradually reduces over the time following the desorption material kinetic. It is noteworthy that such kinetic results slower compared to those obtained in Figs 11 and 12. This effect is attributable to the fact that here the gas removal is spontaneous, contrarily to the previous tests in which butane was removed using the convective motion of a fan.
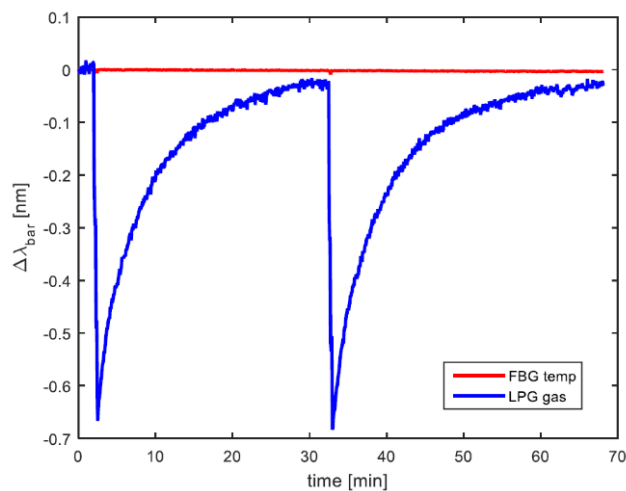


**Figure 14** Butane sensor behavior of a-PS coated device (UV-induced LPG with a-PS thickness of about 300nm).

In all performed tests, the gas concentration was not known, but to obtain a calibration curve it is necessary to study the relationship between gas concentration and consequent signal shift. Calibration curve (Fig. 15) of the selected device has been obtained using the GPL sensing test set-up previously described. The curve is not linear but rather it has a polynomial behavior.
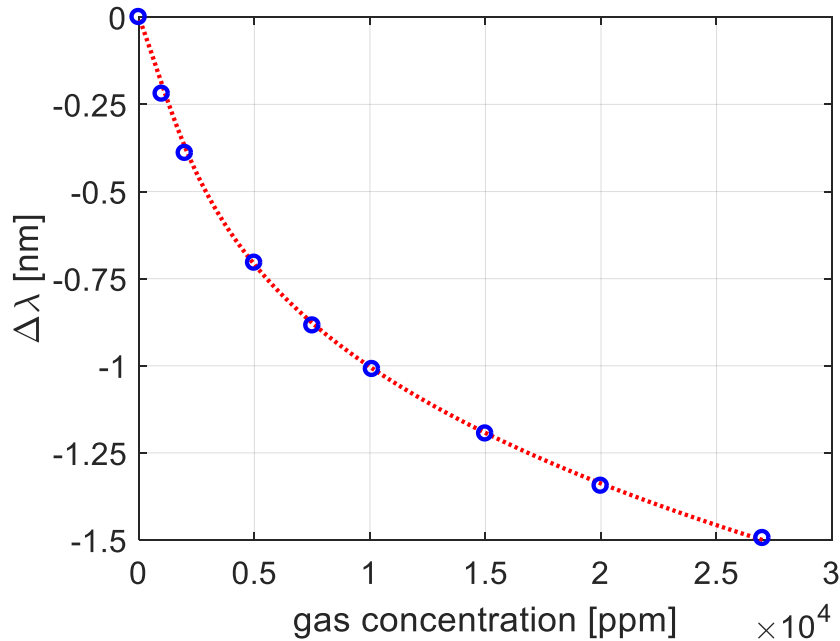


**Figure 15** Shift as function of gas concentration (Calibration curve) for the a-PS coated device (UV-induced LPG with a-PS thickness of about 300nm).

In order to completely characterize the developed GPL sensor, its humidity and temperature sensibilities have been evaluated. As reported in fig. 16.a, the device results sensible to temperature: this behavior is not attributable to the material, but to the intrinsic sensibility to temperature of the employed transducer. Despite the hydrophobicity of the a-PS film, the sensor results sensible to the humidity over 70% RH, probably because the water condensation on the polymer surface; instead, up to 70% RH the device is completely insensible to the vapor presence.

As required by the OPTOFER Project, the sensor has been installed under the railway tunnel near the Porta Rufina station (in Benevento). Fig. 17 shows the picture of the GPL sensor package installed under the tunnel.
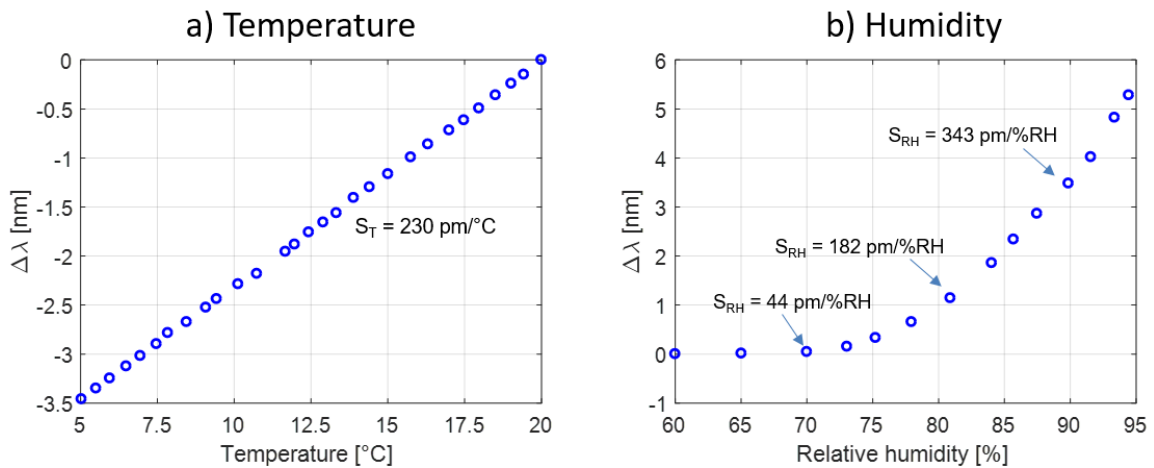
**Figure 16** Temperature and humidity for the a-PS coated device (UV-induced LPG with a-PS thickness of about 300nm).
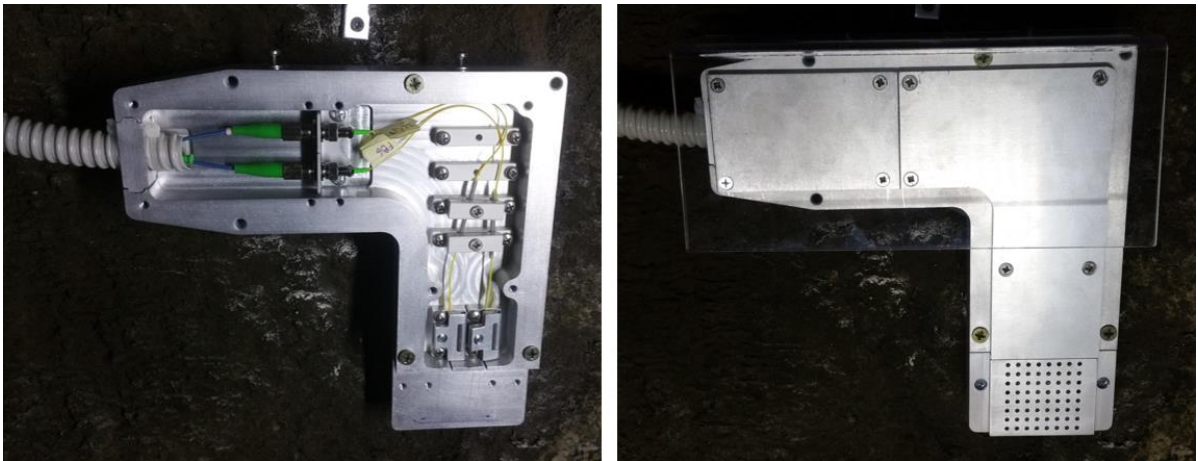


**Figure 17** GPL sensor package installed under the railway tunnel near Porta Rufina Station (BN): package without *(left)* and with *(right)* the protection cover.

After the installation, the device has been tested in presence of GPL: the gas was sprayed directly on the package, in order to simulate a real condition of accidentally GPL leak during rail transport. The measured output signal is the shift of the analyzed LPG peak as function of time, but the PC connected to the transducer convert this signal in GPL concentration (in ppm), thanks to the calibration curve previously obtained. Fig. 18 reports the results of the performed tests.
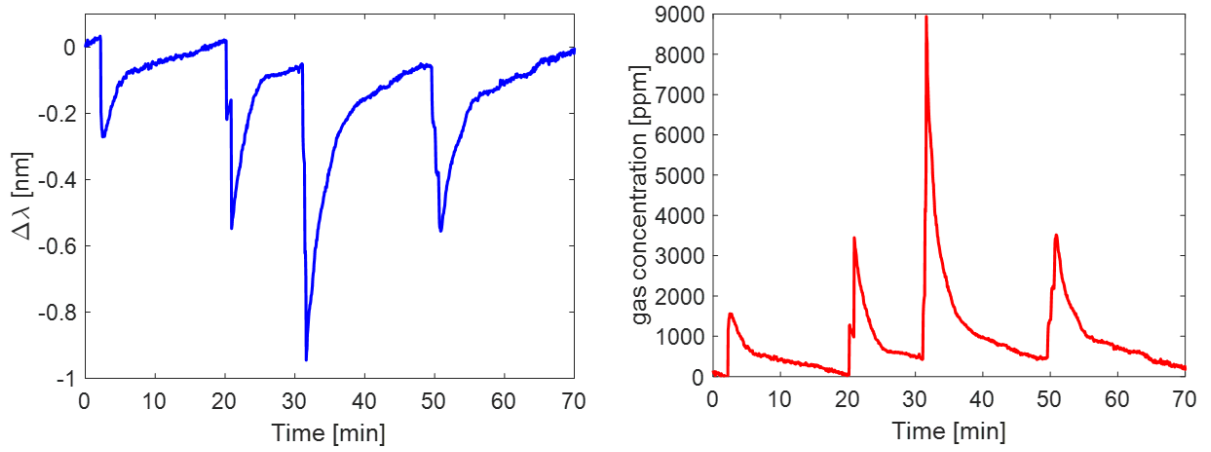
**Figure 18** (left) Shift as function of time for the sensor during the test and (right) consequent concentration calculated by the connected PC using the calibration curve.

# References

[1] A. Cusano, A. Iadicicco, P. Pilla. *Opt. Express*, **14**(1), 19-34, (2006).

[2] A. Cusano, A. Iadicicco, P. Pilla. *Appl. Phys. Lett*, **89**(20), 201116:1-3 (2006).

 [3] A. Cusano, P. Pilla, M. Giordano. *Advanced Photonic Structure for Biological and Chemical Detection*, Ed. X. Fan, pp. 35-75 (Springer, 2009).

[4] P. Pilla, C. Trono, F. Baldini. *Opt. Lett.*, **37**, 4152-4154 (2012).

# 6. Humidity sensors based on TiO₂ coatings

## 6.1 Introduction

Collaboration agreement with CERN (Conseil Européen pour la Recherche Nucléaire - European Organization for Nuclear Research), named "Relative humidity fiber optic sensors based on Long Period Gratings", led to the development of optoelectronic humidity sensors working in cryogenic environment.

The Compact Muon Solenoid (CMS) is one of the two large general-purpose particle detectors built on the Large Hadron Collider accelerator, running at the European CERN in Geneva. Its innermost detector, immersed in a 4 Tesla magnetic field, is a particle tracker where silicon pixel and microstrip sensors measure the momentum and trajectory of particles emerging from the LHC collisions. In order to reduce the radiation-induced loss of the sensors, the subdetectors are cooled at $-20°C/-25°C$. To avoid water condensation and ice formation, the volume needs to be kept sealed and dry. A distributed thermal and hygrometric monitoring of the air is, however, required in the external area surrounding the tracker, where cold services are distributed in complex geometries and a safe control of the environmental parameters is more difficult. In addition, each tracking detector needs to be as much as possible transparent to particles, requiring mass minimization of the devices to be installed in situ, radiation resistance from 1 to 100 Mrad doses, and magnetic field insensitivity. All the commercial miniaturized RH sensors used by CMS are capacitive, multiwired, and not designed with radiation hard characteristics [1]. On the other hand, fiber optic sensors are able to provide many attractive features that overcome the electrical sensors limitations. In addition, modern fabrication technologies allow us to obtain fibers tolerating high radiations levels [2], and this promoted renewed interest in their use in high-energy physics environments.

During this collaboration, titanium dioxide (TiO$_2$) has been used as a sensitive element for the development of high-sensitivity LPG based humidity sensors, due to its high RI (n = 1.96) [3] and hygrosensitive characteristics [4, 5]. Furthermore, the use of an oxide is expected to avoid the typical aging problems characteristic of polymeric overlays.

## 6.2   Materials and climatic chamber

Titanium dioxide (or titania) with formula $TiO_2$ exists at room temperature in three forms: rutile, anatase and brookite, each of which occurs naturally. Rutile is the only stable phase of coarse-grained titania, whereas anatase and brookite are metastable at all temperatures and convert to rutile when heated. The rutile structure is based on a slightly distorted hexagonal close packed (hcp) of oxygen atoms with half the octahedral interstices being occupied by titanium atoms. The tridimensional structure can be seen in Fig. 1.
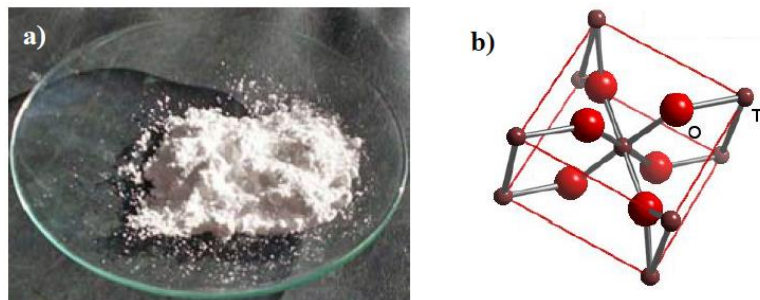


**Figure 1** Titanium oxide $TiO_2$ a) sample in powder form, b) 3D crystal structure.

Titanium oxide thin film is one of the most commonly used materials for optical thin films due to its good durability and high transmittance in the visible spectral region. It is commonly used as high index layer to achieve the high-low index contrast for multiple layer interference films [6]. Thin film properties, including refractive index, are very much dependent on film structure that is controllable by the deposition method and parameters, fixing the operational wavelength.

The sol-gel dip coating method has been selected for the integration of nanoscale $TiO_2$ layers onto the LPG surface, mainly due to its ability to guarantee a good optical quality, a ring-shaped symmetry, and an adequate longitudinal uniformity over the grating length. For $TiO_2$ sol preparation, titanium (IV) isopropoxide ($Ti(OR)_4$) has been used as titania precursor; it needs a solvent and a reaction activator: when the reaction activator is mixed to the precursor, the reaction starts and the oxide is obtained. Several dilutions of titania precursor in ethanol have been experimented in order to obtain a layer as smooth and

homogeneous as possible. The activator also plays a key role: different solutions involving different activators (water or acid) have been prepared to get an appropriate (and optimized) procedure. During this collaboration, UV-induced LPGs were bought by O/E Land Inc., a company based in Quèbec (Canada) that is one of the leader in the manufacturing of fiber gratings devices. These optical devices has been used in reflection mode, and therefore a silver mirror was deposited on the tip of the fiber.
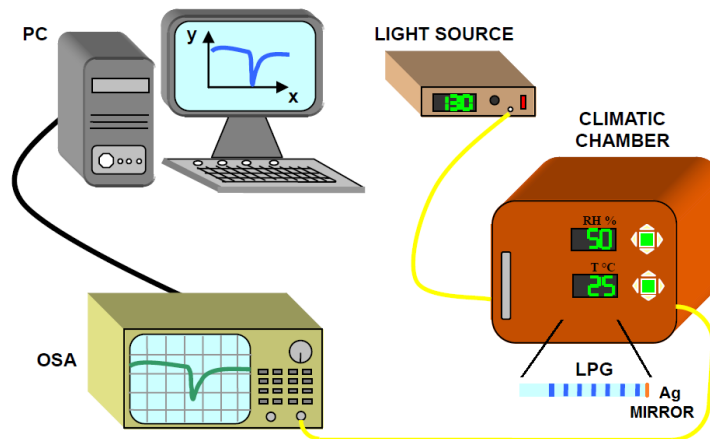


**Figure 2** Schematic representation of the experimental setup used for LPG sensor characterization.

The experimental tests have been performed in a climatic chamber (Angelantoni, Challenge 1200). Temperature and relative humidity can be controlled using the front panel buttons with an uncertainty of +/- 0.1 °C and +/- 1%, respectively. A chamber internal temperature of 25 °C has been fixed for measurements. The LPG sample is placed inside the climatic chamber, letting the fiber patch-cord coming out from the front door (see Fig. 2).

## 6.3  Results and discussion

### 6.3.1  Sol-Gel Process Optimization

Different sols has been prepared. In the following, the experimented solutions are listed.

- The first solution (here indicated as P1t): 6 ml of ethanol, 2.52 ml of $Ti(OR)_4$ and vapours of hydrochloric acid (HCl).

- The second solution (P2t): 5.85 ml of ethanol, 2.52 ml di $Ti(OR)_4$ and 0.15 ml of bidistilled water (H2O). When the water is added in the container, some precipitations appear (Fig. 3), thus meaning that this solution is not useful for sol-gel depositions.
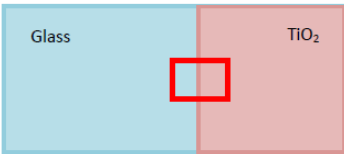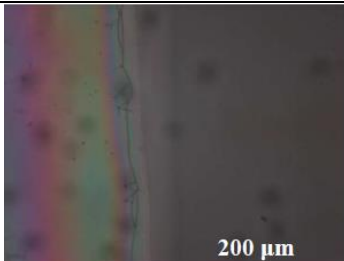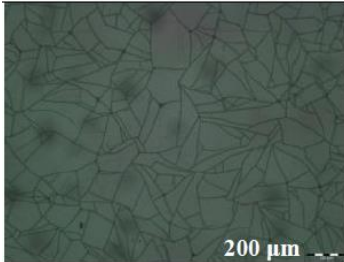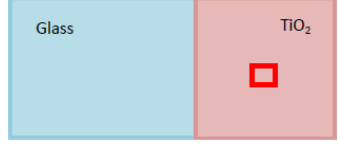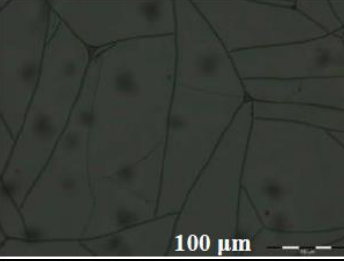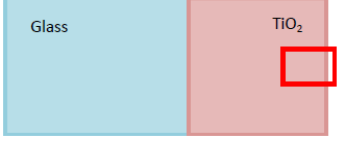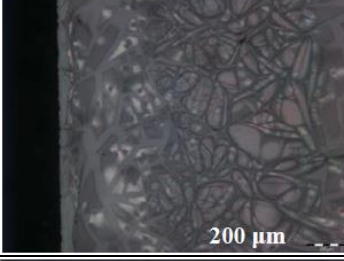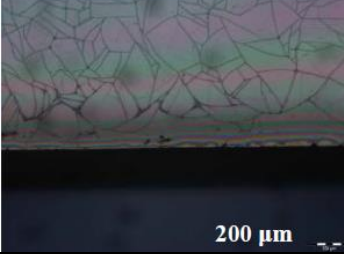


**Figure 3** Sol-gel solutions with precipitation (P2t).

- The third solution (here indicated as P3t): 5.85 ml of ethanol, 0.05 ml of bidistilled water, 2.52 ml of $Ti(OR)_4$ and vapours of hydrochloric acid.

- The fourth solution (P4t): 5.85 ml of ethanol, 0.05 ml of hydrochloric acid and 2.52 ml of $Ti(OR)_4$.

- The fifth solution (P5t): 2.25 ml of ethanol, 0.05 ml of hydrochloric acid and 6.25 ml of $Ti(OR)_4$.

- The sixth solution (P6t): 9.07 ml of ethanol, 0.0765 ml of bidistilled water and 3.85 ml of $Ti(OR)_4$.

A reaction time of 12 hours has been waited before using the prepared solutions for the deposition procedure. Preliminary deposition has been performed on glass planar substrates, in order to evaluate the solution that provide the best titania films, in term of homogeneity and uniformity.
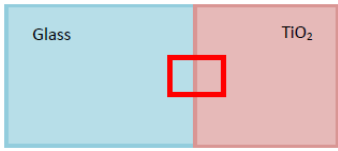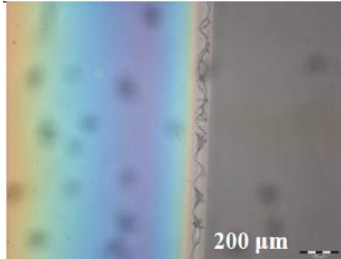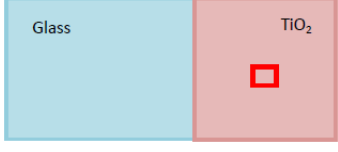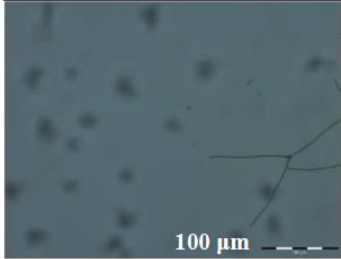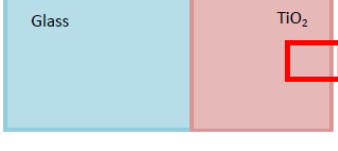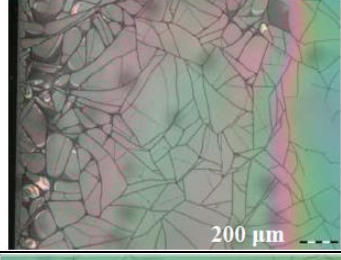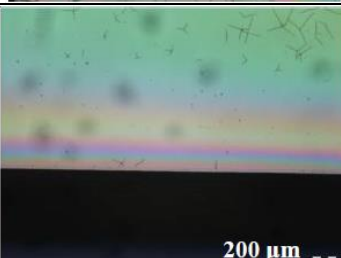
A quality analysis of the deposited layers is obtained by an optical microscope inspection of the films. For each of the prepared solutions, a table is reported: in the first column a schematic picture of the deposited substrate is shown, on which the observed area (red square) is highlighted; second column contains the film pictures, respectively. In the third column the magnification zoom of the microscope is indicated. Finally, in the fourth column it is specified the solution used for the deposition.

**Table 1** Microscope images of a titania layer deposited on a planar glass substrate using the solution P1t (Black circular shadows are due to impurities on microscope lenses).

| Selected area | Micrograph | Zoom | Solution |
|---|---|---|---|
|  |  | 5X | P1t |
|  |  | 5X | P1t |
|  |  | 20X | P1t |
|  |  | 5X | P1t |
|  |  | 5X | P1t |

The TiO$_2$ deposition results on planar glass substrates using the solution P1t are shown in Table 1. As can be seen, the deposited films show a cracked surface with isolated domains. The various colors are due to the different thicknesses of the domains. From these results, it is possible to conclude that the P1t solution does not result in high quality film, especially in terms of homogeneity and uniformity.
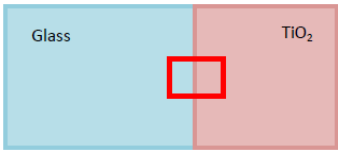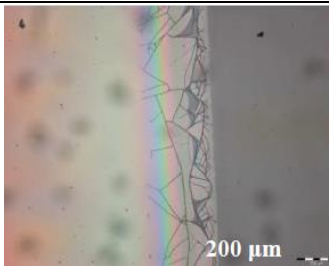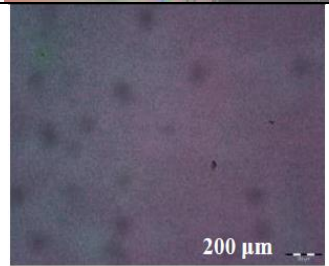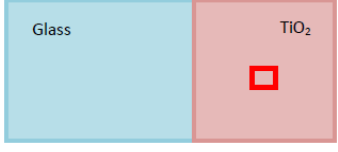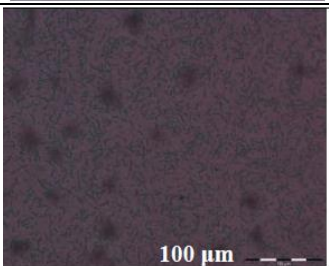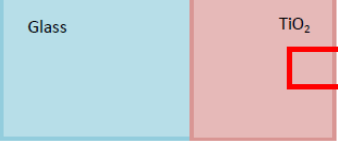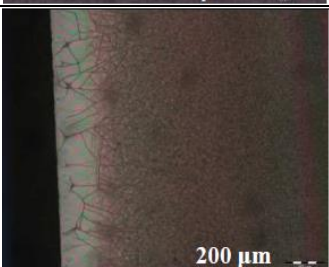
**Table 2** Microscope images of a titania layer deposited on a planar glass substrate using the solution P3t (Black circular shadows are due to impurities on microscope lenses).

| Selected area | Micrograph | Zoom | Solution |
|---|---|---|---|
|  |  | 5X | P3t |
|  |  | 5X | P3t |
|  |  | 20X | P3t |
|  |  | 5X | P3t |
|  |  | 5X | P3t |

The TiO$_2$ deposition results on planar glass substrates using the solution P3t are shown in Table 2. Also in this case the deposited films show a cracked surface. It is evident that films deposited from P3t solution result in bad quality layers, and thus cannot be employed for deposition on LPGs.

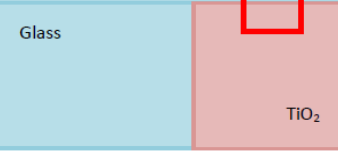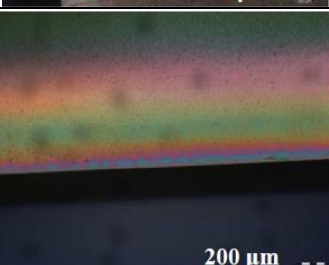The TiO$_2$ deposition results on planar glass substrates using the solution P4t are shown in Table 3.
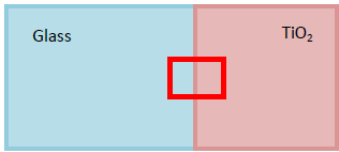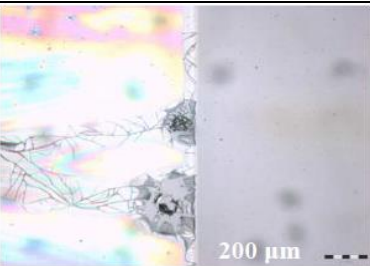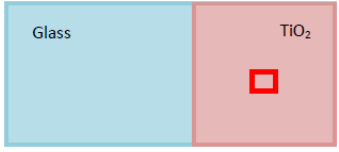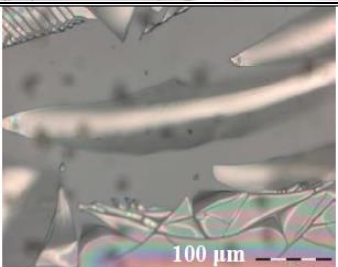
**Table 3** Microscope images of a titania layer deposited on a planar glass substrate using the solution P4t (Black circular shadows are due to impurities on microscope lenses).

| Selected area | Micrograph | Zoom | Solution |
|---|---|---|---|
|  |  | 5X | P4t |
|  |  | 5X | P4t |
|  |  | 20X | P4t |
|  |  | 5X | P4t |
|  |  | 5X | P4t |

68

The deposited film shows a slightly cracked surface with small domains. The quite good uniformity of the layer is shown by the pinkish homogeneous color of the whole surface. From these results we can therefore conclude that the P4t solution can be effectively used for obtaining high quality layers.

The $TiO_2$ deposition results on planar glass substrates using the solution P5t are shown in Table 4.
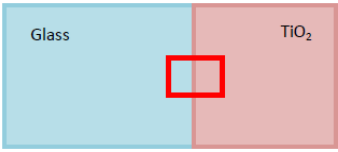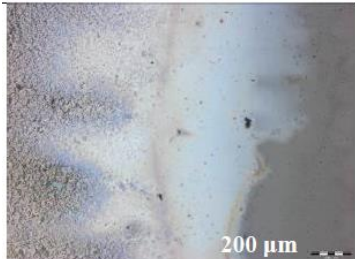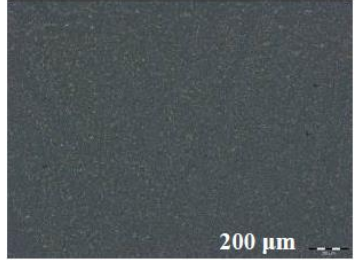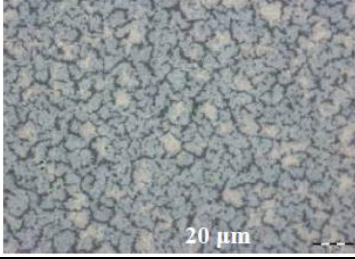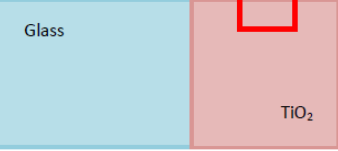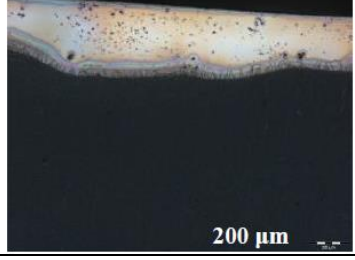
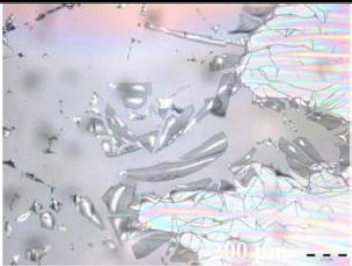**Table 4** Microscope images of a titania layer deposited on a planar glass substrate using the solution P5t (Black circular shadows are due to impurities on microscope lenses).

| Selected area | Micrograph | Zoom | Solution |
|---|---|---|---|
| Glass / $TiO_2$ |  200 μm | 5X | P5t |
| Glass / $TiO_2$ |  200 μm | 5X | P5t |
| Glass / $TiO_2$ |  100 μm | 20X | P5t |
| Glass / $TiO_2$ |  200 μm | 5X | P5t |
| Glass / $TiO_2$ |  200 μm | 5X | P5t |

When using the P5t solution, the deposited film results to be discontinuous with large void areas. These results exclude the P5t from the possible solutions for dip-coating deposition.

Similar (bad) results were also obtained in the case of P6t solution (see Table 5), that led to a cracked surface with small domains.
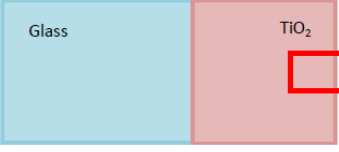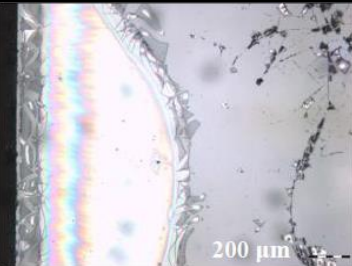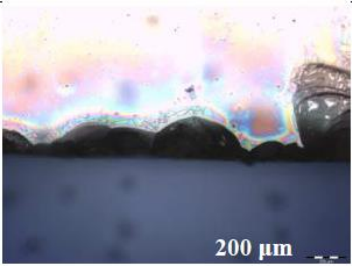
**Table 5** Microscope images of a titania layer deposited on a planar glass substrate using the solution P6t (Black circular shadows are due to impurities on microscope lenses).
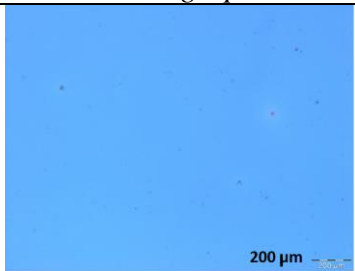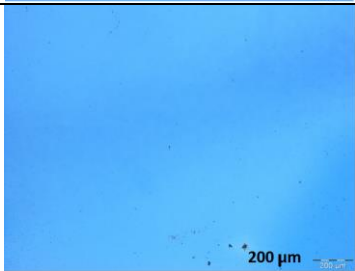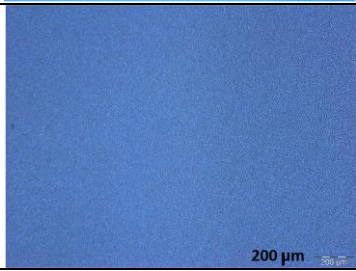
| Selected area | Micrograph | Zoom | Solution |
|---|---|---|---|
| Glass — TiO$_2$ | 200 µm | 5X | P6t |
| Glass — TiO$_2$ | 200 µm | 5X | P6t |
| Glass — TiO$_2$ | 20 µm | 20X | P6t |
| Glass — TiO$_2$ | 200 µm | 5X | P6t |

By resuming the results previously shown, it is possible to state that, on planar substrates, the best titania layers, in terms of homogeneity, uniformity and dimensions of cracks, were obtained using the solution P4t.

Another aspect that was considered is the reaction time of the sol. During sol-gel process, the oxide precursor is hydrolyzed and then the hydroxide molecules react forming oxide macromolecules. If the reaction time is brief, the resultant macromolecules are short, reducing the mechanical properties of the relative wet film. Conversely, it is possible the formation, coalescence, and consequent precipitation, of oxide particles if the reaction time are too long: that induces the formation of layers of particles, which do not result very homogeneous.

To obtain the optimized reaction time, 3 glass substrate have been coated with a P4t sol: deposition has been performed after exactly 3 time interval: 1hour, 1 day and 7 days. Table 6 shows the samples micrographs. It is evident that the sample coated with 7 day after the sol synthesis results inhomogeneous due to the particles that constitute it.

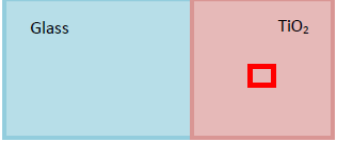**Table 6** Microscope images of a titania layer deposited on planar glass substrate at different reaction times.

| Selected area | Micrograph | Sol Reaction time |
|---|---|---|
| Glass TiO$_2$ | 200 µm | 1 hour |
| Glass TiO$_2$ | 200 µm | 1 day |
| Glass TiO$_2$ | 200 µm | 7 days |

The other samples are, instead, homogeneous and defect free. For this reason, $TiO_2$ sol has been deposited on the lateral surface of an optical fiber: results (Fig. 4) shows the comparison between the fiber coated after 1 hour from the sol synthesis and the fiber coated after a day. The first shows large fracture due to the shrinkage during the drying process, making it unusable as LPG coating. The last is instead very homogeneous and consequently the optimized reaction time is 24 hours.
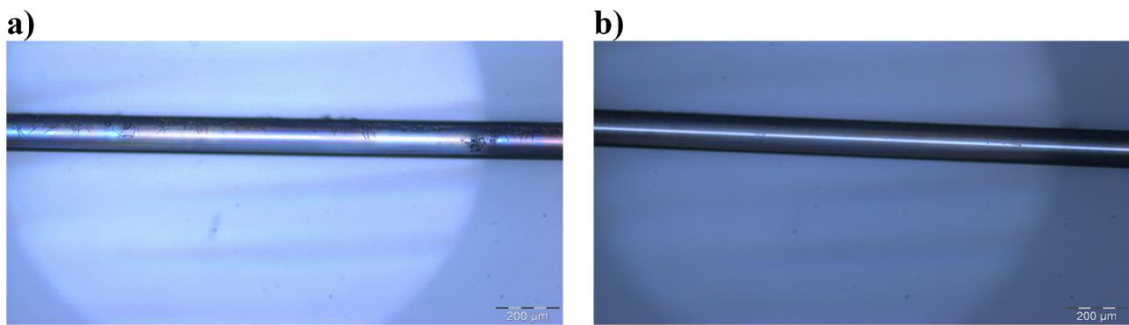


**Figure 4** P4t sol deposited on optical fibers with different reaction time: a) 1 hour and b) 24 hours.

## 6.3.2 Fabrication of coated LPGs

Established that the best titania layer has been obtained using the P4t sol, it is possible to precede to the LPG manufacturing. The main manufacturing steps (summarized in the table below) refer to three main objectives to achieve, such as the realization of a reflection type LPG transducer, the realization of the coated LPG working in transition mode and the characterization and validation of the manufactured LPG probe.

**Table 7** Manufacturing steps of the titania coated LPG.

| Objective | Manufacturing steps |
|---|---|
| Reflection type LPG transducer | - Cleaning of the LPGs surface<br>- mirror integration at the end-face of the cut optical fiber |
| Coated LPG working in transition mode | - titania deposition |
| LPG probe characterization and validation | - humidity sensing characterization |

The surface of the grating must be accurately cleaned to avoid that impurities (dust and/or fingerprints) can affect the homogeneity of the deposited film. Because a mechanical cleaning could damage the grating, it is necessary to use a chemical etching to perform

the fiber treatment. In this case, a basic ("piranha") etching is performed. A solution of water, ammonia ($NH_4O_4$) and hydrogen peroxide ($H_2O_2$) in the ratio of 3:1:1 is wormed up to the boiling point (80 °C). The basic reaction and the boiling bubbles clean the surface from impurities leaving the glass surface perfectly smooth and scratch free. Before the application of the piranha solution, the optical fiber is dipped in chloroform for about 30 minutes to remove the any polymeric coating traces.

As done for the GPL sensors, also in the case of humidity sensor it is necessary to work in reflection mode. For this purpose, tollens' reactant was employed to deposit the silver mirror on the tip of the LPG. Fig.5 reports the increase in optical transmission signal after the mirror deposition.
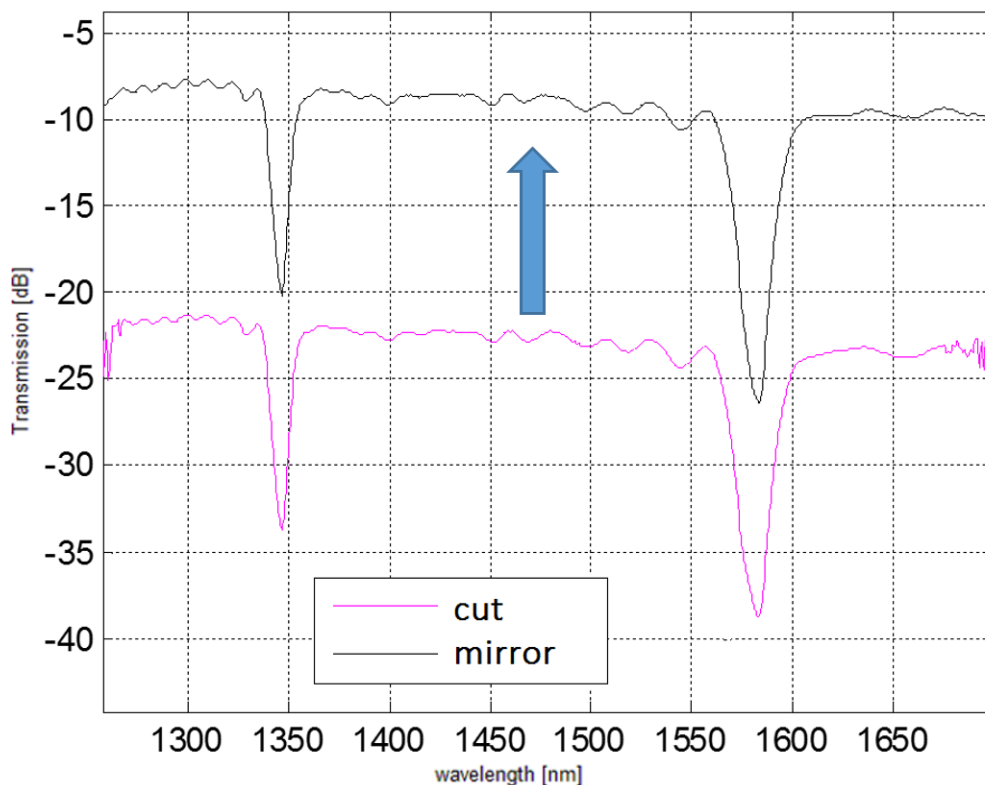


**Figure 5** Baseline variation due to the silver mirror deposition.

After the silver deposition, LPGs has been coated with titania layer. As previously stated, this inorganic material was deposited using the dip-coating technique. The solution selected for the integration of $TiO_2$ layers with optical fiber substrates (P4t) has been used for the integration of $TiO_2$ overlays on the LPGs (Fig. 6). In this case, it can be seen that

the obtained $TiO_2$ layer is homogeneous and only few imperfections are visible along the fiber. This result thus confirms the capability of the solution P4t of producing films with good optical quality and high uniformity, as already observed also in the case of glass planar substrates.
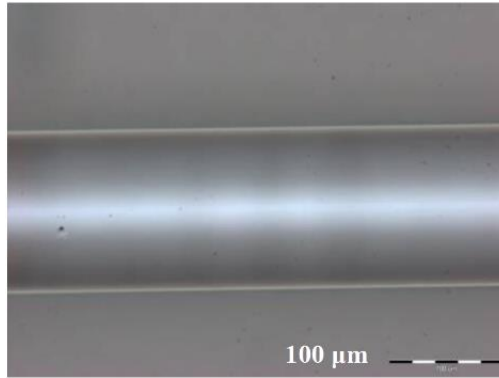


**Figure 6** Microscope image of a titania layer deposited on the optical fiber using the solution P4t.

To work in transition mode, multiple depositions are performed in order to get thicker final layers (of approximately 100 nm), since $TiO_2$ layers result very thin. In case of multilayer depositions, a thermal annealing (10 mins @150°C) between the deposition of two consecutive layers has been proposed.

**Table 8** Microscope images of 6 titania layers deposited on two LPGs and shift undergone by the device after deposition.

| Sample | Zoom | Micrographs | Shift |
|--------|------|-------------|-------|
| LPG1 | 5x |  |  |
| | 20x |  | |
| LPG2 | 5x |  |  |
| | 20x |  | |

As starting point, two UV-Induced LPGs have been coated with 6 layers of titania. Table 8 contains the micrographs of the coated fibers and the shift undergone by the device after the 6 layers deposition. It is evident that the number of layer deposited does not affect the homogeneity of the film, being it as smooth as that obtained with only on layer (Fig. 6).

However, it is noteworthy that the shift undergone by the fibers is very low (only 2-3 nm after 6 $TiO_2$ layers). This result could be attributable to the thermal annealing between the deposition of two consecutive layers: the high temperature of the annealing process (150°C) can increase the hydrophobicity of the deposited layer, making the deposition of the next layer harder (being the titania sol an alcoholic solution). The change in hydrophobicity could be attributable to chemical and/or morphological transformation undergone by the titania layer after the increase in temperature.



**Figure 7** Contact angle goniometer.

To verify this hypothesis, a contact angle test has been performed, using a contact angle goniometer (Fig. 7). Titania was deposited on two glass planar substrates, but only one of these samples has been thermal annealed @150°C. Comparison between the contact angles of these two layers is shown in Fig. 8. It is evident that the sample without temperature annealing shows high hydrophilicity, with a contact angle significantly lower

than 90° (contact angle = 13.6°); on the other hand, annealed titania is characterized by a hydrophobic behavior, with a contact angle higher than 90° (contact angle = 131.2°).
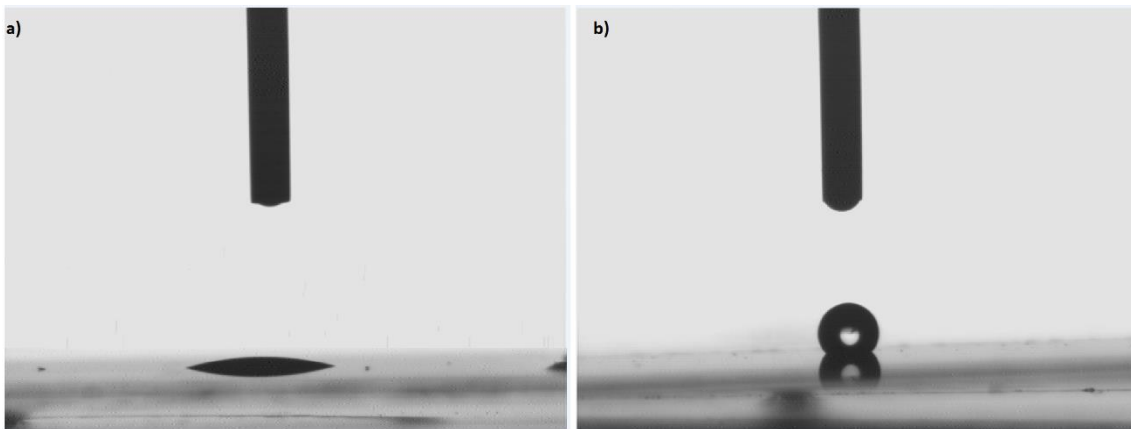


**Figure 8** Contact angle of the titania layers: a) without and b) with annealing @150°C for 10 mins.

On the basis of this observation, the procedure to manufacture the humidity sensors is changed, removing the annealing process between consecutive layer depositions, and replacing it with a drying cycle performed in oven for 10 mins at room temperature under vacuum: vacuum allows to dry the titania film without chemical and morphological transformations that can affect the layer hydrophilicity.

The final manufacturing scheme is shown in Fig. 9. Higher is the thickness needed to operate in transition mode higher is the value of N.
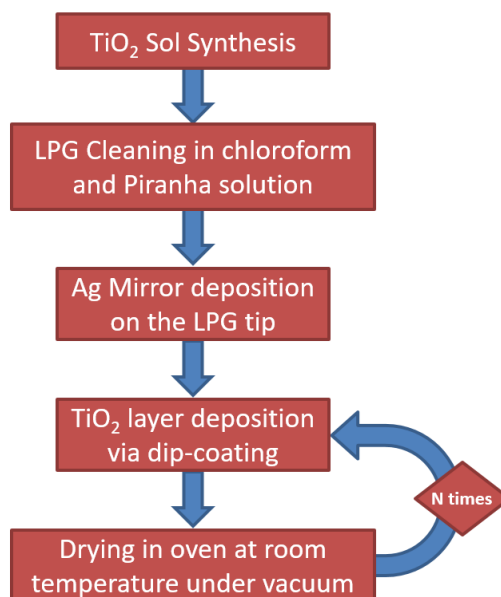


**Figure 9** Humidity sensor manufacturing procedure.

Using this procedure an LPG based device has been manufactured. In fig. 10 is shown the LPG spectrum during the deposition of titania: it is evident that with 12 layers (12 dips) there is a remarkable change in the shape of the curve, with a shift of the $6^{th}$ order cladding mode of about 37nm. Simulations estimate a $TiO_2$ thickness of about 88nm associated to this shift.
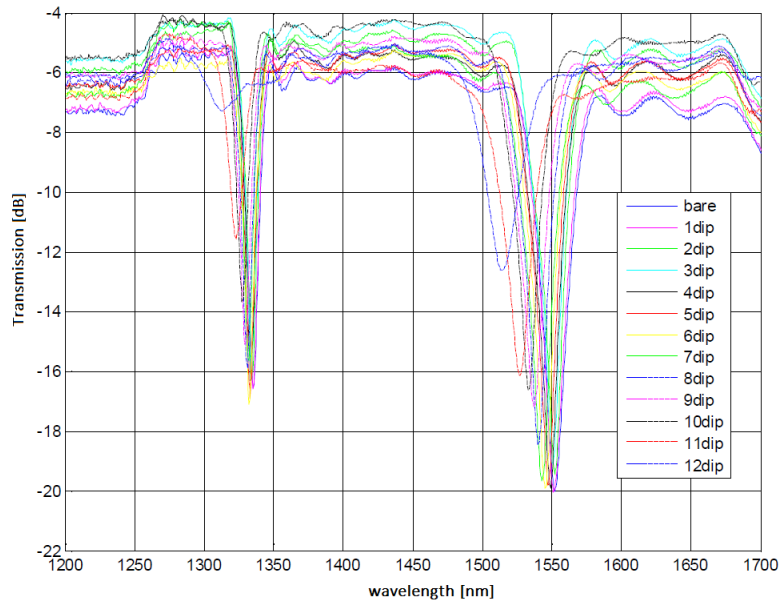


**Figure 10** LPG optical spectrum during $TiO_2$ deposition.
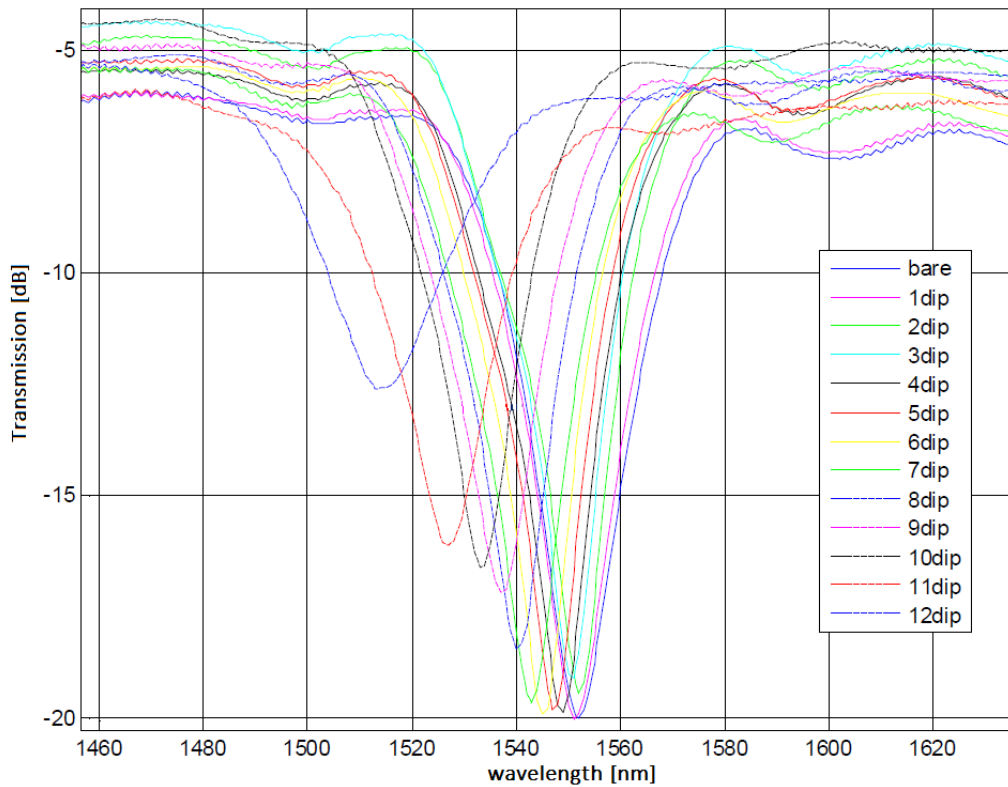


**Figure 11** LPG optical spectrum during $TiO_2$ deposition: zoom in the region 1460-1630 nm.

Fig. 11 shows a zoom of the optical region that contains the 6th order cladding mode (1460-1630 nm). The loss in depth of the attenuation band is ~7.5dB.

### 6.3.3 Preliminary humidity characterization

In this section are reported the first experimental results of a preliminary RH test carried out using the realized LPG sensor coated with a 12 layer $TiO_2$ overlay (with thickness of approximately 88nm). Information about its performances in detecting RH changes in the range 10-80% RH at 25°C (Fig. 12) is detailed in the following.
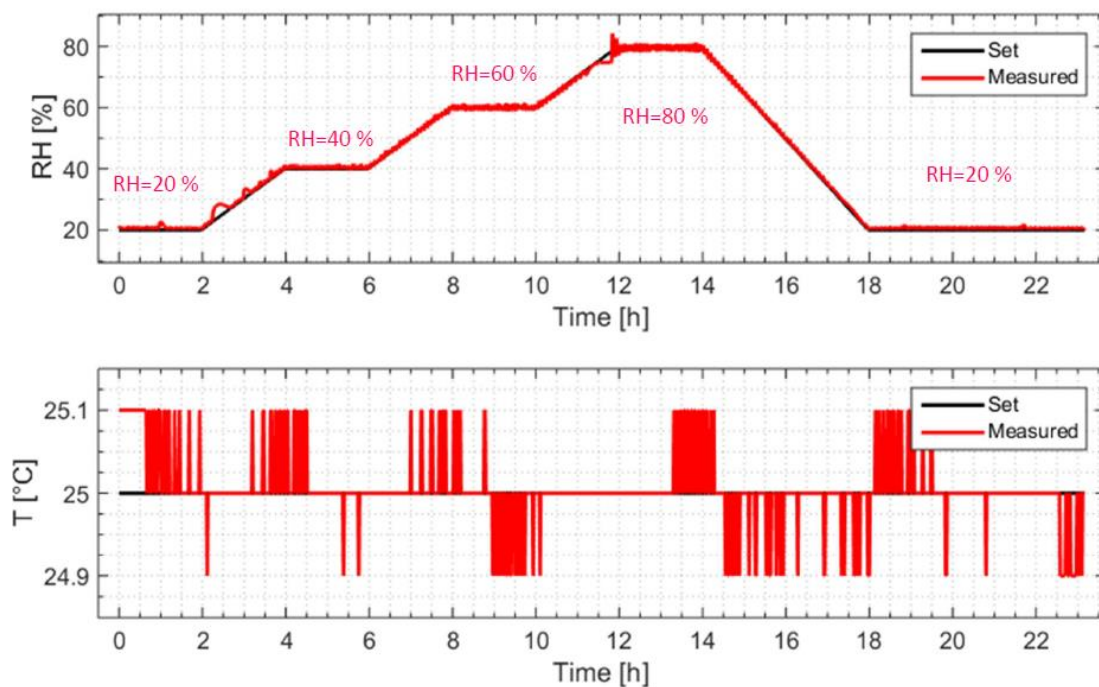


**Figure 12** Settings of the climate chamber.

Figure 13 shows the typical spectral variations of the $TiO_2$-coated LPG sensor during a characterization test carried out at 25°C. As theoretically expected, increasing the humidity content inside the test chamber causes a blueshift the 6th order cladding mode. This is due to the $TiO_2$ coating RI increase caused by the higher amount of adsorbed water molecules, which in turn leads to an increase of $n^{0i}_{eff;cl}$. The loss in depth of the attenuation band is ~1dB.

In Fig. 13 it is plot the time variation of the barycentral wavelength of the resonance dip occurred upon RH changes within the chamber from 10 to 80%, with 20% steps.
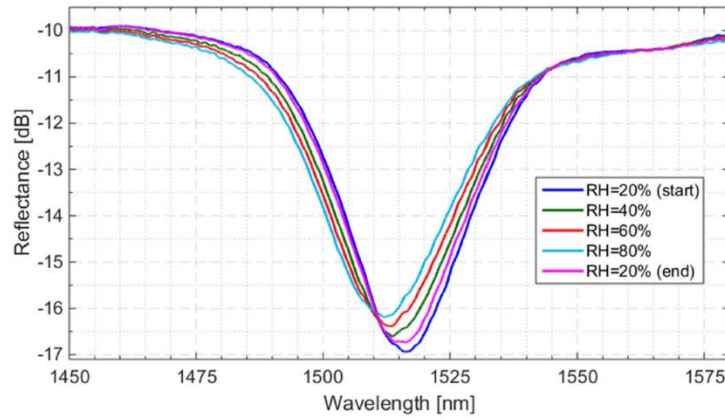
**Figure 13** Transmittance spectra of LPG1 acquired at different RH values.
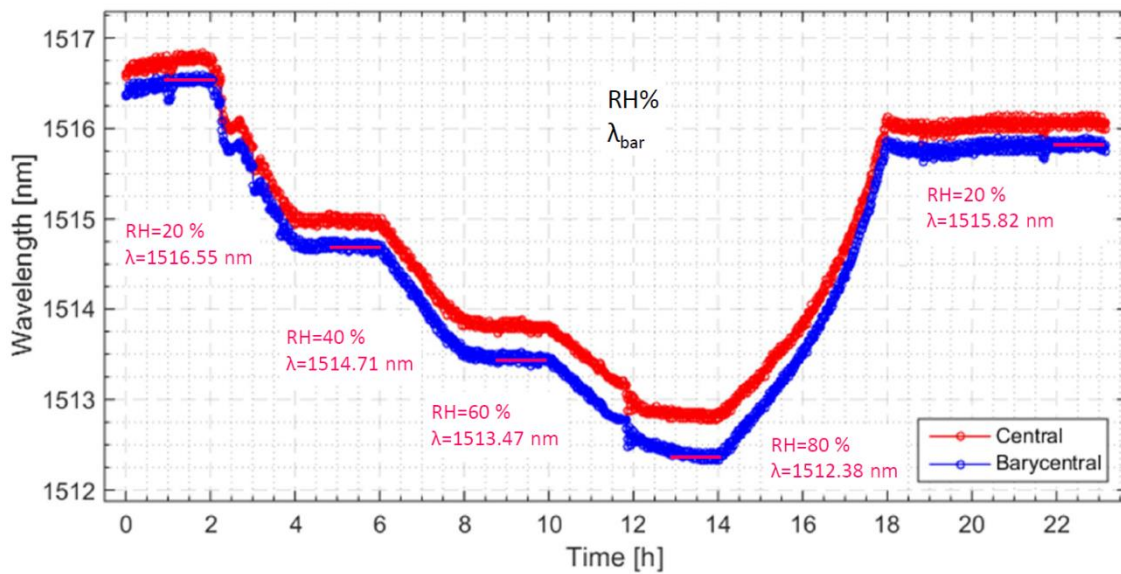


**Figure 13** Time evolution of central and barycentral wavelengths variation occurred for different RH values for TiO$_2$ sample.

As can be noted, the response time of the sensor to a humidity variation is related to the setting time of the chamber. Thin TiO$_2$ layers on the LPG results in an instantaneous response of the sensor to humidity variations. Each RH step is kept for several minutes and the small variations illustrated in Figure 13 are related to humidity control of the chamber and cannot be attributed to LPG sensor instability. In Table 9 the relative wavelength shift for each RH step is resumed.

**Table 9** Microscope images of 6 titania layers deposited

| RH Step | $|Δλ|$ [pm] |
|---------|------------|
| 20-40%  | 1840       |
| 40-60%  | 1240       |
| 60-80%  | 1090       |

The barycentral wavelength variations of the resonance dip versus the RH values are plotted in Figure 14. It is evident that the wavelength shift is higher for lower RH values: from RH=20% to RH=40% the shift is about 1840 pm while from RH=60% to RH=80% the shift is 1090 pm.
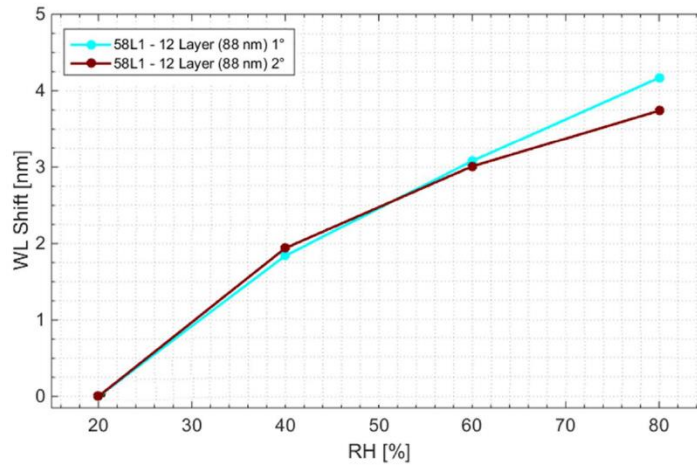


**Figure 14** Barycentral wavelength variations of the resonance dip versus the RH values during two different tests (1° and 2°).

# References

[1] M. Fossa, P. Petagna. "Use and calibration of capacitive RH sensors for hygrometric control of the CMS tracker," CMS Note 2003/24 (2003).

[2] A. Cusano, A. Cutolo, J. Albert. *Fiber Bragg Grating Sensors: Recent Advancements, Industrial Applications and Market Exploitation*, Ed. Bentham Science, pp. 218-237 (2011).

[3] E. Davies, R. Viitala, M. Salomäki. *J. Opt. A Pure Appl. Opt.*, **11**, 015501 (2009).

[4] G. Montesperelli, A. Pumo, E. Traversa. *Sens. Actuators B*, **25**, 705 (1995).

[5] B. C. Yadav, N. K. Pandey, A. K. Srivastava. *Meas. Sci. Technol.*, **18**, 260 (2007).

[6] H. Xie, X.T. Zeng, W.K. Yeo. *Temperature dependent properties of titanium oxide thin films by spectroscopic ellipsometry*, SIMTech technical reports vol. 9 (2008).

# BIOSENSORS

# 7. Drug resistant bacteria biosensor based on a-PS/PMMA coatings

## 7.1 Introduction

This work deals with the development of advanced optical biosensors able to perform a rapid detection of drug resistant bacteria carried out within the FP7 European project "Multianalyte automatic system for the detection of drug resistant bacteria - OPTObacteria"[1]. Resistance to infecting microorganism represents a key threat to human health and cause high human and socio-economic burden. Among the largest diffused infections, β-lactamases expressing pathogens, methicillin-resistant Staphylococcus aureus, and gram-negative hospital opportunistic pathogens are among the most aggressive ones. In particular Extended-spectrum BL have emerged as an important mechanism of resistance in Gram-negative bacteria. Delay in appropriate therapy for infections with ESBL producers not only prolongs hospital stay, but is associated with increased mortality. Methods currently known for detecting ESBLs are expensive and generally used to only test pre-screened individuals. In addition, 24-48 hours are typically needed before having a resistance profile, thus meaning that they cannot be used to obtain rapid results which would allow infection control measures to be implemented at the earliest possible opportunity [2].

Highly sensitive optical probes able to detect unlabeled biomolecules are of great interest in this concerns, as they would enable a true real-time (and in situ) screening with minimal sample consumption and treatment. Among all, LPGs are the most promising fiber optic refractive index (RI) transducers to be employed for unlabeled biochemical assays [3]. The number of biosensing applications exploiting different designs of LPGs is rapidly growing and they are expected to become a key technology in next few years [4-6]. A strong impulse to this growth was recently given by the integration on the LPG surface

of nano-scale polymer overlays and by the discovery of the modal transition phenomenon. As previously stated, it is well known that the SRI sensitivity of LPGs can be optimized at the desired working point through the deposition of a high RI (HRI) layer by acting on its thickness (ranging in hundreds of nanometers). Shifts of the spectral features as high as thousands of nanometers for a unitary change of SRI can be easily obtained, thus making HRI-coated LPGs very much exploited for chemical and biomolecular sensing applications [7]. However, essential condition to fully exploit the benefits of transition mode LPGs is that the attenuation bands would not loose visibility while working in transition mode. This is not verified for some materials and related deposition techniques [8-9] and it is achieved only when high optical quality overlays (low absorption and roughness) are used. Up to now the best results have been obtained with thin polymer layers deposited by dip-coating, in particular with ordinary a-PS [7]. It is worth pointing out that the quality of a biosensing system not solely relies on the sensitivity of the transducer (the a-PS coated LPG), but also involves its interfacial properties where suitable bioactive species (i.e. the bioreceptors) are immobilized, providing the final sensitivity and specificity to the target molecules.

In the framework of OPTOBACTERIA Project, due to the difficulty to directly biofunctionalize the a-PS overlay, it has been used a recently proposed multilayer strategy [10], where the a-PS overlay serves to tune the working point of the device in the transition region, while a second thinner overlay of poly(methyl methacrylate-co-methacrylic acid) (PMMA-co-MA) provides the desired interfacial properties for a stable bioreceptor immobilization. The LPG biosensors manufacturing is reported, from the realization of the reflection type LPG transducer working in transition mode to the biochemical functionalization of its surface. Finally, preliminary experimental results revealing the biosensor capability to successfully detect the binding of a specific BL (AmpC) are also reported.

## 7.2 Materials and SRI characterization

As previously stated, using a multilayer approach for the coating of the LPG allow to independently tune the working point in transition region and achieve an efficient surface functionalization without incurring the problem of the attenuation bands fading. In particular, a-PS is a primary HRI coating, which tunes the working point of the device in transition region. A secondary very thin layer of PMMA-co-MA, whose refractive index is 1.49, was then deposited to provide a caroboxyl-containing surface minimizing at the same time its impact on the optical design of the device.

A-PS and PMMA (see Fig. 1) are probably the most exploited polymers for optical waveguide fabrication so far [11, 12]. They are inexpensive, easily processable and highly transparent.
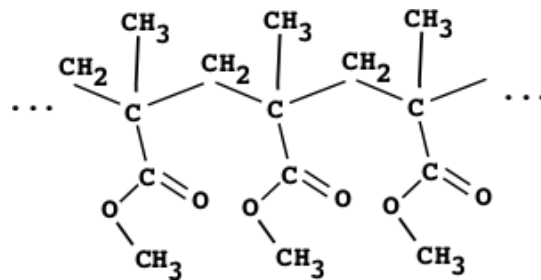


**Figure 1** PMMA chemical structure.

It should be possible to use only a thick PMMA layer (without using a-PS layer) to achieve the maximum sensitivity and the desired functionality of the interface, but there are different drawbacks that does not allow to use this approach. First of all, although the PMMA-co-MA has a slightly higher RI than the cladding that enables the modal transition phenomenon, nonetheless it has a much lower RI than PS. This would result both in a thicker overlay (approx. 2.7 times thicker than a single a-PS overlay) to tune the LPG in the transition region and in a less steep transition region (peak sensitivity approx. 2.3 times lower than with a single a-PS overlay), as determined from a numerical analysis based on the theory reported in [13]. Moreover, thicker overlays to be deposited require high density solutions (up to 20% by weight of PMMA-co-MA) which can be difficult to

prepare. In addition, PMMA-co-MA absorbs a small amount of water which anyway can cause a considerable change of the optical properties of the polymer.

In light of these considerations, it is convenient to use a double-layer approach and minimize the thickness of the outer PMMA-co-MA layer.

UV-induced LPGs have been used in the framework of this project: three different grating periods (350μm, 370μm and 390μm) were employed to study its effect on the sensitivity of the final device.

The SRI characterization was performed by submerging the realized LPG transducer into aqueous glycerol solutions characterized by different refractive index in the range 1.335-1.46. The refractive index of each solution was measured by means of an Abbe refractometer, working at 589 nm.

## 7.3 Results and discussion

### 7.3.1 Fabrication of multilayer coated LPG reflection probes working in transition mode

In order to obtain the multilayer coated LPG ready to the next step, i.e. the biochemical functionalization, a specific procedure has to be performed. As done in the previous chapter, the main manufacturing steps are summarized in the table below.

**Table 1** Manufacturing steps of the multilayer coated LPG transducers prototypes.

| *Objective* | *Manufacturing steps* |
|---|---|
| Reflection type LPG transducer | - mirror integration at the end-face of the cut optical fiber |
| Multilayer coated LPG working in transition mode | - a-PS layer deposition<br>- PMMA-co-MA layer deposition |
| LPG probe characterization and validation | - SRI characterization<br>- prototype acceptance |

After the deposition of silver mirror on the tip of the LPG, the optical fiber has been coated with an a-PS layer. For the deposition of the ordinary a-PS film (RI=1.555), the fiber containing the LPG was first immersed into a PS solution and successively withdrawn with a well-controlled speed. The extraction step was 100 mm/min. Before the deposition, the LPG was thoroughly cleaned in boiling chloroform. Deposition solution was 9.5% (w/w) of PS in chloroform.
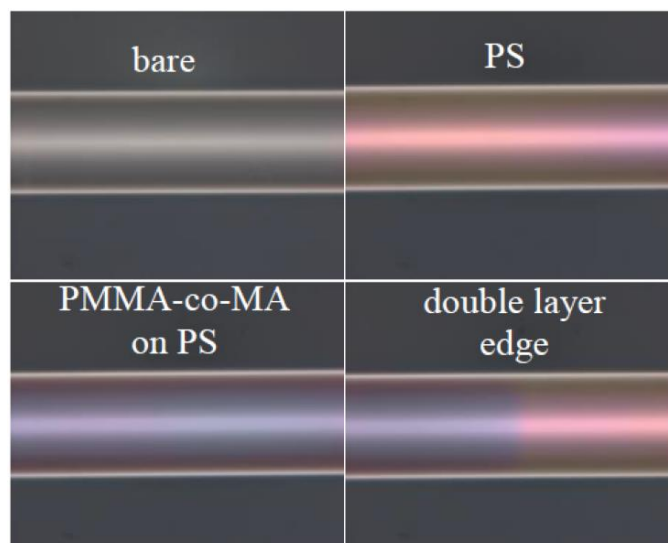


**Figure 2** Optical microscopy images of a double-layer coated optical fiber. Clock wise: bare, PS (pink), transition from PS to PMMA-co-MA on PS, central zone with the double layer of PMMA-co-MA on PS (violet).

The PS coated LPG was subsequently dip-coated into a solution 10% (w/w) PMMA-co-MA (Mw = 34,000 - Aldrich) in chloroform:isopropanol (1:3, v/v) for the formation of the secondary very thin layer of PMMSA-co-MA. Considering the relatively small amount (1.6%) of methacrylic acid in this PMMA co-polymer we assume its RI to be the same as the homopolymer, i.e. 1.49.

In Fig. 2 are reported some typical optical microscopy images of an optical fiber coated with the polymer double-layer in different positions along the fiber axis. The pictures reveal smooth and homogenous layers. Since a-PS and PMMA-co-MA are transparent polymers, the apparent colors are due to interference of the light reflected back from the different interfaces.

It is important at this point to highlight that the deposition of a second layer by DC implies the need for a solvent/nonsolvent strategy. In other words, the second layer should be deposited from a solution whose solvents would not damage the underlying layer. One important difficulty to consider in this system is that a-PS is an highly hydrophobic polymer while PMMA-co-MA has an hydrophilic nature, therefore the use of solvents with a higher polarity, with respect to chloroform, could prevent the good adhesion of the secondary layer and cause its slipping as well as de-wetting defects, as it was experimentally verified in the case of acetone, acetic acid, ethanol:water (1:1, v/v), MEK:isopropanol (1:1). The problem was solved by using a mixture of solvents containing a small amount of a mutual solvent for both polymers, in our case chloroform, and a major part of mutual nonsolvent, in our case isopropanol, in a volumetric ratio 1:3. In this way, the integrity of the first layer was preserved and good adhesion and uniformity of the secondary layer was ensured.

Once the realized LPG transducer has been realized and characterized, the final step before the prototype acceptance relies on the comparison between expected (i.e. from simulations) and experimental performances in terms of SRI sensitivity at an SRI=1.34

(because biological measurements will be conducted in a PH7 aqueous solution, which is characterized by a refractive index ~1.34). In the following paragraph, it is reported the results obtained for the manufacturing of the first three prototypes, carried out by using LPG 1, LPG 2 and LPG 3 ($\Lambda$ = 350μm, 370μm and 390μm, respectively).

*Prototype 1: Manufacturing, characterization and validation*

In this paragraphs the manufacturing, characterization and functional validation of Prototype 1 has been reported. According simulations for this device, to work in transition region the a-PS layer thickness must be 280 nm, enabling to reach a sensitivity as high as 1738nm/RIU.

The first manufacturing step relies on the realization of the reflection type LPG. To this aim, in Fig. 3 is shown the spectra in air of LPG 1, acquired just before the optical fiber cut (i.e. in transmission configuration), just after the optical fiber cut (i.e. in reflectance configuration before the mirror formation) and after the mirror integration at the end of the cut fiber (with Tollens' reactant).



**Figure 3** Experimental spectra acquired in air for LPG 1 before the optical fiber cut (i.e. in transmission configuration), just after the optical fiber cut (i.e. in reflectance configuration before the mirror formation) and after the mirror integration at the fiber termination.

It can be seen that, after the optical fiber cut, a strong baseline reduction occurs. Nevertheless, as soon as the Ag mirror is formed at the fiber termination, almost all the initial power is recovered.

The prototype manufacturing continued with the double layer (a-PS and PMMA-co-MA) deposition onto the LPG surface. Figure 4 shows the spectral position of the attenuation band related to the 6th order cladding mode for the bare LPG and for the a-PS coated device (both in reflection configuration). In particular the resulting overlay thickness after DC from the 9.5% a-PS solution was ~260 nm while the secondary layer obtained from the 10% PMMA-co-MA solution was estimated to be ~30 nm, as inferred by numerical simulations carried out by means of the developed virtual environment.

As previously described, when an HRI overlay is deposited onto the grating the effective RI of the cladding modes is increased; therefore the central wavelengths of the attenuation bands experience a blue shift, which for the 6th order cladding mode in Fig. 4 was about 13.8 nm. The second layer of PMMA-co-MA produced a cumulative effect of 4.2 nm on the attenuation band shift. The goodness of the deposition process is also testified by the subsistence of the attenuation band visibility. In fact, a secondary layer with defects would have determined a dramatic decrease of the attenuation bands depth due to scattering losses [14].
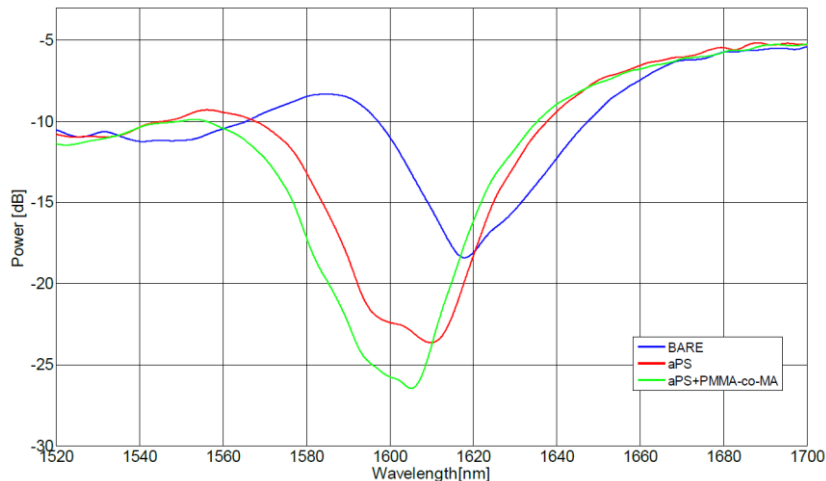


**Figure 4** Effect of the a-PS and PMMA-co-MA overlays deposition on the sixth order cladding mode attenuation band of LPG 1.

The spectral characterization to SRI changes obtained with Prototype 1 is reported in Fig. 5.a in terms of central wavelengths of the attenuation bands position. It refers to the sixth order cladding mode. Experimental data were fitted with a Lorentzian-Cumulative function. The resonance-shaped sensitivity characteristic of the coated device is reported in Fig. 5.b, as extrapolated from the experimental results.

In particular, it can be seen that the SRI sensitivity in correspondence of an SRI=1.34 turned out to be ~1918nm/RIU. This experimental value resulted slightly higher than the expected one (1738nm/RIU): this is probably due to the slight differences between numerical and experimental values of the refractive indexes of the a-PS and PMMA-co-MA layer, as well as of the glycerol solution used for the SRI sensitivity characteristic. However, the realized prototypes was clearly accepted, as it performs even better than the designed device.
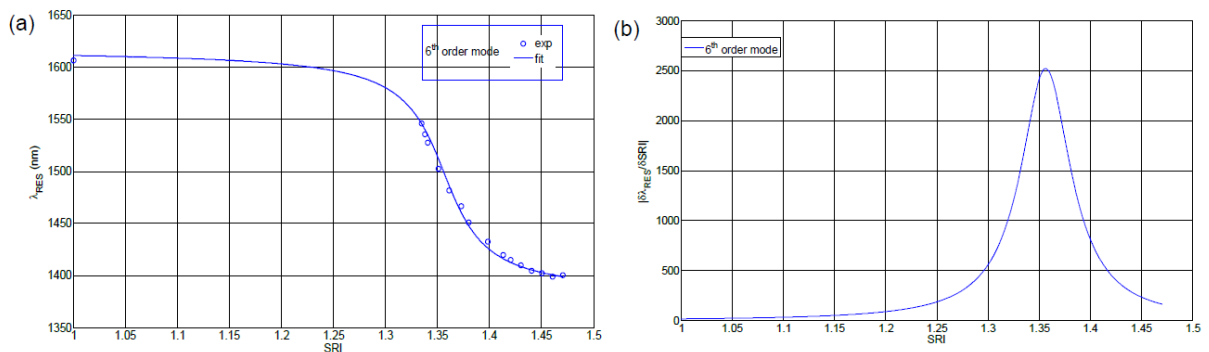


**Figure 5** a) SRI characterization in terms of attenuation bands minima position for the 6$^{th}$ order cladding mode; b) SRI sensitivity ($|\partial\lambda res/\partial SRI|$) of the sixth order cladding modes extrapolated from data reported in (a).

*Prototype 2: Manufacturing, characterization and validation*

In this paragraphs the manufacturing, characterization and functional validation of Prototype 2 has been reported. According simulations for this device, to work in transition region the a-PS layer thickness must be 270 nm, enabling to reach a sensitivity as high as 1304 nm/RIU. The spectra in air of LPG 2, acquired before the optical fiber cut, after the optical fiber cut (i.e. in reflectance configuration before the mirror formation) and after the mirror integration are reported in Fig. 6.
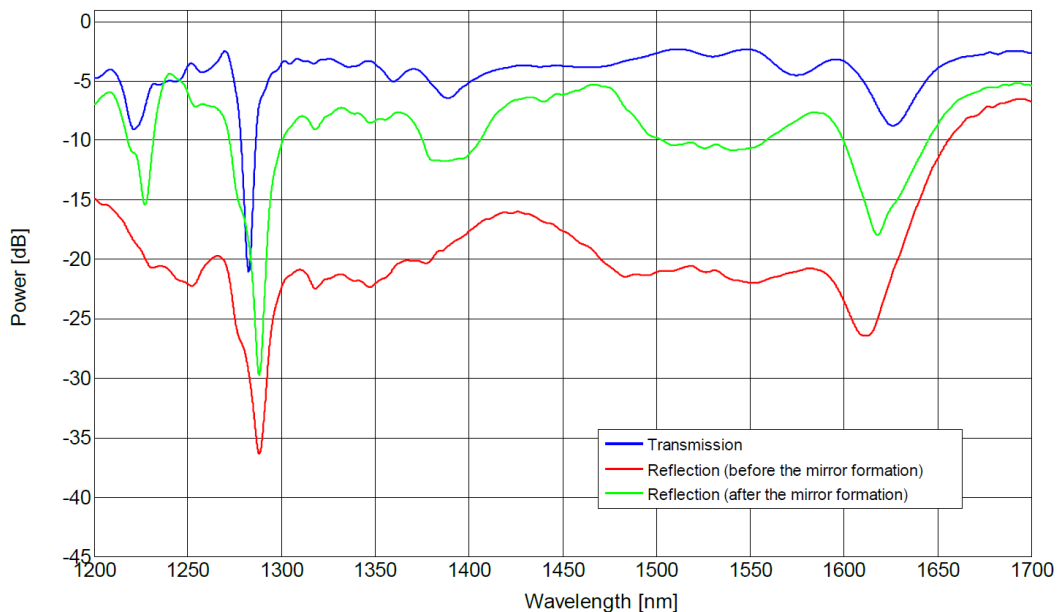
**Figure 6** Experimental spectra acquired in air for LPG 2 before the optical fiber cut (i.e. in transmission configuration), just after the optical fiber cut (i.e. in reflectance configuration before the mirror formation) and after the mirror integration at the fiber termination.

Also in this case, a strong baseline reduction is observed when cutting the fiber containing the LPG 2, which is almost recovered after the integration of the Ag reflecting metallic layer.



**Figure 7** Effect of the a-PS and PMMA-co-MA overlays deposition on the 5th order cladding mode attenuation band of LPG 2

Figure 7 shows the spectral position of the attenuation band related to the fifth order cladding mode for the bare LPG and for the a-PS coated device. The resulting overlay thickness after DC from the PS solution was estimated to be ~270 nm while the secondary layer obtained from the 10% PMMA-co-MA solution was estimated to be ~40 nm. The

92

a-PS deposition caused the central wavelengths of the attenuation bands of the fifth order mode to blue shift of about 11.5 nm, while the second layer of PMMA-co-MA produced a cumulative effect of about 4.0 nm on the attenuation band shift.

Fig. 8.a reports the spectral characterization to SRI changes obtained with the fifth order mode of Prototype 2, whereas its sensitivity vs. SRI is reported in Fig. 8.b. Also in this case the experimental results are slightly better than the expected ones: indeed a sensitivity for an SRI=1.34 of ~1498nm/RIU was estimated, with respect to the expected 1304nm/RIU.



**Figure 8** a) SRI characterization in terms of attenuation bands minima position for the 5th order cladding mode; b) SRI sensitivity ($|\partial\lambda res/\partial SRI|$) of the 5th order cladding modes extrapolated from data reported in (a).

*Prototype 3: Manufacturing, characterization and validation*

In this paragraphs the manufacturing, characterization and functional validation of Prototype 2 has been reported. According simulations for this device, to work in transition region the a-PS layer thickness must be 270 nm, enabling to reach a sensitivity as high as 1146 nm/RIU. The spectra in air of LPG 3, acquired before the optical fiber cut, after the optical fiber cut (i.e. in reflectance configuration before the mirror formation) and after the mirror integration are reported in Fig. 9.
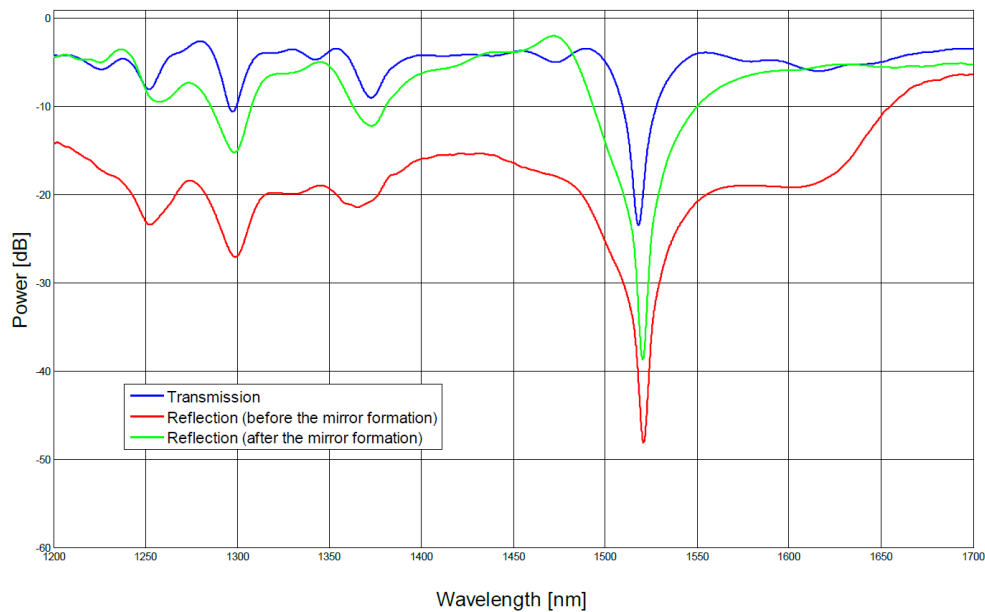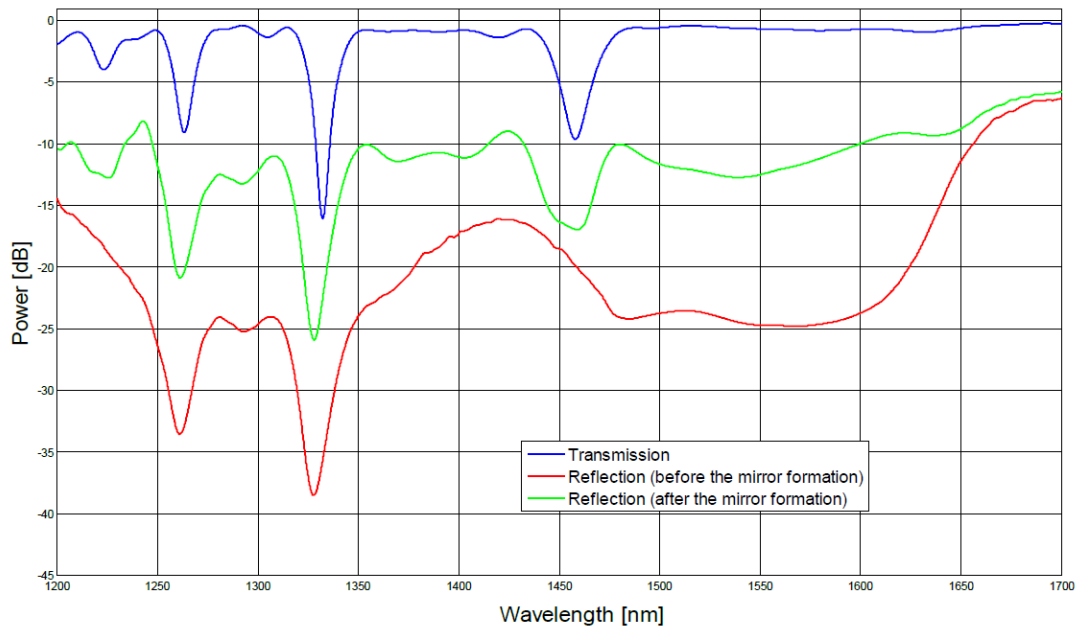
**Figure 9** Experimental spectra acquired in air for LPG 3 before the optical fiber cut (i.e. in transmission configuration), just after the optical fiber cut (i.e. in reflectance configuration before the mirror formation) and after the mirror integration at the fiber termination.
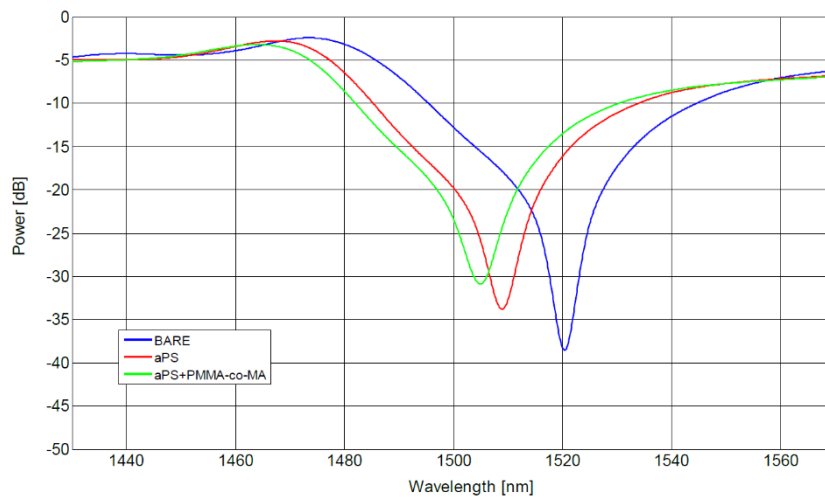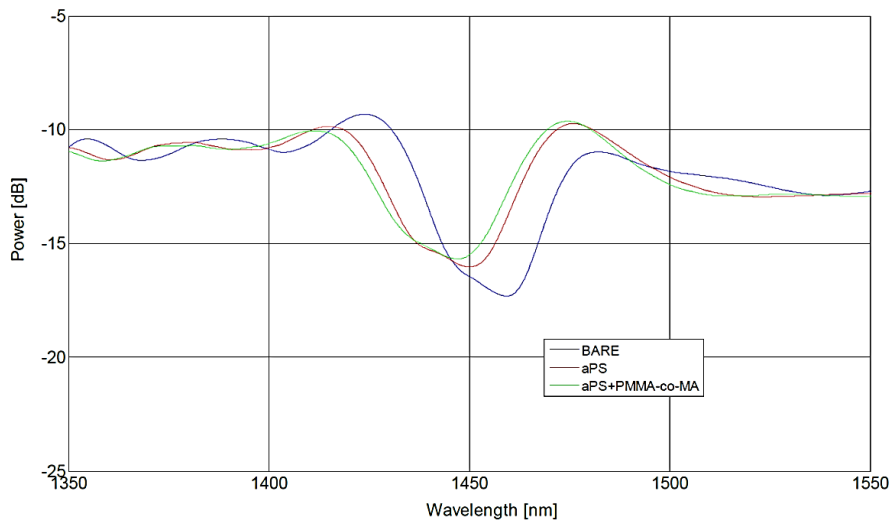


**Figure 10** Effect of the a-PS and PMMA-co-MA overlays deposition on the $5^{th}$ order cladding mode attenuation band of LPG 3.

Figure 10 shows the spectral position of the attenuation band related to the $5^{th}$ order cladding mode for the bare LPG and for the a-PS coated device. The resulting overlay thickness after DC from the PS solution was estimated to be ~260 nm while the secondary layer obtained from the 10% PMMA-co-MA solution was estimated to be ~30 nm. The a-PS deposition caused the central wavelengths of the attenuation bands of the $5^{th}$ order

mode to blue shift of about 9.4 nm, while the second layer of PMMA-co-MA produced a cumulative effect of about 2.58 nm on the attenuation band shift.

Fig. 11.a reports the spectral characterization to SRI changes obtained with the 5th order cladding mode of Prototype 3, whereas its sensitivity vs. SRI is reported in Fig. 11.b.
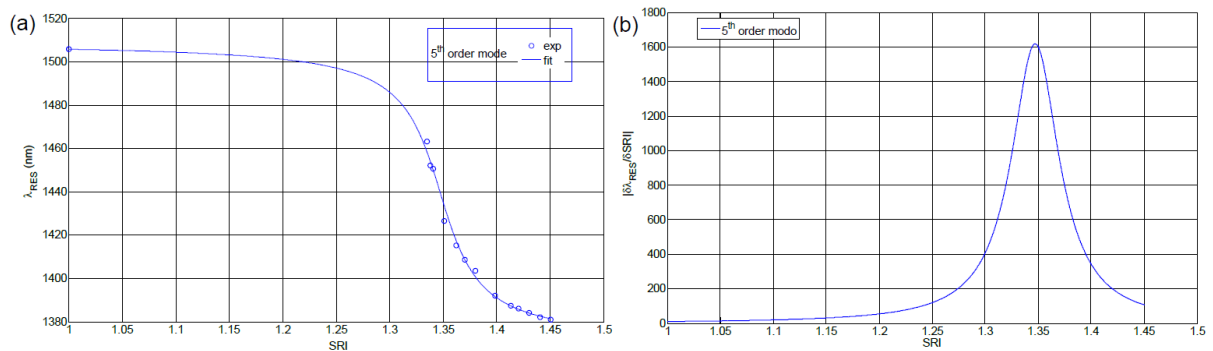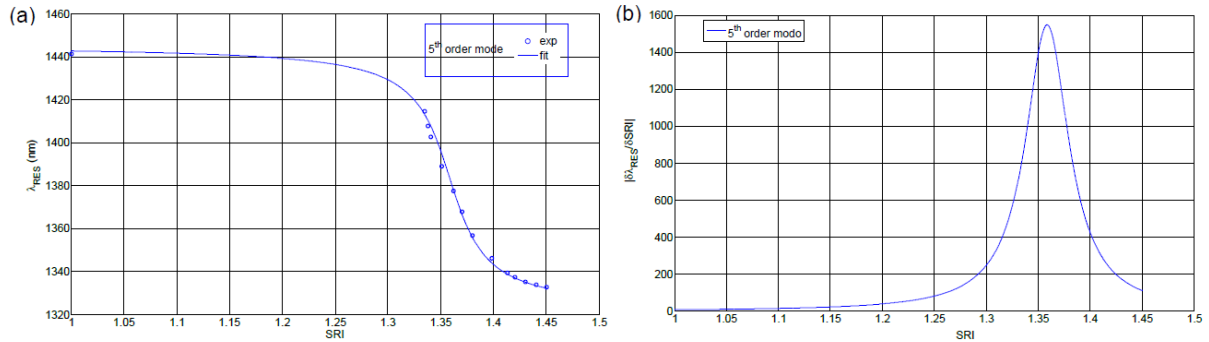


**Figure 11** a) SRI characterization in terms of attenuation bands minima position for the 5th order cladding mode; b) SRI sensitivity ($|\partial\lambda res/\partial SRI|$) of the 5th order cladding modes extrapolated from data reported in (a).

Once more, the experimental performances are slightly better than the expected ones, since a sensitivity for an SRI=1.34 of ~1188 nm/RIU was estimated, with respect to the expected value of 1146 nm/RIU.

## 7.3.2 Chemical functionalization of sensor surface

After a ligand-BL (3-APBA) was chosen, anchoring of the ligand was carried out exploiting established covalent coupling techniques. The proper linkage chemistry was carried out to anchor the bioreceptor to the external layer of the probe. With the carboxylic functions chosen as anchoring points on the probe surface and $-NH_2$ groups presents on the ligand, the linkage chemistry is consisted in well-established protocols developed for solid-phase peptide synthesis. These is consisted in the initial activation of the carboxyl group through a reaction with EDC and NHS, leading to an amine-reactive ester, and a successive reaction with a primary amino group present on the ligand. Once the probe surface had been functionalized by the ligand, the retention of its biological activity is evaluated carrying out the interaction studies with the complementary BL, also taking

into consideration local parameters that may influence the binding, such as aggregation, pH and ionic strength.

The a-PS and PMMA-co-MA coated sensor ('Prototype 2') surface was immersed in a phosphate buffer solution at pH=5. After the optical stabilization of the sensor, a solution of 0.05M of EDC (~98%, Sigma-Aldrich) with 0.03M of NHS (~98%, Sigma- Aldrich) was added, to activate the carboxylic groups (-COOH) of PMMA-co-MA. In Fig. 12 it is reported the chemical reaction.
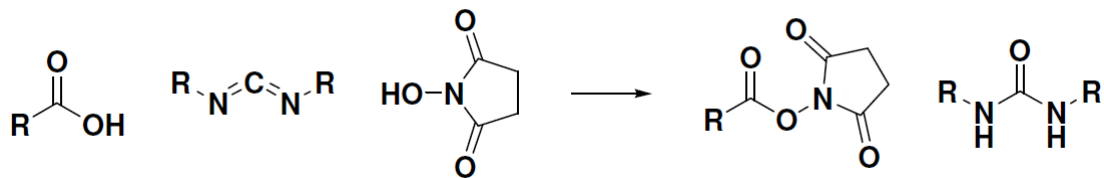


**Figure 12** The chemical reaction of the –COOH groups of the sensor surface with the EDC/NHS to obtain the esterification of carboxyl group.

After the stabilization of the optical signal, the sensor was immersed in a clean buffer solution at pH=5. It is worth observing that each time grating is extracted/submerged into an aqueous environment there is a sort of acclimation of the polymeric layer expressed through a quite fast red wavelength shift. Dynamics of chemical functionalization were continuously monitored through automated spectral acquisition.
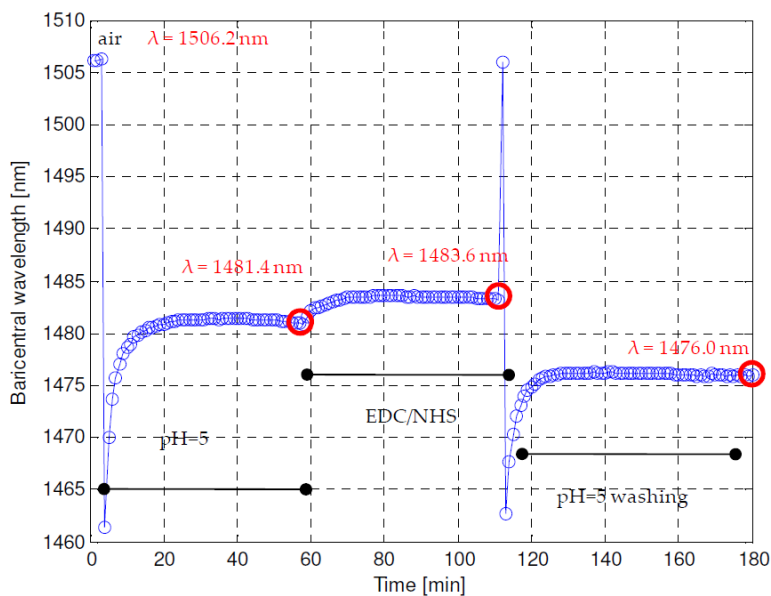


**Figure 13** Baricentral wavelength variation vs. time due to the chemical functionalization of sensor surface.

In Fig. 13 it can be observed the dynamic of the barycentral wavelength shift of sensor surface during the time; in the first step the sensor surface was immersed in a phosphate buffer solution at pH=5 for about 40 min, after the stabilization of the optical signal, the sensor surface was immersed in the EDC/NHS solution for about 40 min. In the second step, the sensor surface was immersed in a clean buffer phosphate solution at pH=5. The so functionalized sensor surface was immersed in a phosphate buffer solution at pH=7; after the stabilization of the optical signal, a 3-APBA solution, was added. In Fig. 14 it is reported the chemical reaction.
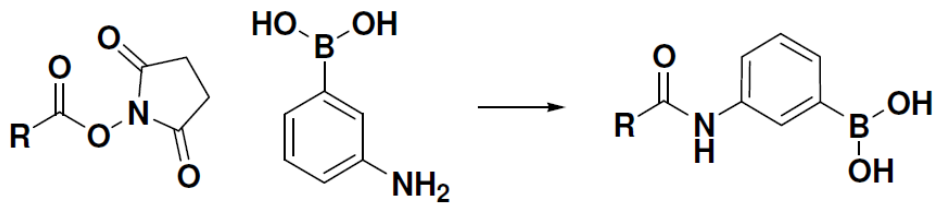


**Figure 14** The covalent attachment of the chosen ligand of 3APBA.
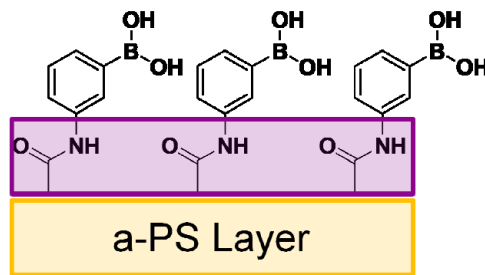


**Figure 15** A scheme of the sensor surface.
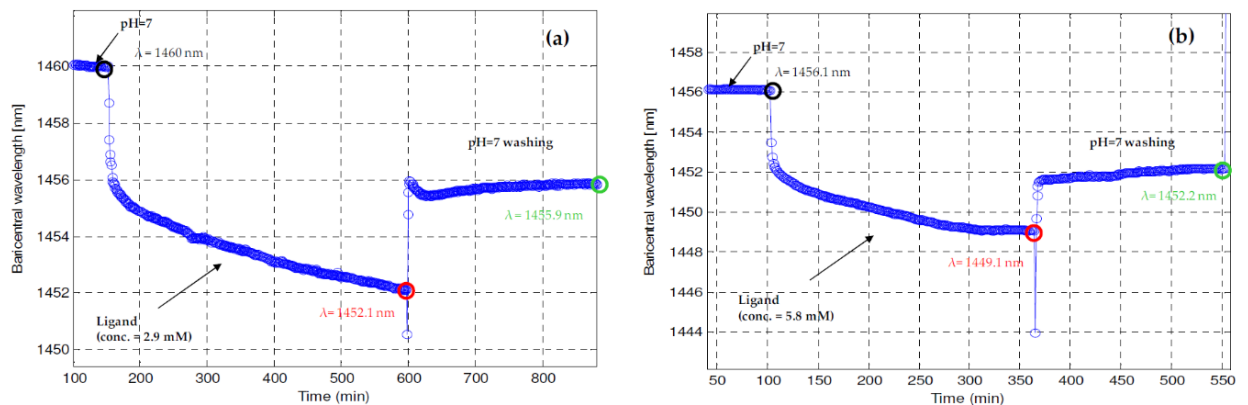


**Figure 16** Barycentral wavelength variation vs. time due to the bioanchoring of 3-APBA at (a) 2.9 mM and (b) 5.8 mM.

The 3-APBA solutions used are at different concentrations of 2.9 and 5.8 mM. Dynamics of chemical binding of ligand were continuously monitored through automated spectral acquisition. After the chemical functionalization by means of EDC/NHS solution, the LPGs sensor surface was immersed into a phosphate buffer solution at pH=7.

In Fig. 16.a it can observe the dynamic of the barycentral wavelength shift of sensor surface during the time; in the first step the sensor surface was immersed in a phosphate buffer solution at pH=7, after the stabilization of the optical signal, the sensor surface was immersed in the 3-APBA solution at 2.9 mM. In the second step, the sensor surface was immersed in a clean buffer phosphate solution at pH=7. In Fig. 16.b it can observe the dynamic of the barycentral wavelength shift of sensor surface during the time; in the first step the sensor surface was immersed in a phosphate buffer solution at pH=7, after the stabilization of the optical signal, the sensor surface was immersed in the 3-APBA solution at 5.8 mM. Also in this case, the sensor surface was immersed in a clean buffer phosphate solution at pH=7.

## 7.3.3 First verification of the preservation of 3-APBA capability of binding the BL
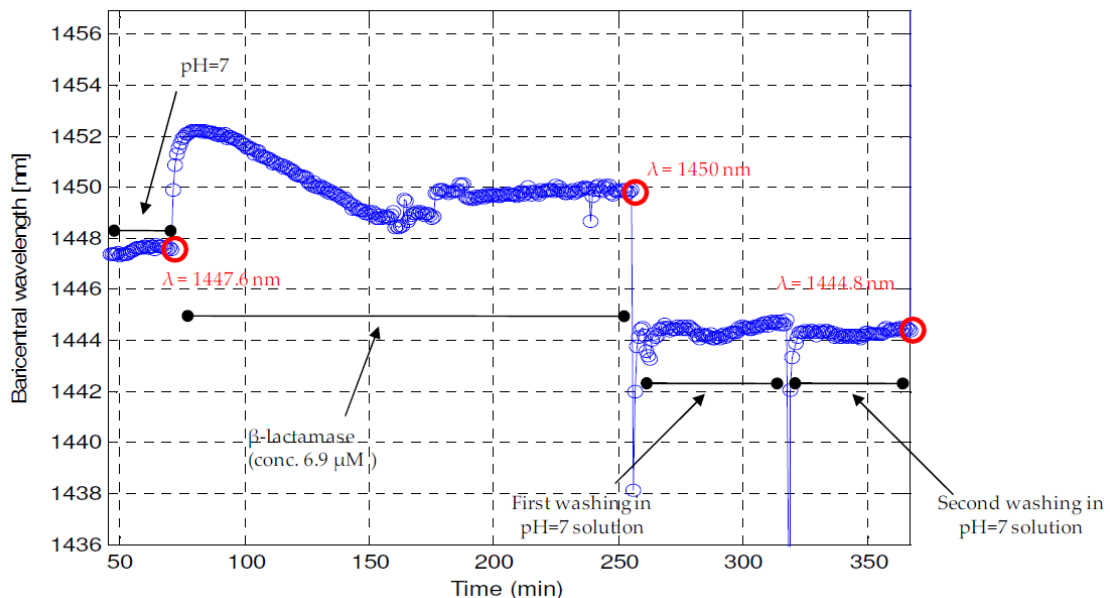


**Figure 17** Barycentral wavelength variation vs. time related to the affinity binding of the ligand to the β-lactamase.

After optical stabilization, the coated LPG was immersed in a phosphate buffer solution at pH=7, after the stabilization of the optical signal the β-lactamase solution (6.9 μM) was added. In Fig. 17 is reported the dynamic related to the affinity binding of the ligand to the β-lactamase. In Figure 11 it is possible to note that there was a wavelength shift when the β-lactamase was added, that means that the protein is binding.

## 7.4 Data analysis interpretation

### 7.4.1 Analysis of the LPG biosensor response to the permanent attachment of 3-APBA

In this section, it is provided an analysis of the LPG biosensor ('Prototype 2') response to the permanent attachment of the 3-APBA onto its chemically functionalize surface. In particular, here we analyze the barycentral wavelength variation of the attenuation band of the LPG biosensor that occurs when it is immersed in 3-APBA solutions with two different concentrations, namely 2.9 and 5.8 mM.

As described in the previous sections, the test of ligand attachment essentially consists of three main steps:

1) the LPG probe (after the EDC/NHS coupling chemistry) is first immersed in a vial containing a phosphate buffer solution at pH=7. After a sort of acclimation of the polymeric layers, the biosensor response reaches a plateau value ($\lambda_{pH7}$);

2) successively a varying volume of ligand solution is added to the vial so as to obtain the desired 3-APBA concentration; the whole ligand binding kinetic is monitored until the LPG response reaches a baseline value ($\lambda_{ligand}$); this is carried out by means of an automated spectral acquisition system enabling a continuous tracking of the LPG attenuation band as well as the recovery of its baricentral wavelength;

3) finally, the probe is extracted from the vial and is immersed in a clean phosphate buffer solution at pH=7 (the same solution used in the step 1 ) in order to remove the ligand molecules that are not permanently bound to the probe surface. Once completed the washing procedure the LPG signal reach a new plateau (henceforth referred to as $\lambda_{pH7washing}$).

As evident from Figure 18, where the sensorgram (i.e. the baricentral wavelength variation of the LPG attenuation band vs. time) of a generic test of ligand attachment has been reported, it is possible to identify two different LPG output signal variations:

$$\Delta_{\textbf{before-washing}} = \lambda_{\textbf{ligand}} - \lambda_{\textbf{pH7}} \text{ (red arrow)}$$

and

$$\Delta_{\textbf{after-washing}} = \lambda_{\textbf{pH7 washing}} - \lambda_{\textbf{pH7}} \text{ (green arrow)}$$
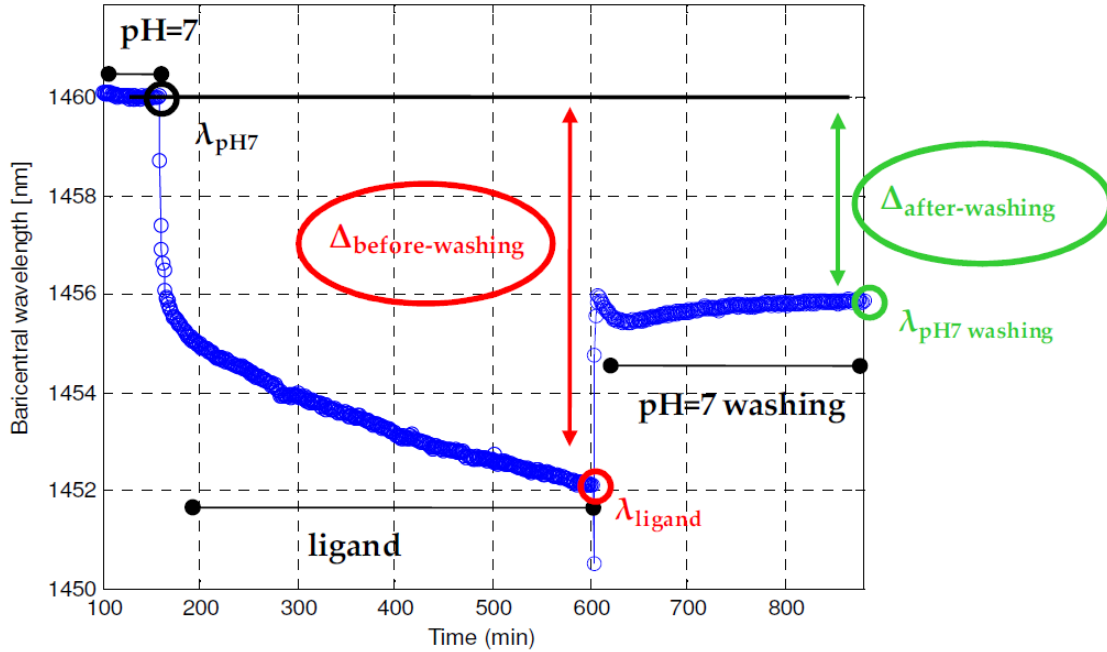


**Figure 18** Generic test of ligand attachment.

$\lambda_{\text{before-washing}}$ is the baricentral wavelength shift of the LPG attenuation band due to the attachment of ligand on the sensor surface evaluated before the washing procedure, i.e. when the probe is still immersed into the 3-APBA ligand solution. In the most general case, in absence of thermal variations, this quantity can be expressed as the sum of three contributions:

$$\Delta_{\textbf{before-washing}} = \Delta_{\textbf{bulk}} + \Delta_{\textbf{Permanent}} + \Delta_{\textbf{not-Permanent}}$$

where $\Delta_{\text{bulk}}$ is the output signal variations (wavelength shift of the attenuation band) due to the difference between the refractive indices of the clean pH=7 solution (used in the step 1) and the ligand one (used in the step 2), $\Delta_{\text{Permanent}}$ is the wavelength shift due to the ligand permanently bound to the chemically functionalized surface of the LPG (or better to the formation of a layer of ligand permanently bound to the LPG surface), $\Delta_{\text{not-Permanent}}$

is the wavelength shift due to the adsorption of ligand that is not permanently bound to the sensor surface.

On the other hand, $\Delta_{\text{after-washing}}$ is the barycentral wavelength shift of the LPG attenuation band due to the ligand attachment on the sensor surface evaluated after the washing procedure, i.e. when the probe is immersed into a clean phosphate buffer solution at pH=7. In absence of thermal variations, it can be expressed as:

$$\Delta_{\textbf{after-washing}} = \Delta_{\textbf{permanent}}$$



**Figure 19** Baricentral wavelength variation vs. time obtained by two ligand attachment tests using a 3-APBA solution concentration of 2.9 mM (a) and 5.8 mM (b), respectively.

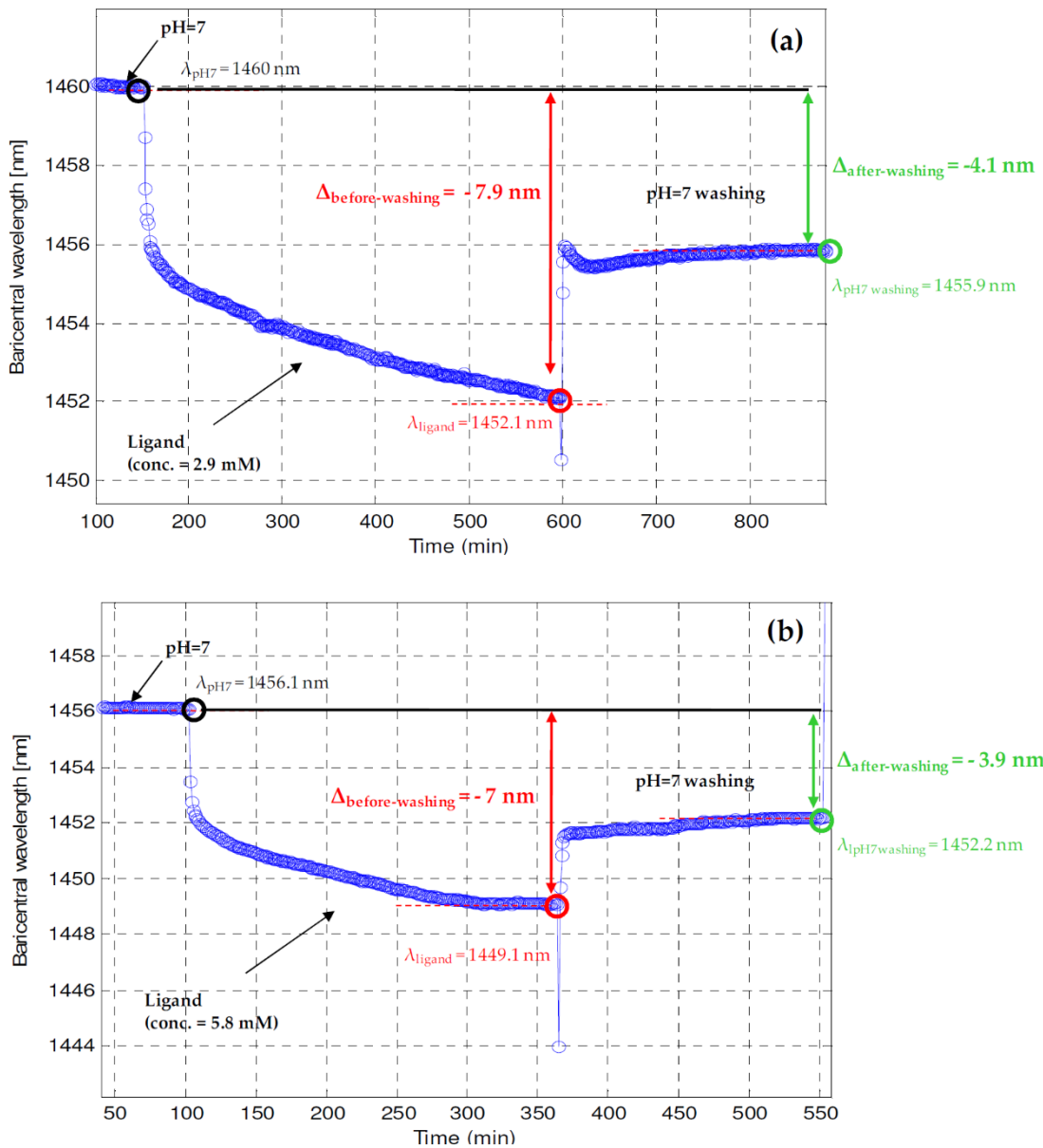In this case, indeed, the ligand not-permanently bound to the surface is completely removed by the washing cycles ($\Delta_{\text{not-Permanent}} = 0$) and the refractive indices of the phosphate buffer solutions at pH=7, before and after the ligand insertion, are the same ($\Delta_{\text{bulk}} = 0$).

Therefore, on the basis of these considerations, it is clear that by evaluating the $\Delta_{\text{after-washing}}$ for each ligand solution concentration, it is possible to evaluate the LPG signal variation due exclusively to the formation of an ultra-thin layer of 3-APBA (of the order of a few nanometers) that is permanently attached on the chemically functionalized LPG surface. After this brief introduction useful to elucidate the analysis methodologies and the quantities under investigations, let analyze further in detail the LPG biosensor response to the permanent attachment of the 3-APBA occurred by using two ligand solutions with different concentrations, namely 2.9 and 5.8 mM.

In Fig. 19 the sensorgrams obtained by using a 3-APBA solution with concentration of 2.9 mM (a) and 5.8 mM (b) have been reported. In particular, Fig. 19.a refers to a first test, where a 3-APBA concentration of 2.9 mM has been used. As it can be seen, the baseline of the sensor response when the LPG is immersed into the phosphate buffer solution at pH=7 (before the ligand addiction) is $\lambda_{\text{pH7}}=1460.0$ nm. As soon as the 3-APBA solution is added to the buffer solution, the LPG output signal decreases (the attenuation band undergoes a blue-shift) until it reaches a plateau level at $\lambda_{\text{ligand}}=1452.1$ nm. During the washing procedure, the ligand molecules not permanently bound to the probe surface tend to detach from it (and the $\Delta$bulk become equal to 0), thus leading to a recovery (the attenuation band red-shifts) of the sensor response until the plateau value $\lambda_{\text{pH7washing}}=1455.9$ nm. The observed values for $\Delta_{\text{before-washing}}$ and $\Delta_{\text{after-washing}}$ are 7.9 nm and 4.1 nm, respectively, in correspondence of a 3-APBA solution concentration of 2.9mM. When a higher 3-APBA solution concentration (5.8 mM) was used, the $\lambda_{\text{pH7}}$,

$\lambda_{\text{ligand}}$ and $\lambda_{\text{pH7washing}}$ were respectively 1456.1 nm, 1449.1 nm and 1452.2 nm, with a $\Delta_{\text{before-washing}}$ equal to 7.0 nm and a $\Delta_{\text{after-washing}}$ of 3.9 nm.

From the reported results, it is possible to state that the signal recovery is not complete ($\Delta_{\text{afterwashing}} \neq 0$), demonstrating that an ultrathin layer of 3-APBA effectively remains permanently attached on the functionalized LPG surface.

These results confirm that:

- the chemical functionalization allows the carboxylic groups activation and enables the permanently attachment of the 3-APBA ligand onto the coated LPG surface;

- the high surface sensitivity of the coated-functionalized LPG allows the detection of a 3-APBA ligand ultrathin layer, permanently attached onto the LPG probe surface. It is important to remark that the ligand size is significantly lower than the size of the target β-lactamase protein;

The following table summarizes the $\Delta_{\text{before-washing}}$ and $\Delta_{\text{after-washing}}$ values for the two used 3-APBA ligand concentrations:

**Table 1** Resume of the $\Delta_{\text{before-washing}}$ and $\Delta_{\text{after-washing}}$ obtained for the two used 3-APBA ligand concentrations.

| *3-APBA solution concentration* | *Δbefore-washing* | *Δafter-washing* |
|---|---|---|
| 2.9 mM | 7.9 nm | 4.1 nm |
| 5.8 mM | 7.0 nm | 3.9 nm |

It is worth considering at this point, that the ligand attachment in the test so far reported takes place in successive addictions, i.e. the 3-APBA attachment occurring in case of the highest concentration (5.8 mM) takes place on the LPG functionalized surface already covered (completely or only partially) by an ultra-thin ligand layer (i.e. the one formed when the lowest concentration was used).

Therefore, in this case it is preferable defining two further quantities ($\Delta_{\text{before-washing\_cumulative}}$ and $\Delta_{\text{after-washing\_cumulative}}$) enabling to take into account this cumulative effect:

$$\Delta_{\textbf{before-washing\_cumulative}} = \sum\nolimits_{\textbf{i=1-n}} \Delta_{\textbf{before-washing(concentration\_i)}}$$

$$\Delta_{\text{after-washing\_cumulative}} = \sum_{i=1-n} \Delta_{\text{after-washing(concentration\_i)}}$$

In Figure 20, it is plotted these cumulative quantities $\Delta_{\text{before-washing\_cumulative}}$ (blak squares) and $\Delta_{\text{after-wahing\_cumulative}}$ (red circles), as a function of the 3-APBA cumulative concentration. It can be observed that they both increase with the cumulative ligand concentration, with the $\Delta_{\text{afterwahing\_cumulative}}$, in particular, showing a quadratic trend.
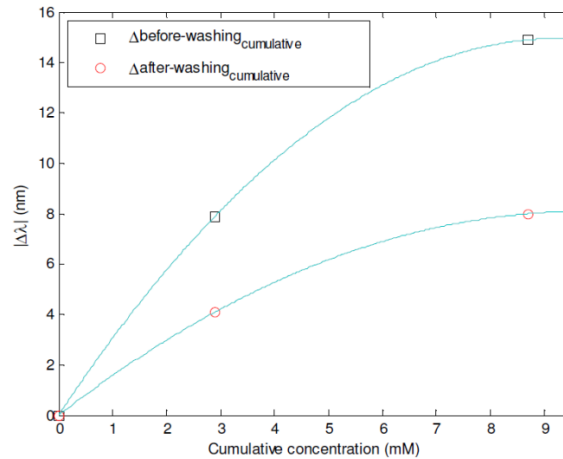


**Figure 19** $\Delta_{\text{before-washing\_cumulative}}$ and $\Delta_{\text{after-wahing\_cumulative}}$ as a funtion of the 3-APBA ligand cumulative concentration

## 7.4.2 Analysis of the LPG biosensor response to the 3-APBA capability of binding the BL

After previously analysis, devoted to investigates the LPG biosensor response to the permanent attachment of 3-APBA, let analyze further in detail the sensor response to the binding capability of the β-lactamase. In Fig. 20 the sensorgrams obtained by using a β-lactamase with concentration of 6.9 μM has been reported. As it can be seen, the baseline of the sensor response when the LPG is immersed into the phosphate buffer solution at pH=7 (after the ligand attachment procedure) is $\lambda_{\text{pH7}}=1447.6$ nm. As soon as the β-lactamse solution is added to the buffer solution, the LPG output signal increases (the attenuation band undergoes a red-shift) until it reaches a plateau level at $\lambda_{\text{β-lactamase}}=1450$ nm. During the washing procedure, the β-lactamase molecules not permanently bound to the probe surface tend to detach from it (the $\Delta_{\text{bulk}}$ become equal to 0), and the sensor response until the plateau value $\lambda_{\text{pH7washing}}=1444.8$ nm.
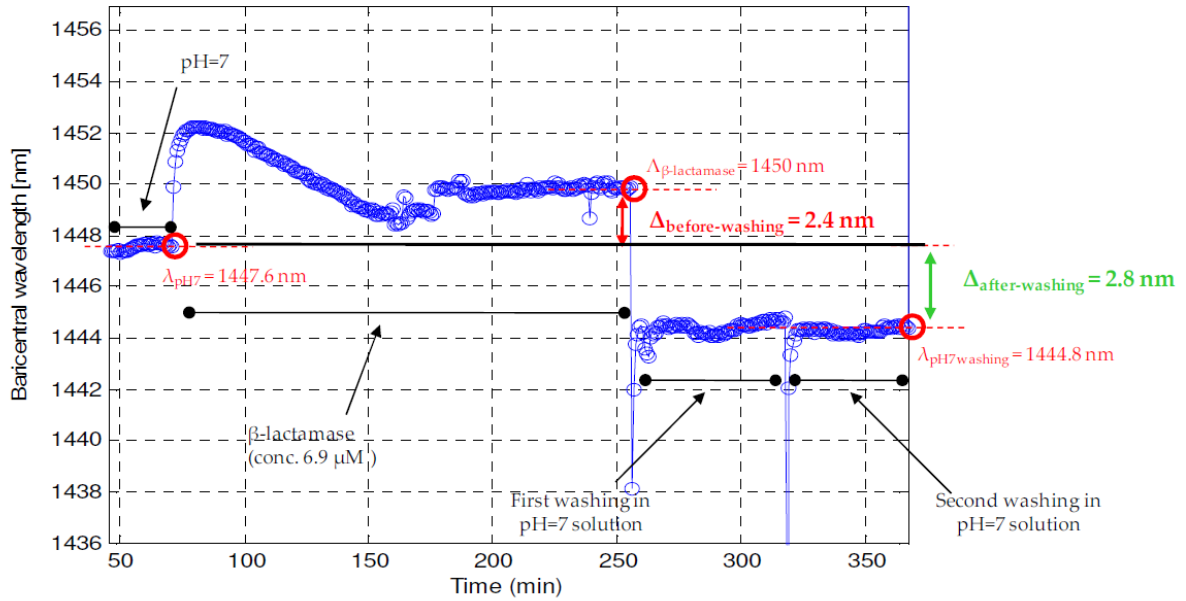
**Figure 20** Baricentral wavelength variation vs. time obtained by the β-lactamase binding with the 3APBA ligand.

The calculated values for $\Delta_{\text{before-washing}}$ and $\Delta_{\text{after-washing}}$ are respectively 2.4 nm and 2.8 nm.

In particular, the $\Delta_{\text{after-washing}}$ is the wavelength shift due to the β-lactamase molecules permanently attached onto the LPG surface.

These results confirm that:

-   the attachment of the 3-APBA ligand onto the chemical functionalized surface of the LPG probe (as described in the previously section) allows the β-lactamase protein binding;

-   the proposed biosensor is able to detect the β-lactamase binding onto the biofunctionalized LPG surface.

## 7.5   Design and realization of an automated robotic arm.

Aim of the OPTOBACTERIA Project was the design of an Automated Laboratory Detector (ALD), mainly consisting on an automatic robot able to perform repetitive and controlled tests on a series of biological samples by using multiple LPG biosensors simultaneously. The design phase started from a general view of the ALD, a schematic representation  of which is shown in Figure 5.1. Here, the ALD has been conceived as composed of:

1)   a sensing head holder, allowing the control of up to eight fiber optic biosensors simultaneously;

2)   a couvettes carousel, having Functionalization, Samples and Rinse areas, divided according to the specific needs, in order supply the ALD with the additional functionality of being able to automatically realize the chemical functionalization, the ligand immobilization along with the biological tests starting from a general purpose probe (i.e. from the LPG transducer, with the a-PS and the PMMA coatings);
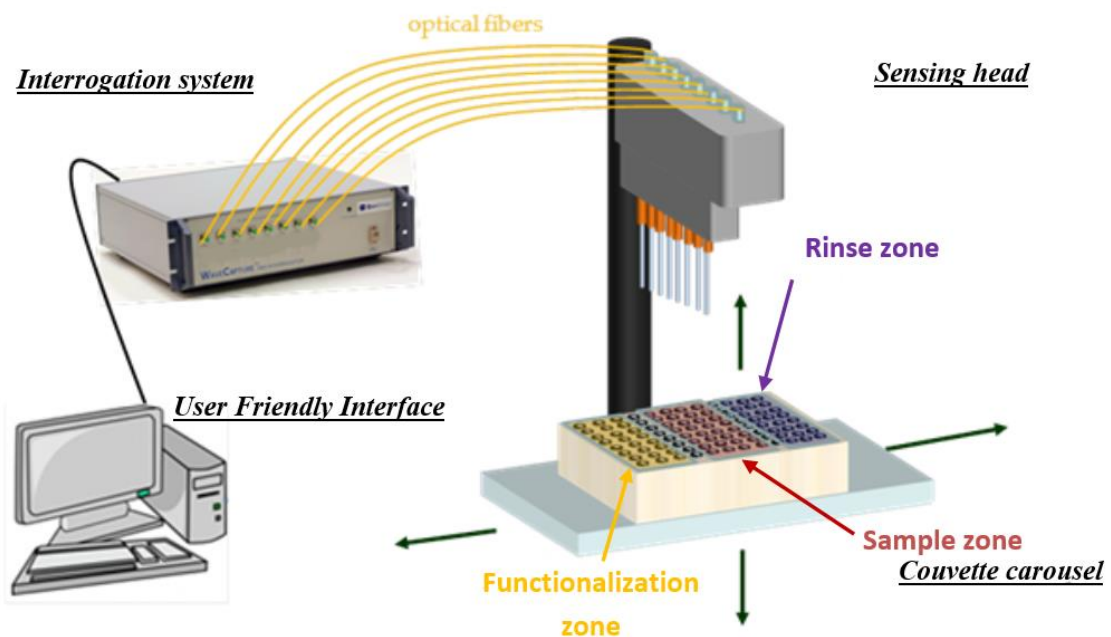


**Figure 21** General view of the ALD.

3)  a proper optoelectronic unit for the interrogation of the LPG–based reflection probes;

4)  a PC with dedicated software for command and control of the Robotic work.

The designed system is composed of two main parts: the <u>test chamber</u>, containing a sensor mount, able to hold up to eight LPG biosensor, a couvette carousel holding a 96-well plate, and two linear actuators, responsible for the movements of the well-plate along the vertical and the horizontal directions, and the <u>rear region</u>, hosting the optoelectronic interrogation unit and the electronic circuits for the control of the entire system, the connection with the host PC and the power supply.

Once defined the design criteria, the ALD system has been assembled, and all its components have been included in a suitable enclosure. The test chamber, where the biological tests take place, is shown in Fig. 22, where the enclosure has been opened to show the inside. It is possible to distinguish the two-dimensional translation stages (horizontal, X and vertical, Z), the sensor holder with eight LPG transducers mounted, and the couvettes carousel with a 96-well plate.
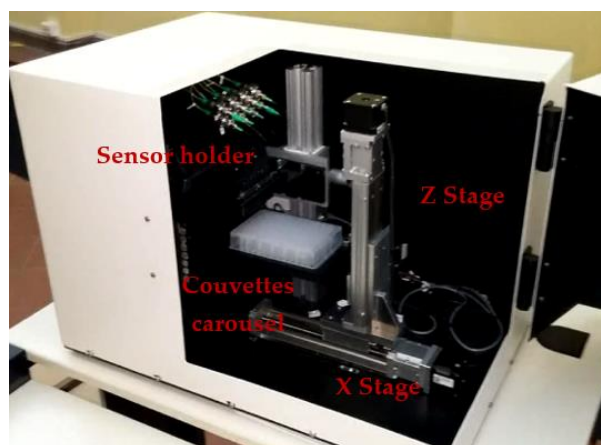


**Figure 22** A view of the manufactured ALD, showing the test chamber.

The developed ALD, comprising both the mechanical stages and the optoelectronic interrogation unit and its related software, has been subjected to a phase of test and debugging. Once carried out the test of the single parts, the whole system operation was

tested for making simultaneous biological tests with up to eight LPG probes. The complete kinetics of the binding of a ligand on the surface of each LPG probe and a typical β-lactamase detection tests have been monitored.

# References

[1] http://www.optobacteria.eu.

[2] N.M. Mitchell, G.G. Rao, J. Wong. *ESBL Detection Kit and Method*, US Patent 20100203567 (2010).

[3] X. Fan, I.M. White, S.I. Shopova. *Analytica Chimica Acta*, **620**(1-2), 8-26 (2008).

[4] X. Chen, L. Zhang, K. Zhou. *Opt. Lett.*, **32**, 2541-2543 (2007).

[5] M. Smietana, W.J. Bock, P. Mikulic. *Opt. Express*, **19**, 7971-7978 (2011).

[6] Z. Wang, J.R. Heflin, K.V. Cott. *Sensors and Actuators B: Chemical*, **139**(2-4), 618-623 (2009).

[7] A. Cusano, A. Iadicicco, P. Pilla. *Opt. Express*, **14**(1), 19–34 (2006).

[8] P. Pilla, P. Foglia Manzillo, V. Malachovska. *Opt. Express*, **17**, 20039–20050 (2009).

[9] I. Del Villar, I. R. Matías, F.J. Arregui. *Opt. Express*, **13**(1), 56–69 (2005).

[10] P. Pilla, V. Malachovská, A. Borriello. *Opt. Express*, **19**, 512–526 (2011).

[11] K.M. Stoeffler, C. Dubois, A. Ajji. *Polym. Eng. Sci.*, **50**, 1122-1127 (2010).

[12] H. Ma, A.K.Y. Jen, L.R. Dalton. *Adv. Mater.*, **14**, 1339-1365 (2002).

[13] D. Ennis, H. Betz, H. Ade. *J. Polym. Sci. Part B: Polym. Phys.*, 44, 3234-3244 (2006).

[14] I. Del Villar, I.R. Matias, F.J. Arregui. *J. Lightwave Technol.*, **23**, 4192 (2005).

# 8.  Conclusion

The aim of this thesis is the realization of integrated optic sensors based on fiber grating devices. In order to obtain chemical and biological sensors, a Long Period Gratings transducer was used as transduction platform. Different organic and inorganic materials were used as sensitive elements at the interface between the LPGs and the external environment. Since the selectivity and sensitivity of a LPGs based sensor depend upon the interface materials, careful study of the sensing materials, as well as of the deposition process was done.

Results of this PhD work has been obtained thanks to the integration of interdisciplinary knowledges in different scientific and technological areas, such as optical engineering, biochemistry, polymer materials, synthetic chemistry.

In the framework of the OPTOFER Project it has been manufactured a GPL sensor based on LPGs coated with a-PS thin films. This polymeric film has been chosen for the physical affinity between the hydrophobic polystyrene chains and the short aliphatic molecules that constitute GPL. Preliminary results have shown the good sensitivity of the devices in presence of unknown GPL concentrations: the signal is stable and the sensor is characterized by fast response time and reversibility (absence of hysteresis in consecutive gas on/gas off cycles). An accurate study, both of the material and of the interaction between the LPG transducer and the a-PS film, has allowed the development of a device able to clearly detect GPL concentration between 1000 to 30000 ppm. These sensors have been installed and tested under the railway tunnel of Porta Rufina station, in Benevento.

"Relative humidity fiber optic sensors based on Long Period Gratings" is the name of the collaboration agreement with CERN during which have been designed, developed and manufactured humidity sensors resistant to radiation and to cryogenic temperature. LPGs,

used as transducers, were coated with thin film of sol-gel synthesized titania, an inorganic oxide that shows different interesting features: 1) hygrosensitive characteristics, 2) ageing and high energy radiation resistance and 3) thermal stability. The sol-gel synthesis and the deposition process optimization has led to the development of humidity sensors with good sensibility and reversibility, and the inorganic nature of the titania coating guarantees the mechanical and thermal stability of the device.

In the framework of the OPTOBACTERIA Project, has been developed a highly-sensitive reflection-type LPG biosensor, useful for the detection of antibiotic resistance bacteria. The reflection-type LPG was coated by a primary a-PS layer and by a secondary very thin overlay of PMMA-co-MA. a-PS was used has HRI layer in order to tune the LPG to operate in the transition region. PMMA-co-MA has been employed as thin film to provide carboxylic groups on the external surface of the fiber. A standard linkage chemistry has been carried out to anchor the bioreceptors to the probe surface. Preliminary experimental results demonstrate the capability of the fabricated LPG biosensor to successfully monitor all the steps of the biochemical immobilization strategy as well as to detect the BL binding to its functionalized surface.

# Acknowledgement

Firstly, I would like to express my sincere gratitude to my Ph.D tutor Dr. Anna Borriello for the continuous support of my Ph.D study and related research, for her patience, motivation, and immense knowledge. Her guidance helped me in all the time of research and writing of this thesis, both from the scientific and human point of view.

I would also like to thank my Ph.D tutor Prof. Giuseppe Mensitieri for the support given to me during these three years and for the useful scientific discussion.

My sincere thanks also goes to Eng. Mauro Zarrelli for encouraging my research and for allowing me to grow as a research scientist: your advice on both research as well as on my career have been priceless.

I would like to thank also Miss. Paola Desidery, who has always answered my administrative questions with patient and courtesy, and Miss. Mariarosaria Marcedula, who has constantly helped me in samples manufacturing and characterization.

Moreover, I would like to thank my mother for supporting me spiritually throughout the Ph.D period, for teaching me to endure until the achievement of my goals and to share my work results with the people who helped me.

A special thanks goes to the love of my life, P. M., who made me understand the true meaning of love making me feel happier than I thought was possible. I will never stop to thank you for the patience that you have had and for the love you show me every day.

Finally, I dedicate this work to the memory of my father, who until the last day of his life has always been able to counsel and help me. Thanks for all you have done for mom and me.